A STUDY ON CROSS-SHORE SEDIMENT TRANSPORT DUE TO NON BREAKING WAVE

BADAL MAHALDER

DEPARTMENT OF WATER RESOURCES ENGINEERING
BANGLADESH UNIVERSITY OF ENGINEERING AND TECHNOLOGY
DHAKA

JANUARY, 2011

A STUDY ON CROSS-SHORE SEDIMENT TRANSPORT DUE TO NON BREAKING WAVE

BADAL MAHALDER

A thesis submitted to the Department of Water Resources Engineering in partial fulfillment of the requirements for the Degree of Master of Science in Water Resources Engineering

DEPARTMENT OF WATER RESOURCES ENGINEERING
BANGLADESH UNIVERSITY OF ENGINEERING AND TECHNOLOGY (BUET)
DHAKA

January, 2011

CERTIFICATE OF RESEARCH

This is to certify that this thesis work has been done by me and neither this thesis nor any part thereof has been submitted elsewhere for the award of any degree or diploma.

Countersigned by the Supervisor

Signature of the Candidate

Dr. Umme Kulsum Navera
Professor
Department of Water Resources Engineering
BUET

Badal Mahalder

BANGLADESH UNIVERSITY OF ENGINEERING AND TECHNOLOGY, DHAKA

DEPARTMENT OF WATER RESOURCES ENGINEERING

Certification of Thesis

The thesis titled **"A Study on Cross-shore Sediment Transport Due to Non Breaking Wave"**, submitted by Badal Mahalder, Roll No. 040816001P, Session April 2008, to the Department of Water Resources Engineering, Bangladesh University of Engineering and Technology, has been accepted as satisfactory in partial fulfillment of the requirements for the degree of Master of Science in Water Resources Engineering and approved as to its style and content. Examination held on January 30, 2011.

_____

Dr. Umme Kulsum Navera
Professor, Department of Water Resources Engineering
BUET, Dhaka-1000, Bangladesh

Chairman (Supervisor)

_____

Dr. M. A. Matin
Professor and Head, Department of Water Resources Engineering
BUET, Dhaka-1000, Bangladesh

Member (Ex-Officio)

_____

Dr. M. Monowar Hossain
Professor, Department of Water Resources Engineering
BUET, Dhaka-1000, Bangladesh

Member

_____

Dr. M. R. Kabir
Professor and Pro Vice-Chancellor
The University of Asia pacific, Dhaka, Bangladesh

Member (External)

30 JANUARY, 2011

ACKNOWLEDGEMENT

The author expresses his profound gratitude and respect to his supervisor, Dr. Umme Kulsum Navera, Professor, Department of Water Resources Engineering, BUET for her constant supervision, scholastic guidance and patience help throughout the thesis work and for the report preparation. She makes the author interested and enthusiastic to the field of coastal hydraulics. Her continuous direction, advice and help encouraged the author throughout the research work with a great extent.

The author wishes to express his sincere appreciation to Dr. M. A. Matin, Professor and Head, Department of Water Resources Engineering, BUET, for his timely co-operation and guidance.

The author is also intended to express his gratitude to Dr. M. Monowar Hossain, Professor, Department of Water Resources Engineering, BUET, for his valuable comments and suggestion. The author is also grateful to Dr. M. R. Kabir, Professor and Pro Vice-Chancellor, The University of Asia pacific, Dhaka, Bangladesh for his kind consent to be a member of the examination board. The author is very much grateful to Dr. Md. Sabbir Mostafa Khan, Professor, Department of Water Resources Engineering, BUET for valuable suggestions to improve the quality of Laboratory work. The author is also grateful to Mr. Biswajit Nandi, Assistant Professor, Department of Water Resources Engineering, BUET for providing help to collect relevant literatures.

The author acknowledges the great help and support provided by all laboratory staff of Hydraulics and River Engineering Laboratory, DWRE, BUET. The author cannot but express his appreciation to River Research Institute (RRI), Faridpur, Bangladesh, especially to Mr. Md. Lutfor Rahman of RRI for his kind help by providing velocity meter to carry out the laboratory work.

Finally, the author would like to dedicate this dissertation to his parents who were the source of his constant encouragement.

ABSTRACT

Cross-shore sediment transport is mainly influenced by the wave orbital motion when the sediment properties are uniform for different wave conditions. The attainment of equilibrium beach profile where cross-shore sediment movement is responsible mainly depends on sediment size and wave condition. This is a major field of interest for the researchers to evaluate the formation of natural beaches. In the Hydraulics and River Engineering Laboratory of Water Resources Engineering Department, BUET, such an experimental setup was constructed to understand the process of sediment transport in the cross-shore direction due to non breaking wave incidence.

In the experiment the slope of the artificial laboratory beach profile was taken as 1:15 and the mean grain diameter was 0.125 mm. The experiment was conducted with three different water depths of 50 cm, 40 cm and 35 cm. For each water depth the wave periods were taken as 1 sec, 2 sec and 2.5 sec. On the experimental slope, 3 cm thick sand layer was placed for every experimental run and the run time was taken as 1 hr and 15 minutes. The run time was selected by carrying out different trial runs with the selected wave period before conducting the experiment.

Different wave parameters such as wave period and wave height were measured for each experimental run. The mean flow velocity due to wave was measured at different locations on the slope half of still water depth from the water surface with the help of 2-D programmable Velocity Meter. After completing each run, the bed profile was measured with a point gage. The final bed profile obtained from the experimental result was compared with numerical model namely Parabolic Wave Model was found satisfactory. Again the actual velocity profile was compared with the model data, the comparison was found reasonably satisfactory.

In this study, different standard non-dimensional parameters for sediment transport were reviewed and these parameters were established for this experimental setup. The parameters obtained from the experiment showed good correlation with the standard parameters. It was found that the offshore sediment transport rate was dominant for this experiment. Hence, the beach was an erosion type beach. The non-dimensional correlation established form this study shows affirmative result with the similar experiment conducted by previous researchers. This study result may be a basis to identify the parameters responsible for beach formation and construction of any coastal structures where sediment movement is a serious problem.

The effect on the change of gradation for cohesionless sandy slope due to wave attack was also observed form the study. It was found that, the mean sediment grain size increased after completing a run in the onshore region. The change in sediment gradation was found significant where the incident wave breaks on the slope. But the grain diameter did not change or the change was very much negligible towards the offshore region, especially where the water depth was higher. In this study it was also found that use of CC blocks on the onshore area produce stable beach compared to that of a breakwater.

Table of Contents

Notations

Symbol	Meaning
ρ	density of water
s	specific gravity of sediment
g	acceleration gravity
τ	shear stress
U_m	maximum horizontal velocity of water particle on sea bed
f_ω	wave friction coefficient
$\emptyset_m$	friction angle for a moving grain
T	wave period
L	wave length
H_w/H	wave height
H_0	deep water wave height
L_0	deep water wave length
C	wave celerity
C_g	group velocity of wave
ω	wave angular frequency
k	wave number
η	instantaneous water surface elevation
$\bar{\eta}$	time independent mean free surface displacement
ξ_{-h}	maximum particle excursion at the bottom
d_{50}	median grain size
h	water depth
w_s/w_0	sediment fall velocity
Ω	energy flux
Ψ_{cr}	critical Shields Parameter
θ'	mobility parameter
$\hat{U}_\delta$	peak value of near-bed orbital velocity (m/s)
$\hat{A}_\delta$	the peak value near-bed orbital excursion
ω	angular frequency
$\hat{U}_{crest}$	peak value of near-bed orbital velocity under wave crest (m/s)
$\hat{U}_{trough}$	peak value of near-bed orbital velocity under wave trough (m/s)
$tan\beta$	bottom slope
Ur	Ursell parameter
Ψ'	flow intensity parameter
d_0	excursion length of the near bottom orbital motion
q_{net}	net sediment transport rate

$\bar{q}$	mean value of sediment transport over one half wave cycle
u	Velocity component in X-direction
v	Velocity component in Y-direction
$\emptyset$	velocity potential
Φ	non-dimensional onshore and offshore sediment transport rates
u_{*w}	bed shear velocity due to wave
$\overline{U}$	independent mean flow
$\hat{u}$	wave induced flow
u'	arbitrarily fluctuating component of flow
P	mean pressure
$\equiv$	equivalent
S_{xx}	radiation stress in X-direction
S_{yy}	radiation stress in Y-direction
S_{zz}	radiation stress in Z-direction
τ_{sx}	mean surface stress in x-direction
τ_{sy}	mean surface stress in y-direction
$\bar{\tau}_b$	bottom friction stress

List of Figures

List of Tables

List of Photographs

CHAPTER 1
Introduction

1.1 Background

Wave driven current is an important parameter for near-shore sediment transport and morphological changes in the coastal area. The fundamental parameters for evaluating the morphological changes in the beach are waves, near-shore currents and sediment transport processes due to these waves and currents. Accurate prediction about these parameters play a key role in solving coastal engineering problems related to beach formation behavior. Waves and currents are the main factors which start the initiation of motion, mobilize and then transport the sediment. The gradients in the sediment transport cause deposition or erosion of sediment, affecting the local as well as the beach topography. Gradients in sediment transport rate may occur naturally or can be induced by man-made structures such as groins, seawalls, detached breakwaters, dredging and beach nourishment. In order to predict the beach morphological changes for the purpose of engineering analysis and design a robust model of near-shore waves, currents, and sediment transport is required.

Sediment transport along the coasts can be divided into two processes: longshore sediment transport and cross-shore (onshore-offshore) sediment transport (Wellen et al, 2000). The former has been studied for many years and can be adequately modelled to predict this type of transport (Dyksterhuis, 1998). The later, however, has only recently been studied to develop mathematical models to help predict changes in beach profiles (Hibma et al, 2004). Sediment transport is now considered to be a combination of longshore and onshore-offshore processes.

In order to estimate changes in beach topography, a quantitative evaluation of the net (difference between onshore and offshore) sediment transport rate is required at every point on the cross-shore position. For this purpose, sediment transport in the near-shore region is required to calculate by using both the cross-shore and longshore

transport process. Cross-shore transport is mainly produced by the wave orbital motion, whereas longshore transport is primarily associated with wave-induced longshore currents. In this study, the net onshore and offshore sediment movement has been calculated through experimental investigation.

The estimation of net cross-shore sediment transport rate is more difficult because the net rate in the cross-shore direction occurs as an accumulation of small differences between the large values of the onshore and offshore directed transports. To obtain an accurate estimate of the net cross-shore transport rate, each of these large quantities must be evaluated separately and correctly. In order to provide a reliable estimation of the net sediment transport rate due to wave action, the evaluation for the transport direction, instantaneous values of the transport rate in the respective direction and the effects of various bed forms are the fundamental requirements to evaluate. The modes of sediment transport are traditionally classified into two types: bed load and suspended load.

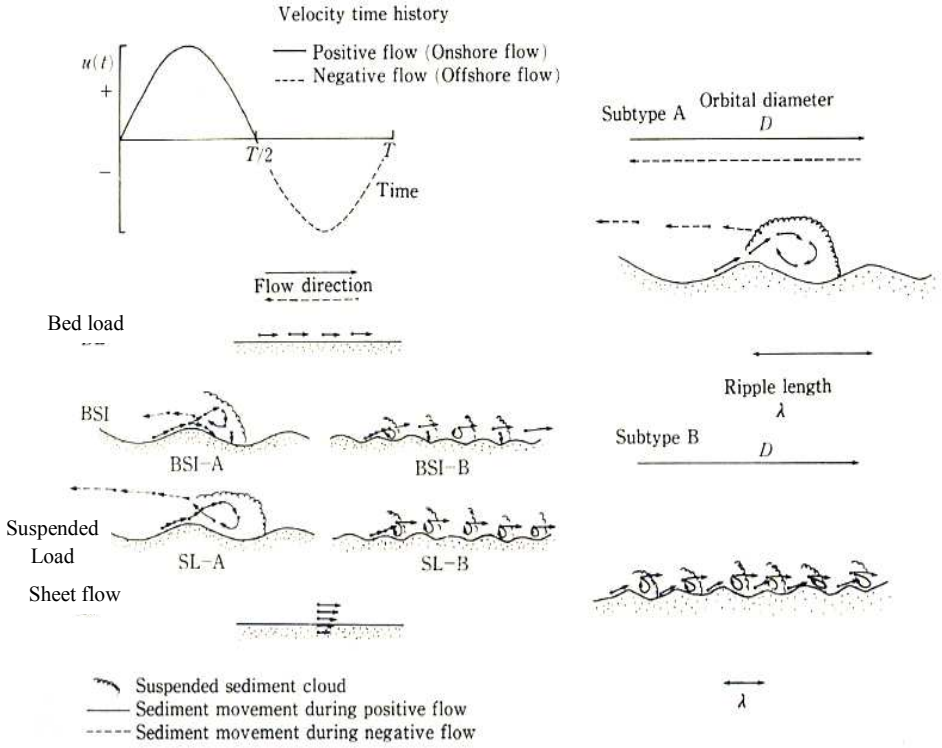

Figure 1.1.1: Sediment transport type (Source: Shibayama, 1984)

For estimating the sediment transport, the effect of sinusoidal wave (Shibayama, 1984) orbital velocity in the non-breaking zone is the fundamental parameter to know

the complex phenomena. As the flow is sinusoidal, so the classification of sediment transport under oscillating flow can be represented by the Fig. 1.1.1. The resultant classification of transport modes denotes positive and negative direction of flow in the first (on shore direction) and second (offshore direction) half of the wave period respectively.

However, because of the one step forwards and one step backwards nature of water particle movement due to waves, current will usually be the main transporter of the sediments stirred up by the waves, except for wave breaking zones, where a longshore current is produced due to wave breaking.

Theory has been developed (Camenen et al, 2003) which incorporates the effect of sediment gradation on the onshore-offshore transport or cross-shore sediment transport and the resulting equilibrium beach slope. Two main approaches to the phenomena have been studied: an energetics approach developed by Bagnold (1966) and a probabilistic approach introduced by Einstein (1972).

Some well known sediment transport formulas have been developed on the basis of experimental data from the laboratory and field data. Some of them to be mentioned as Bijker (1968), Bailard (1981), Bailard and Inman (1981) Van Rijn (1984 a, b, c, 1989, 1993), Quick (1991), Dibajnia and Watanabe (1992), Dibajnia (1995), Ribberink and Al Salem (1994, 1995), Camenen and Larson (2005, 2007, 2008).These formulas have been developed with experimental flume data involving different grain sizes and wave condition and has compared with mathematical model for that purpose.

In this research an experimental approach has been carried out to understand the sediment transport process in the laboratory flume by using the local representative soil sample. The experimental result has been compared with well known sediment transport formula to observe the sediment transport process. In this study, the experimental result has been compared with Parabolic Wave Model (Navera, 2004). This model is based on the Small Amplitude Surface Wave theory and the van Rijn (1989) formula is used for sediment transport calculation.

1.2 Objectives of the study

This research work mainly focuses on the non-breaking wave induced sediment transport process in the near-shore zone. For this purpose a laboratory setup has been established to investigate the following specific objectives:

1 To investigate the flow pattern, bed profile and sediment transport process with different combination of water depth, wave height and wave period.
2 To compare the results obtained from the experiment in the laboratory with the Parabolic Wave Model.
3 To observe the change of sediment transport pattern and bed profile response by using two types of breakwaters (submerged and floating) and with CC Blocks.
4 To investigate the change of the gradation of beach material due to wave attack.

1.3 Organization of the Thesis

This research work has been stated step by step through six chapters.

Apart from this first chapter which states the background and objective of the study, there are five more chapters. The essence of each chapter is stated below shortly:

Chapter 2 mainly focuses on the reviews of literature related to the theme of this study. Here some previous formulae for sediment transport in cross-shore direction due to wave induced current has also been studied.
Chapter 3 deals with the general theory behind the wave propagation techniques, boundary condition for solving the wave propagation parameters, measurement of different wave properties etc. has been discussed.
Chapter 4 represents the detail experimental setup, data collection processes in the laboratory and the formulation process of Parabolic Wave Model that has been used to verify the experimental data.

Chapter 5 illustrates the data analysis, results and discussion related to the sediment transport processes, total change in sediment volume in the offshore or onshore direction, the response of bed profile and the gradation change on the slope in a comprehensive manner. In this chapter the comparison between the experimental and theoretical data for bed profile and velocity has been represented.

Chapter 6 discusses major findings of the study. In this chapter the limitations of the study and recommendations for further study have also been discussed.

CHAPTER 2

Literature Review

2.1 General

In this chapter, some laboratory studies which are related to investigate the near-shore sediment transport due to wave induced current has been discussed. Furthermore, some modern and classical approaches that had been practiced earlier for the development of different sediment transport formulas have been illustrated. Here some formulas related to the wave induced current effect on sediment transport in the near-shore region have been studied. In addition to this, the effect of sediment size on sediment transport has been studied in detail to identify the effect of sediment size on cross-shore sediment transport process.

2.2 Review on Previous Laboratory Study

The historical development for investigating the beach development process or sediment movement in the near-shore region in laboratory flume has possessed long history (Dette et al, 2002). The first steps to study this process, was conducted by the Army Corps of Engineers (CE). They conducted two series of movable bed model experiments for beach profile change in the tank of the Beach Erosion Board in 1956-1957 and 1962. The study has been distinguished mainly by the grain size of the bed material on experimental beach slope. Nine major tests were carried out with two sand sizes using essentially the same water depth and offshore wave conditions. Tests for a given grain size were characterized by waves of varying steepness, producing either accreting or eroding profile shapes. All tests were performed with monochromatic waves. The experiments included extensive profile surveys during each test to document the approach to attain equilibrium. Only limited hydraulic measurements were made, mainly wave heights at incipient breaking and run-up heights. The CE experiments were a pioneering effort involving the first prototype size tests for profile

evolution under waves. Since then, tanks and flumes comparable in size have been constructed in several countries and similar experiments have been carried out. The capabilities of modern instrumentation have allowed for more efficient and accurate measurements of profile change, sediment transport, waves and fluid flow than was possible during these experiments. However, a wealth of data were collected in the CE experiments that constitute a valuable resource for researchers as well as practicing engineers in understanding beach profile response to waves.

Another series of experiment in Grosser Wellenkanal (GWK) were conducted since 1986 to 1997. The aim of the experiments with sandy beach profiles was to investigate the profile development and morphodynamic processes under given wave and water depth conditions. The purpose of the first set of experiments in 1986-1987 was to study beach and dune erosion under monochromatic and random waves. Dette and Uliczka (1986) analyzed velocity and sediment suspension measurements along the surf zone. Dette (1986) focused on the dune erosion investigations. The absorption control system for reflected waves was not installed at the time. Suspension measurements in 1990 and 1991 were used by Raudkivi and Dette (1991, 1993) to develop an empirical model for the description of the vertical distribution of suspended sediments inside and outside the surf zone. Investigations on profile development by means of the 1993 GWK experiments by Peters et al. (1996) showed that beach profiles reached their equilibrium state under erosional and accretional wave conditions in small time scales. In these two test series grain sizes were different.

Several approaches have been developed after these two approaches in the field of cross-shore sediment transport. Some researchers have developed different non-dimensional parameters to predict sediment transport for different wave and slope condition. Dibajnia and Watanabe (1992) pointed out that, the effect of the critical Shields parameter was fundamental for sediment transport in the cross-shore direction. They also found that ripples formation was dominating in monochromatic waves and there remains stronger suspension and phase- lag effects for sediment transport.

Dette et al. (2002) investigated the effect of beach slope on erosion rate during wave similar to storm surges or short term waves in nature. The slopes for this experiment were taken as 1:20, 1:15, 1:10 and 1:5. They found that, the sand loss from the beach above the raised water level was a function of beach slope. The erosion rate and thus the volume loss increases rapidly on slopes steeper than 1:15. The 1:15 slope discourages wave run-up, so that an erosion escarpment, which accelerates erosion from the beach. According to the study, the cross-shore transport rates diminish rapidly as the underwater profile approaches equilibrium form. This study supports the concept of zero net cross-shore transport on an equilibrium profile and minimum amount of sediment is mobilized on such a profile. The beach slope of the initially dry beach had a major effect on the erosion of the beach by raised water levels. The sand losses increase rapidly once the beach slope becomes steeper than 1:15. Hence, the annual sand demand can be minimized if the storm tides can run onto a flat beach, with an additional wave run-up zone.

Dohmen Janssen and Hanes (2002) carried an experiment in a large- scale wave flume (LWF) to investigate the sediment transport where waves are dominating. They found that, for non-breaking waves the bed load sediment transport represents around 90% of the total load. The experiment with real waves showed that the results were quite consistent with those observed in oscillating water tunnels (OWTs). Net transport rates under waves were found to be about a factor 2.5 larger than in uniform horizontal oscillatory flows. They explained this by referring to the differences between boundary layer flows in OWTs and under free surface gravity waves.

Sekiguchi et al. (2004) conducted a laboratory study on a fixed slope of 1/20 with a piston-type wave generator was equipped at the one end of the flume. The study was carried out to investigate the formation of ripple under asymmetrical oscillatory flows. In this study three median grain sizes soil of 0.021, 0.038, and 0.054 cm with density between 2.6–2.7 g/cm^3 were used. Water depth above the horizontal portion of the sand bed was kept constant throughout each experimental run. The range of wave period was from 1.0 to 3.5 s, and wave height from 1.7 to 13.0 cm. By combining these experimental parameters, approximately 250 runs were carried out. Each run

had 30min wave action. Ripple formation was recorded using a digital video camera and photographs were taken at a certain interval of time.

2.3 Study on Different Theoretical Formulation

The calculation of near-shore sediment transport rate is quite challenging due to the complexity of the hydrodynamics and the variety of the governing parameters. Actually it is very much difficult to estimate sediment fluxes on beaches due to the combination of steady flows (currents) and oscillatory flows (waves). Moreover, many other parameters should be integrated such as the variations in mean water level, breaking wave effects (turbulence and undertow) and topographic influence (mean slope and bed forms). Furthermore, these parameters induce different types of transport (bed load, suspended load and sheet flow) with very different physical implications for the movement of sand.

Different formulas are available to estimate sediment transport on beaches, most of them based on a macroscopic approach to the phenomena. Two main approaches to the phenomena have been studied: an energetic approach developed by Bagnold (1963) and a probabilistic approach introduced by Einstein (1972).

Hughes et al. (1997) conducted a study for detailed measurements of flow velocity and total sediment load in the swash zone on a steep beach. The findings of their study was, during wave uprush the onshore flow increased almost instantaneously from zero to its maximum velocity. According to the study result, during backwash the offshore flow increased steadily from zero to its maximum towards the end of the backwash and dropped rapidly to zero as the beach fell dry. They found that, the duration of backwash was typically longer than that of uprush and maximum water depth on the beach was attained just prior to the end of the uprush. The amount of sediment transported by a single uprush was typically two to three orders of magnitude greater than the net transport per swash cycle (difference between uprush and backwash) inferred from surveys of beach profile change.

Butt et al. (1999) observed that the time-series from in the swash-zone and identified two possible mechanisms for accretion and erosion. Sediment becomes in suspension by the action of sudden offshore to onshore velocity transition and the turbulence in the swash-front. This movement leads subsequent onshore advection by the uprush and offshore transport due to low-frequency. For fast flowing backwashes the threshold velocity for sediment movement exceeds. They also suggested that the erosion in beach takes place during the high energy conditions due to a decrease in bed level. Though, the flux calculations show a bias towards accretion. They suggested that, this was probably due to the inability of the instruments to measure backwash flows very close to the bed.

Elfrink et al. (2002) concluded that, dominant hydrodynamic forcing and resulting sediment transport mechanisms in the swash zone were important for the future measurement and modelling requirements of sediment transport. The hydrodynamics of the swash zone were largely governed by the boundary conditions imposed by the inner surf zone and the underlying beach. These boundary conditions include the wave height, wave frequency, wave shape, spectral bandwidth, orbital velocities, currents, turbulence, slope and beach composition. These hydrodynamics are important phenomena for understanding the cross-shore sediment transport. In addition to these, the beach composition (grain size, permeability, degree of saturation) largely expected to influence the hydrodynamics at micro-scales (e.g. infiltration/exfiltration and boundary layers).

Meijer et al (2002) conducted a study to determine the effects of grain size and density gradation in oscillatory sheet-flow. Experiments were conducted in an oscillating water tunnel to observe the size gradation on sediment transport rates. The experiments on density graded sediments indicate that total mass-transport rates were larger than the mass-transport rates of quartz material, whilst the transport rates of the quartz fraction show that this fraction is not hindered by the availability at the bed.

Camenen et al. (2005) showed that the sediment transport in the cross-shore direction is proportional to the total Shields parameter to the power 1.5. For purely oscillatory

flows, the mean Shields parameter for each half-period (when $u>0$ and $u\leq 0$) is important to computed in order to take into account the effect of asymmetric waves.

The study conducted by Hsu et al. (2006) suggested that when mean-current-induced transport was small, wave-induced transport leads to the observed onshore bar migration. To calculate the net cross-shore sediment transport, Hsu et al. formed a simplified phase-resolving process. This process was wave-averaged energetics-type (e.g., only moments of the near-bottom velocity field are required) with different friction factors for oscillatory and mean flows. Although the assumptions underlying the models differ, the similarity of model results precludes determination of the dominant mechanisms of sediment transport during onshore bar migration.

From the above mentioned studies it has been observed that, very few studies had been conducted to compare the behavior of different formulae with respect to the main sediment transport parameters. King and Seymour (1982) performed some comparisons with Shields parameter. More recently, Dohmen- Janssen (1999) compared the Bailard, Ribberink, and Dibajnia and Watanabe formulae with experimental flume data involving different grain sizes, currents, and orbital velocities. Camenen and Larroude´ (2000) pointed out there are great dependence of sediment fluxes on these parameters. Several authors have hence made some comparisons but only between their own formula and one other, or have only studied the influence of one parameter.

Shore Protection Manual (SPM, 1984) suggested that, the dimensionless fall velocity is the key component in onshore-offshore sediment transport in the littoral zone. The littoral zone is defined as extending from the shoreline to just beyond the seaward where most waves breaks. Earlier studies had indicated that sediment suspension in the surf zone may form a significant portion of the material for longshore transport. However, the SPM admits that it cannot recommend suitable prediction procedures and it can only provide useful guidance. In the Shore Protection Manual, it has been illustrated that, the beach slope depends on the wave exposure, the specific gravity, porosity and permeability of beach materials and to some degree on the tides. For design of replacement beach materials it is essential to ensure that the sediment

supplied to the artificial beach is at least as coarser in texture as that are existed in naturally developed beach.

For developing reliable correlation for sediment transport Watanabe (1982) formed a new non-dimensional parameters. This was related to the Shields parameter and the sediment transport process in the cross-shore direction. The study result indicated that, sediments start to move if the Shields parameter is bigger than the critical Shields parameter. The Shields parameter is defined as

$$\theta = \frac{u_*^2}{(s-1)gd} = \frac{\tau}{\rho(s-1)gd} \tag{2.1}$$

Laboratory results have shown that the Shields diagram for currents can be used directly for wave, with the current-induced bottom shear stress replaced by Jonsson's (1966) definition of wave-induced bottom shear stress.

$$\tau_{\omega,max} = \frac{1}{2}\rho f_\omega U_\omega^2 \tag{2.2}$$

Where, U_m is the maximum horizontal velocity of water particle on sea bed, given by the linear wave theory,

$$U_m = \frac{\pi H}{T}\frac{1}{\sinh\frac{2\pi h}{L}} \tag{2.3}$$

and f_ω wave friction coefficient,

$$f_\omega = exp\left(5.5\left(\frac{K_s}{A}\right)^2 - 6.3\right) \tag{2.4}$$

Where, k_s the bed roughness and A the amplitude of oscillation of water particle on sea bed.

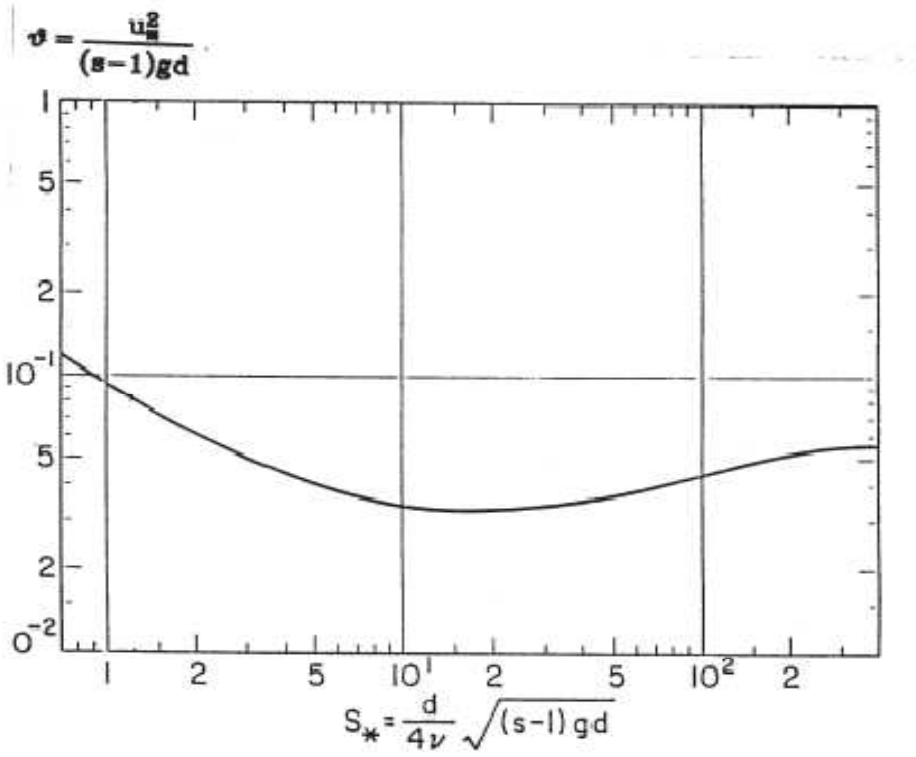

Figure 2.3.1: Shields Diagram (Source: Zhou Liu, 2001)

Larson and Wamsley (2007) developed the formula for the net transport rates in the cross-shore and longshore direction, respectively as:

$$q_{bc,net} = K_c \frac{\tan \emptyset_m}{\tan^2 \emptyset_m - (dh/dx)^2} \frac{u_0^3}{g} \left(\frac{dh}{dx} - \tan \beta_e\right) \frac{t_0}{T} \tag{2.5}$$

$$q_{bl,net} = K_1 \frac{\tan \emptyset_m}{\tan^2 \emptyset_m - (dh/dx)^2} \frac{u_0^2 v_0}{g} \frac{t_0}{T} \tag{2.6}$$

Where, $q_{bc,net}$, $q_{bl,net}$ were the net transport in the cross-shore and longshore direction, respectively, K_c and K_l were empirical coefficients, $\emptyset_m$ the friction angle for a moving grain (≈30°), β_e the foreshore equilibrium slope, u_0,v_0 and t_0 the scaling velocities and time, respectively, and T wave period.

Camenen and Larson (2005, 2007 and 2008) developed a general transport formulation for bed load and suspended load under combined waves and current. According to them, these formulas can be used for both sinusoidal and asymmetric waves. To simplify calculations the waves were assumed to be sinusoidal having no

asymmetry. Thus, the contribution to the transporting velocity from waves was negligible, implying that only the current moves the material. In such case, the bed load transport can be expressed as,

$$\frac{q_{bc}}{\sqrt{(s-1)gd_{50}^3}} = a_c\sqrt{\theta_c}\theta_{cw,m}exp\left(-b_c\frac{\theta_{cr}}{\theta_{cw}}\right) \tag{2.7}$$

where the transport q_{bc} was obtained in the direction of the current, the transport normal to the current was zero, *s* the relative density between sediment and water, d_{50} the median grain size, a_c and b_c empirical coefficients, $\theta_{cw,m}$ and θ_{cw} the mean and maximum Shields parameters due to wave and current interaction, respectively, θ_{cr} the critical Shields parameter and θ_c the Shield's parameter due to current. It was a very interesting idea to compare the dependence of formulae with respect to the main parameters of sediment transport. This approach provided a better understanding of the physics of sediment transport, as different parameters relate to wave (bottom orbital velocity, period, and asymmetry), current and sediment (grain size) were included in these formulas.

One of the first sediment transport formulations that are still used in engineering applications was proposed by Bijker (1968). It was derived from Frijlink (1952) formula for a current only with a modification of the bottom shear stress using a wave–current model. The direction of sediment fluxes is always that of the current since this formula was proposed to estimate longshore transport rate:

$$\mathrm{q_{sb}} = \mathrm{C_b d}\sqrt{\frac{\mu_c\tau_c}{\rho}}\exp\left(-0.27\ \frac{(\rho_s-\rho)gd}{\mu_c\tau_{cw}}\right) \tag{2.8}$$

$$\mathrm{q_{ss}} = 1.83\ \mathrm{q_{sb}}\left(\mathrm{I_1 ln}\left[\frac{33h}{\delta_c}+\mathrm{I_2}\right]\right) \tag{2.9}$$

where q_{sb}, q_{ss} sediment volume fluxes for bed load and suspended load respectively, *d* the median grain size diameter, *h* water depth, C_b breaking wave parameter, μ_c ripple parameter, τ_c shear stress due to current only, τ_{cw} shear stress due to wave–current interaction, ρ_s, ρ sediment and water densities respectively, I_1, I_2 Einstein integrals (suspended load) and $\delta_c = 100d / h$ dimensionless thickness of the bed load

layer. The ripple parameter introduced by Bijker can be defined by the following equation:

$$\mu_c = \left(\frac{f_{ct}}{f_c}\right)^{3/2} \tag{2.10}$$

where f_{ct} the total friction coefficient due to current and f_c the skin friction coefficient due to current. The shear stress due to the wave–current interaction is computed following the method proposed by Bijker introducing a suspension factor:

$$\tau_{cw} = \left[1 + 0.5\left(\xi_B \frac{U_w}{U_c}\right)^2\right]\tau_{cf} \tag{2.11}$$

with $\xi_B = \sqrt{f_{wt}/f_{ct}}$ parameter due to the wave-current interaction, f_{wt} the total friction coefficient due to waves, U_w peak value of the wave orbital velocity at the bottom and U_c mean current velocity. The Einstein integrals for the suspended load are given:

$$I_1 = \int_\delta^1 \left(\frac{1-y}{y}\right)^4 dy \tag{2.12}$$

$$I_2 = \int_\delta^1 \left(\frac{1-y}{y}\right)^4 ln\, dy$$

where $A = W_s/k(\frac{\tau_{cw}}{\rho})^{0.5}$ a function determining the rate of the suspension, k = 0.41 the Von Karman constant and W_s is the settling velocity.

The Bailard (1981) formula was derived directly from the Bagnold's (1966) approach. Bagnold introduced the energetics approach for sediment transport in which the main idea was that the sediment flux is proportional to the energy flux (local rate of energy dissipation). His transport model was able to separate the two classical types of transport:

- bed load transport sustained by the bed via grain to grain interaction,
- suspended load transport sustained by the current via turbulent diffusion.

Thus, the transport was expressed as:

$$q_s = q_{sb} + q_{ss}\alpha\Omega \tag{2.13}$$

$$\Omega = 0.5\rho f_{cw} \left|\overrightarrow{u(t)}\right|^3 \tag{2.14}$$

where, Ω energy flux due to waves and currents, f_{cw} friction coefficient due to the wave-current interaction, $\overrightarrow{u(t)}$ instantaneous velocity vector, $\overrightarrow{u(t)} = \vec{U}_c + \overrightarrow{u_w(t)}$, U_c current velocity averaged over the depth and $u_w(t)$ instantaneous wave velocity. For a horizontal bed, it can ultimately be written as a vector of sediment volume transport:

$$\overrightarrow{q_s} = \frac{0.5 f_{cw}}{g(s-1)}\left(\frac{\epsilon_b}{tan\phi}\ \langle|\vec{u}|^2\vec{u}\rangle + \frac{\epsilon_s}{W_s}\langle|\vec{u}|^3\vec{u}\rangle\right) \tag{2.15}$$

Where, ϵ_b, ϵ_s bed load and suspended load efficiencies respectively, ϕ friction angle of the sediment and $\langle|\vec{u}|\rangle$ average over several periods of the wave. The bed load and suspended load efficiency coefficients are slightly different from those given by Bagnold. Bailard suggested from a calibration with field data that ϵ_b = 0.1 and ϵ_s = 0.02. One difficulty for this formulation was the estimation of the friction coefficient due to the wave–current interaction as Bailard did not specify any expression for this friction factor.

Dibajnia and Watanabe (1992) and Dibajnia (1995) formulated two formulas, where the sediment transport was divided into two half cycles due to the presence of waves (Fig. 2.3.2).

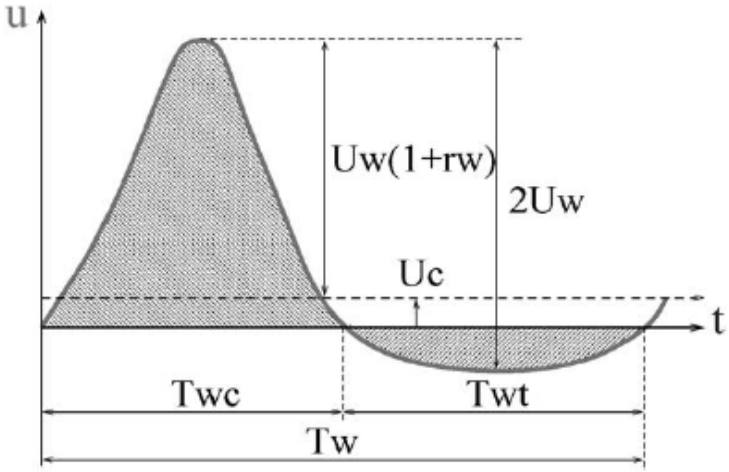

Figure 2.3.2: Bottom velocity profile in the direction of the wave propagation (Source: Debanjinia and Watanabe, 1992)

During the first half-cycle, sediment moves in the direction of the wave, just as it moves in the opposite direction during the second half-cycle. An important aspect of the formula is that possible quantity of sand may present in suspension after each half-cycle. Hence the suspended sediment can move to the other direction which is called phase-lag. This formula enables to calculate the sediment transport rate under a non-linear wave.

The solid volume flux is given by the following equation:

$$\overrightarrow{q_s} = A_{dw} W_s d \frac{\overrightarrow{\Gamma}}{\Gamma} \Gamma^{B_{dw}} \tag{2.16}$$

Where, A_{dw} = 0.001and B_{dw} = 0.55, coefficients of calibration with

$$\overrightarrow{\Gamma} = \frac{T_{wc}\overrightarrow{u_{wc}}\,(\Omega_c^3 + \Omega'^3_t) + T_{wt}\overrightarrow{u_{wt}}(\Omega_c^3 + \Omega'^3_t)}{(u_{wc} + u_{wt})T_w} \tag{2.17}$$

Where, T_w, T_{wc}, T_{wt} period and half periods of wave taking into account the effect of a current (Fig. 2.3), Ω_c, Ω_t amount of sand entrained and settled during the half-period T_{wc} and T_{wt} respectively, Ω'_c, Ω'_tamount of suspended sand remaining from the positive and negative half-cycle respectively and u_{wc}, u_{wt} quadratic velocity over each half-period expressed as

$$u_{wj}^2 = \frac{2}{T_{wj}} \int_t^{t+T_{wj}} u^2\,(t)dt + 2U_c^2 \sin^2\theta \tag{2.18}$$

Where j can be c or t, $u(t) = U_c \cos\theta + u_w\,(t), u_w(t)$ instantaneous wave orbital velocity, θ angle between wave direction and current direction.

$$\begin{aligned}
&\text{If } \omega_j \le \omega_{cr} && \text{then } \Omega_{\mathrm{j}} = \omega_j \tfrac{2W_s T_{wj}}{d} \\
& && \text{and } \Omega'_{\mathrm{j}} = 0 \\
&\text{If } \omega_j \ge \omega_{cr} && \text{then } \Omega_{\mathrm{j}} = \tfrac{2W_s T_{wj}}{d} \\
& && \text{and } \Omega'_{\mathrm{j}} = \left(\omega_j - 1\right) \tfrac{2W_s T_{wj}}{d} \\
&\text{With} && \omega_j = \tfrac{u_{wj}^2}{2(s-1)gW_s T_{wj}}
\end{aligned} \tag{2.19}$$

Where j can be c or t. ω_{cr} is a ripple parameter:

$$\omega_{cr} \begin{cases} = 0.03 & \text{If } \Psi_{cw(max)} \leq 0.2 \\ = 1 - 0.97\left(1 - \left(\frac{\Psi_{cw(max)} - 0.2}{0.4}\right)^2\right)^{0.5} & \text{If } 0.2 < \Psi_{cw(max)} < 0.6 \\ = 1 & \text{If } 0.6 \leq \Psi_{cw(max)} \end{cases} \quad (2.20)$$

Where, $\Psi_{cw(max)}$ maximum shields parameter due the wave-current interaction.

Ribberink (1993) proposed a quasi-steady formula for bed load transport. In this formula the instantaneous solid flux is assumed to be proportional to a function of the difference between the actual time-dependent bed shear stress and the critical bed shear stress (Fig.2.3.3). This formulation has been calibrated towards several flume data sets including wave–current interaction in a plane regime (suspended load negligible) and field data (unidirectional flows in rivers). The following expression for the sand transport rate was obtained:

$$\overrightarrow{q_{sb}} = m_{Rib}\sqrt{(s-1)gd^3} \times \langle\left(\left|\overrightarrow{\Psi(t)}\right| - \Psi_{cr}\right)^{n_{Rib}} \frac{\overrightarrow{\Psi(t)}}{|\Psi(t)|}\rangle \quad (2.21)$$

Where, $\overrightarrow{\Psi(t)} = 0.5 f_{cw}|u(t)|\overrightarrow{u(t)}/[(s-1)gd]$ time dependent Shields parameter (Fig. 2.3.3) with the instantaneous velocity $\overrightarrow{u(t)} = \overrightarrow{U_c} + \overrightarrow{u_w(t)}$, Ψ_{cr} critical Shields Parameter, $\langle\Psi_{cr}\rangle$ time-averaged over several wave periods and m_{Rib} = 11, n_{Rib} = 1.65 adjusted coefficients.

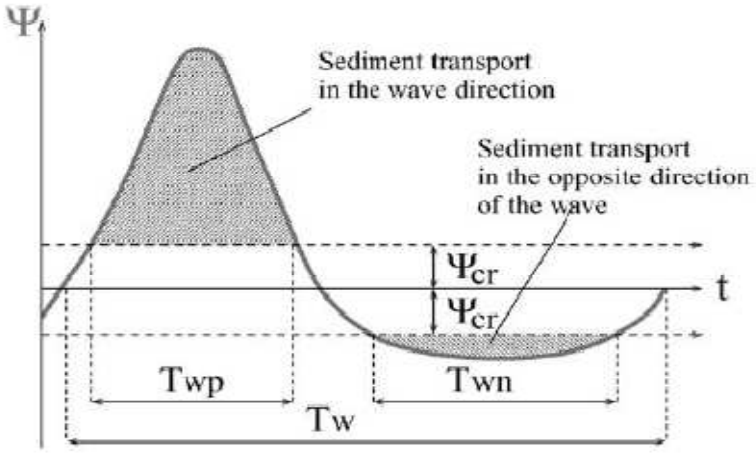

Figure 2.3.3: Profile of the time-dependent shear stress (Source: Ribberink 1993)

In the same way as the Bailard formula, an equivalent wave–current friction coefficient has to be computed. Ribberink proposed to use the Madsen and Grant's (1976) method. At last, several formulations need a friction coefficient due to wave–current interaction.

According to Ribberink, friction coefficients due to current only or due to waves only do not have the same physical basis and display very different values ($f_w/f_c \approx 10–100$). Madsen and Grant suggested a linear combination of the two friction coefficients:

$$f_{cw} = X f_c + (1 - X) f_w \qquad \text{with X} = \frac{\mathrm{U_c}}{\mathrm{U_c} + \mathrm{U_w}} \tag{2.22}$$

However, following the relation between friction coefficient and shear stress, f_{cw} can be computed from the maximum total shear stress over the bottom.

$$f_{cw} = \frac{\tau_{\mathrm{cw,max}}}{0.5\ \rho \langle |\vec{u}|^2 \rangle} \tag{2.23}$$

He also proposed to compute total roughness values as follows:

$$k_{st} = max\left(k_s;\ d\left[1 + 6\left(\frac{\langle |\Psi(t)| \rangle}{\Psi_{\mathrm{cr}}} - 1\right)\right]\right) \tag{2.24}$$

Where, k_s skin roughness height.

Dally (1980), Dally and Dean (1984, 1987) developed another formulation type for calculating net time-averaged flux of suspended sediment (S_{ys}) at any section in the near-shore zone given by:

$$S_{ys} = \int_{bottom}^{water\ level} u(z) C(z) dz \tag{2.25}$$

where *u(z)* average horizontal velocity at level *z*, and *C(z)* suspended sediment concentration at level *z*. The fluid flow regime is divided into an upper layer where only mean flow was considered and a lower layer where mean flow and

orbital velocity were taken into account. The interface between the layers was determined by the distance that the assumed uniform sediment will fall in one wave period. Linear wave theory was used to predict orbital velocities and stream function wave theory had been applied by Dally to obtain second-order mean flow velocities. The concentration profile was exponential and based on the l-D solution of the diffusion equation for unidirectional flow. The shear velocity used in the solution was assumed to be the sum of the shear velocities due to wave-induced bottom shear and breaking-induced turbulence. The continuity equation was then solved in an explicit finite difference scheme. However, to prevent numerical instability just outside the surf zone, empirical transport spreading (smoothing) was applied.

Madsen and Grant (1976) developed another formula for calculating sediment transport rate in the cross-shore direction due to wave induced current.

$$q_{w,half} = 12.5\, w_s d_{50} (\theta')^3 \tag{2.26}$$

In which $q_{w,half}$ the time averaged transport rate over a half cycle (m^2/s), w_s the particle fall velocity, d_{50} median particle diameter, $\theta' = \frac{0.5(\hat{U}_\delta)^2 f_w'}{(s-1)g d_{50}}$ mobility parameter,

$f_w' = exp\left[-6 + 5.2\left(\hat{A}_\delta / d_{50}\right)^{-0.19}\right]$ is grain related friction factor, $\hat{U}_\delta$ peak value of near-bed orbital velocity (m/s) and $\hat{A}_\delta$ the peak value near-bed orbital excursion. The empirical coefficient was based on the calibration of about 110 experiments with d_{50} in the range of 300 to 2800 μm; wave periods in the range of 1 to 6 s; in most tests the bed was flat. This equation yields a net transport rate in the direction of the largest peak velocity (usually onshore). According to Horikawa et al. (1982), this equation is also valid for sheet flow conditions based on a comparison with measured transport rates in the sheet flow regime.

Hallermeier (1982) developed another simple formula for calculating sediment transport due to wave induced current in the cross-shore direction.

$$q_{w,half} = \omega(d_{50})^2(0.1\psi)^{1.5} \quad (2.27)$$

In which, $q_{w,half}$ time averaged transport rate over half cycle (m^2/s), $\Psi = \frac{(\hat{U}_\delta)^2}{(s-1)g\ d_{50}}$ mobility parameter and $\omega = \frac{2\pi}{T}$ angular frequency. This equation was based on about 700 experiments with d_{50} in the range of 150 to 4200 μm and wave periods in the range of 1 to 9 s. The predicted transport rates are in agreement with measured transport rates for $30 < \Psi < 200$. The predicted rates are too large for $0.05 < \Psi < 30$. This equation predicts a net transport rate in the direction of the largest peak velocity.

Sato-Horikawa (1986) formulated another cross-shore sediment transport formula to calculate the sediment movement. Based on tunnel experiments with regular asymmetric wave motion over a rippled sand bed of 180 μm, Sato and Horikawa found:

$$q_{w,net} = -7w_s d_{50}(\theta'_{crest} - \theta_{cr})(\theta'_{crest})^2 \qquad for\ \theta'_{crest} \leq 0.6 \quad (2.28)$$

In which $q_{w,net}$ net transport rate over a wave cycle (m^2/s), $\theta' = \frac{0.5(\hat{U}_{crest})^2\ f'_w}{(s-1)gd_{50}}$ mobility parameter, θ_{cr} critical mobility parameter.

$f'_w = exp\left[-6 + 5.2\left(\hat{A}_\delta/d_{50}\right)^{-0.19}\right]$ friction coefficient, $\hat{U}_{crest}$ is peak value of near-bed orbital velocity under wave crest (m/s) and w_s particle fall velocity of bed material (m/s). This equation was based on 36 experimental data, predicts a net transport rate against the direction of the largest peak velocity and is only valid for the ripple regime.

Sawamoto-Yamashita (1987) developed another formula based on experiments performed in a wave tunnel with sand (d_{50} = 200, 700 and 1800 μm) coal and plastic material, the following empirical formula for the sheet flow regime was proposed:

$$q_{w,half} = 12.5\ w_s d_{50}(\theta')^3 \quad (2.29)$$

In which, $q_{w,half}$ time-averaged transport rate over half cycle (m^2/s), $\hat{u}_{*w} =$

$(0.5f'_w)^{0.5}\widehat{U}_\delta$ peak bed-shear velocity (m/s), $f'_w = exp\left[-6 + 5.2\left(\hat{A}_\delta / d_{50}\right)^{-0.19}\right]$ grain related friction factor, $\widehat{U}_\delta$ peak value of near-bed orbital velocity (m/s) and $\hat{A}_\delta$ the peak value near-bed orbital excursion. This equation yields a net transport rate in the direction of the largest peak velocity.

The Van Rijn (1989) formula was expressed in the same way as the Bijker formula, as the sum of bed load transport (taking into account the influence of waves) and the suspended load flux integrated over depth. The direction of sediment fluxes was also that of the current. Bed load transport could be written as follows:

$$q_{sb} = 0.25 d D_*^{-0.3} \left(\frac{\tau_{cf}}{\rho}\right)^{0.5} \left(\frac{\tau_{cw} - \tau_{cr}}{\tau_{cr}}\right)^{1.5} \tag{2.30}$$

Where, $D_* = ((s\text{-}1)gd^3 = v^2)^{1/3}$ dimensionless sediment diameter, $\tau_{cf} = \mu_c \alpha_{cw} \tau_c$ total shear stress due to current only (taking into account the influence of bed forms), τ_{cr} critical shear stress for sediment transport, $\mu_c = f_c / f_{ct}$ shape factor and α_{cw} coefficient due to the presence of waves. Suspended load transport is computed by solving the equation of concentration over depth.

$$\frac{dc}{dz} = -\frac{(1-c)^5 c W_s}{\epsilon_{scw}} \tag{2.31}$$

Where, $c(z)$ mean volume concentration (time averages) at height z, $(1\text{-}c)^5$ corresponds to the decrease of the settling velocity due to high concentrations and ϵ_{scw} mixing coefficient in case of a wave-current interaction.

Then, integrating sediment fluxes over depth:

$$q_{ss} = \int_a^h \overline{u(z)}\, c(z) dz \tag{2.32}$$

where, h water depth, a= max(k_{sct}, k_{swt}) reference level, k_{sct}, k_{swt} total roughness values due to current and waves and $\overline{u(z)}$ mean velocity at height z.

2.4 Effect on grain size distribution due to wave incidence

Sediments size plays a significant role for the formation of beach profile. Sediment in coastal regions may be composed of any materials that are available in significant quantity and is of a suitable grain size to remain on the beach. Grain size is sometimes given as the ' ϕ ' scale. It relates to the diameter d in millimeter by d = 1/2 ϕ (Fox et al. 1966). Grain size in beach varies from more than 1.0 meter for boulders to less than 0.1 mm for very fine sands. Generally grain size ranges from 0.1 to 2.0 mm in natural beaches. There are three dominant factors controlling the mean grain size of beach sediment: the sediment source, the wave energy level and the beach slope. The sorting of sediments along a beach profile produces cross-shore variations in sediment grain size.

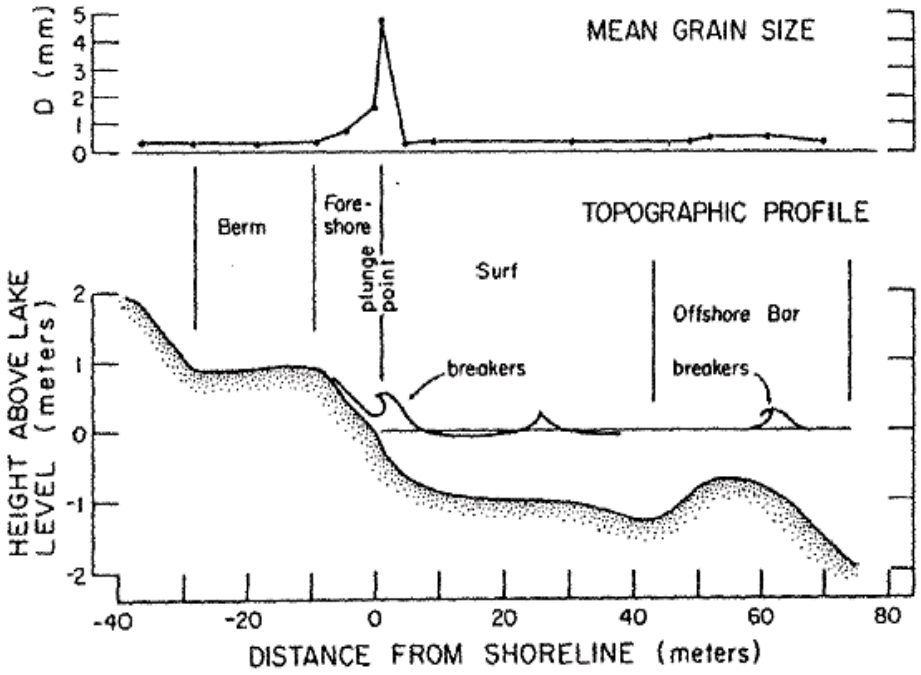

Figure 2.4.1: Grain size across the Lake Michigan beach (Source: Fox et al. 1966)

The Fig. 2.4.1 shows the mean grain size reflects the wave energy loss. It has been found that the incoming waves first break over the offshore bar without much energy dissipation by turbulence. The waves then reform and break for a second time, plunging at the base of the beach face where they expend most of their energy.

Weigel (1964) described that on a sloping beach wave motion becomes translator when wave breaks. The water moves forward as a foam line and then rushes up the beach face carrying fine sand in suspension and moving coarser grains along the bottom. The uprush gradually slows down due to gravity, friction and percolation. Therefore, it deposits a thin layer of sand along the way. At its maximum landward limit on sandy beaches, a thin line of sand grains (called a swash mark) is deposited, the grains usually being of a larger size than the rest of those on the beach. If the upward motion on the beach face has been ceased, the water which has not percolated into the sand returns as gravity flow down the beach face moving sediment with it. This sediment consists mainly of grains greater in size than average (like those in the swash marks). When this backflow comes in contact with the forward moving water of the next breaking wave, the coarse material is deposited and a low seaward facing step is formed.

Theoretical work by Bowen (1980) showed that when a sediment of a given grain size was in equilibrium with a given slope and wave regime net sediment transport parameters were responsible for the variation in direction of sediment.

Gourlay (1980) studied the role of permeability in laboratory experiments. He tested two beaches with significant differences in sediment permeability; one was composed of sand and the other of coal. He considered the dimensionless fall velocity parameter to be a scaling parameter which represented the time taken for a sand particle to fall a distance equal to the wave height. If time was large compared with the wave period, any material stirred up by the breaking waves was likely to remain in suspension and the result was suspended load movement. If it was of the same order of magnitude or less than the wave period, bed load motion scenario was predominating. He found permeability as an important factor in the amount of reflection that occurred on the beach models, as well as the resulting beach profiles. According to Gourlay the sand beach behaved impermeable surface with both the uprush and the backwash flowing parallel to the beach face.

Experiments conducted by Watanabe, Riho and Horikawa (1980) on constant beach slope subjected to selected wave action for one hour. The changes in the beach profile

were measured and the net rate of onshore-offshore sediment transport was calculated. In their results they observed that the shoreward limits of significant beach change in most cases were determined by the locations of maximum run-up. Onshore sediment transport was explained by the asymmetric to and fro water particle motion under large amplitude waves, since the coarse sands are transported essentially as bedload. They found that while net bedload transport was usually onshore net suspended load could be onshore or offshore depending on the wave conditions.

Bird (1984) analyzed the grain size distributions of beach materials. He found that the distributions were commonly asymmetrical and negatively-skewed producing mean grain size coarser than the median. He attributed that to the fining of the beach sediments due to wave action which reduces the relative proportion of fine particles. The incoming swash carried a number of particles with it up the slope against the gravitational forces. However, because of the permeability of the beach, a certain proportion of the swash flowed into the beach the velocity of the backwash was reduced. Consequently, despite the favorable slope the backwash could carry fewer particles seaward.

According to the study result of Bird, the beach water table was also responsible for the response of a beach to incoming waves. A wet sandy beach is more easily eroded by wave scour than a dry one. On some beaches a distinct break occurred in the beach slope at the water table level, a steep coarser upper beach with a shallower, finer lower beach results. Below this break the mean flow was out of the beach during the tidal cycle and this increased the potential mobility of the sediment resulting in a lower slope.

Studies on cross-shore sediment transport of bimodal sediment beaches by Richmond and Sallenger (1984) showed that onshore transport of coarser materials and offshore transport of finer grains may occur simultaneously.

Dyer (1986) observed from the studies of bimodal sediments that for a grain size less than about $l/7^{th}$ of the larger grains, more or less free passage through the pore spaces could occur and the smaller particles could flow into the coarser lattice as a separate

deposition stage. In a binary mixture with a diameter ratio of 1:6.3, there was a minimum porosity when the proportion was 25 per cent small spheres to 75 per cent large. Maximum packing densities for binary mixtures occurred at about 70 per cent large to 30 per cent small spheres. Less roll-able grains were more likely to be transported in suspension or by saltation while more roll-able grains would be transported as bedload. Under extreme conditions where all of the fine material had been winnowed from the surface materials, a coarse lag deposit a few grains left on the surface protecting the material beneath. If this was removed then further erosion of fine grains will occur.

Walsh (1989) reported that if a beach was artificially protected by adding a material that increased the grading, the beach is more susceptible to erosion since the permeability was decreased. The new combined material would be moved more aggressively offshore and the breaking point may move further onshore if enough material was moved offshore.

Dalrymple (1992) used regular waves in a large-scale flume to study the response of sand beaches. His study concluded that there were two types of beach profiles: storm or barred ones and normal or non-barred ones. By combining two dimensionless parameters he formed the profile parameter, P defined in terms of deep-water wave characteristics as

$$P = \frac{gH_0^2}{w_s^3 T} \tag{2.33}$$

Where,

g = gravitational acceleration

H_0 = deep water wave height

w_s = sediment fall velocity

T= wave period

If the profile parameter exceeded 10,400, then the beach was barred; for small values of P, the beach profile was normal.

Years of observations have led geologists and coastal engineers to develop some guidelines that define beach response to its environment. Some of these rules include:

- Fine grained sediments form shallow sloped beaches while coarser grains form steeper slopes when attacked by the same waves,
- Larger waves result in shallower slopes (erosive or 'storm' profiles) while smaller waves cause beaches to steepen.
- Decreasing wave height was associated with a coarsening of the beach sediments and conversely increasing wave heights were followed by a fining of the foreshore.
- There is a continuous sequence of breaking wave types, and the type is a function of the deep water wave steepness and beach slope.

2.5 Summary

Sediment is transported by flowing water and the determination of the sediment flux is a function of water and sediment properties. The main properties needed to estimate the sediment flux are related to the sediment mixture (grain size distribution, porosity, sediment concentration) and to the flow variables (the velocity profile, bed shear stress, shear velocity, stream power). In morphodynamics, channel bed change due to erosion or deposition is considered jointly with its effect on flow dynamics.

From the previous studies conducted by different researchers, it has been found that the sediment size taken into consideration was different in different studies. The size selection was dominated by the representative sediment size of that respective country's beach materials. In Bangladesh some studies have been conducted to identify the sediment size of the beach materials. But study regarding the cross-shore sediment transport with the representative materials has not been conducted yet. Therefore, in this study a very simplified laboratory study has been conducted with non-breaking wave parameter on a constant slope of 1:15. Though the beach slopes of Bangladesh is much milder than this laboratory setup, but the study will enhance the knowledge to identify the mechanism and the physics of sediment transport.

CHAPTER 3

Theoretical Background

3.1 General

Knowledge on waves and wave generated forces are essential for the design of coastal projects since they are the major factor that determines the geometry of beaches, the planning and design of marinas, waterways, shore protection measures, hydraulic structures and other civil and military coastal works. Estimates of wave conditions are needed in almost all coastal engineering studies. In this chapter the detailed parameters of wave and wave related cross-shore sediment transport are discussed.

This chapter also deals with temporally periodic, long-crested, gradually varying progressive waves, propagating over a small bottom slope, which are superimposed on a nearly horizontal mean flow. The main objective was to obtain approximate conservation equations of mass and momentum describing the physical process involved. These equations were time averaged and depth integrated form. The purpose of time averaging was to remove temporal fluctuations due to waves. The resultant velocity was considered as the sum of a time dependent mean flow, a wave induced flow and an arbitrarily fluctuating component. After the derivation of the equations of mass and momentum, the approximate forms of the forcing terms found in the momentum equations have been discussed. The discussed terms are radiation stresses, surface stress, bottom stress and lateral mixing.

3.2 Wave

A wave is the common terms for any periodic fluctuation in water height, velocity or pressure. The effect of water waves are of paramount importance in the field of coastal structures specially embankment and others. Surface waves normally derive their energy from the winds. Waves have potential energy in the form of their surface displacement and kinetic energy in the motion of the water particles. Waves transmit

this energy as they propagate. There has been a relatively small mass transport in the direction of wave propagation (SPM, 1984). When directly being generated and affected by the local winds, a wind wave system has been termed as a wind sea. Wind waves in the ocean are called ocean surface waves.

Waves are characterized by:

- wave height (H)
- wave length (L)
- wave period (T)

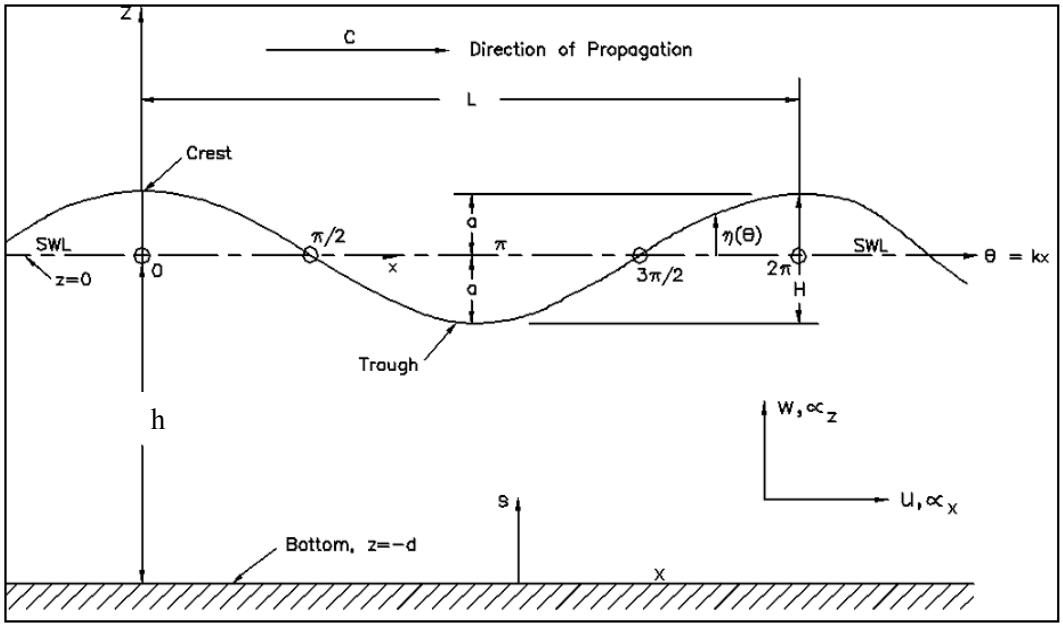

Figure 3.2.1: Definition sketch of wave (Source: CEM part II, 2006)

Wave height (H) is the vertical distance from the crest of a wave (the highest position of a wave) to the trough of the wave (the lowest position of the wave). For a given wind speed, many different wave lengths are produced and for each wave length many different wave heights are developed. The general relationship is that higher waves tend to have longer wave length (lower frequencies).

Wave length (L) is the horizontal distance from one wave crest to the next wave crest or the distance from one wave trough to the next wave trough. Although difficult to measure at sea, this parameter may be measured on aerial photograph.

Wave period (T) is the time, usually measured in seconds, that it takes for a complete wave cycle (crest to crest or trough to trough) to pass a given fixed point. It depends upon the speed of movement of the wave across the surface. It is the one characteristics of a wave that remains constant at all times, no matter what changes occur in height or length.

Other wave parameters include $\omega = 2\pi/T$ which is the angular or radian frequency, the wave number $k = 2\pi/L$, the phase velocity or wave celerity $C = L/T = \omega/k$, the wave steepness $\varepsilon = H/L$, the relative depth h/L and the relative wave height H/h. These are the most common parameters encountered in coastal practice. Wave motion can be defined in terms of dimensionless parameters such as H/L, H/h and h/L. The dimensionless parameters k_a and k_d (CEM 2006) preferred in research works, can be substituted for H/L and h/L, respectively, since these differ only by a constant factor 2π from those preferred by engineers. The speed at which a wave form propagates is termed the phase velocity or wave celerity C. Since the distance traveled by a wave during one wave period is equal to one wavelength, wave celerity can be related to the wave period and length by

$$C = \frac{L}{T} \tag{3.1}$$

An expression relating wave celerity to wavelength and water depth can be given as

$$C = \sqrt{\frac{gL}{2\pi} tanh\left(\frac{2\pi h}{L}\right)} \tag{3.2}$$

The equation below is termed as dispersion relation since it has been indicated that waves with different periods travel at different speeds. For a situation where more than one wave is present, the longer period wave will travel faster.

$$C = \frac{gT}{2\pi} tanh\left(\frac{2\pi h}{L}\right) \tag{3.3}$$

From Equation 3.2 and 3.3 an expression for wavelength as a function of depth and wave period may be obtained as

$$L = \frac{gT^2}{2\pi} tanh\left(\frac{2\pi h}{L}\right) = \frac{gT}{2\pi} tanh(kh) \tag{3.4}$$

To use Eq. 3.4 there involves some difficulty since the unknown L appears on both sides of the equation. Tabulated values of d/L and d/L_0 (SPM 1984) where L_0 is the deepwater wavelength may be used to simplify the solution of this Equation.

$$L_0 = \frac{gT^2}{2\pi} \tag{3.5}$$

Five factors influence the formation of wave:

- wind speed
- distance of open water that the wind has blown over (called the fetch)
- width of area effected by fetch
- time duration the wind has blown over a given area
- water depth

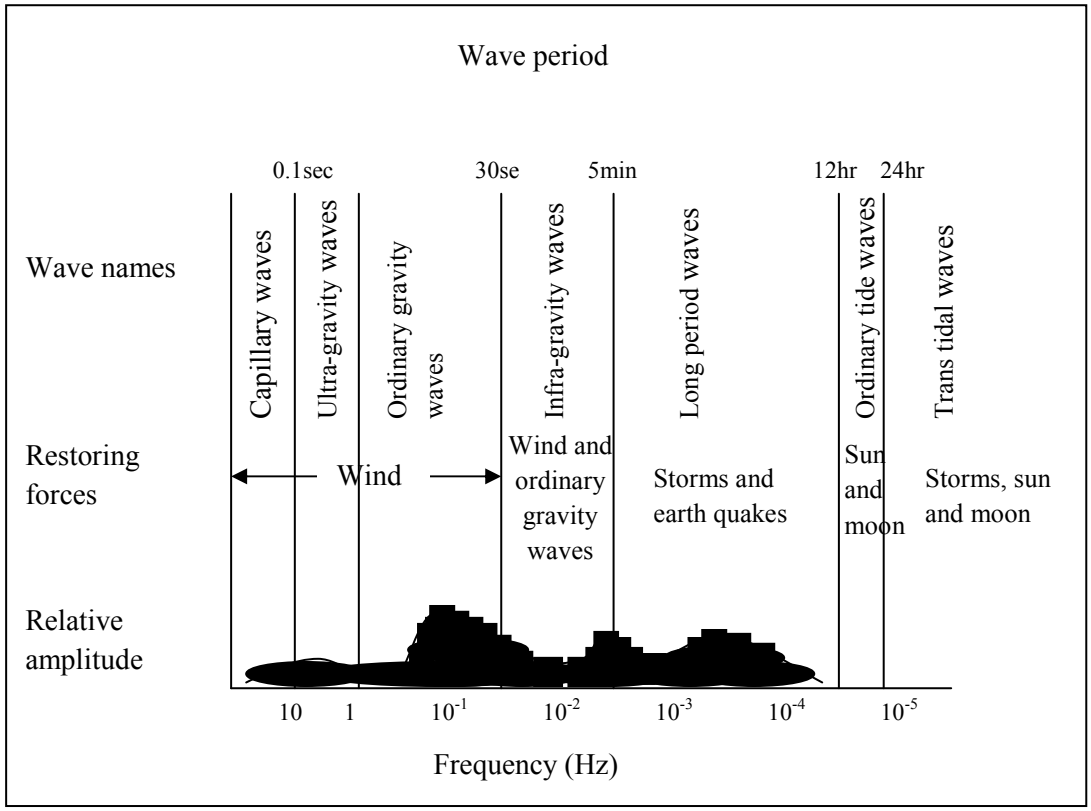

Figure 3.2.2: Classification of ocean waves according to wave period (Source: Munk, 1951).

Waves are classified in various ways. Ocean waves have a very wide range of periods. The energy of waves of fixed period is proportional to Hz, as shown in the Fig. 3.2.2. This diagram was originally drawn by Munk in 1951 which displays the predominant types of waves in the ocean, the names of the various waves for each period range, and the agents generating these waves. The Figure 3.2.2 shows that waves of the greatest energy concentration are wind waves. Wind waves are generated and developed by wind action stated above and their wave period is normally less than 10 to 15 sec, while heights of as much as 34 m have been reported. Swells consist of wind-generated waves that have traveled out of their generating area.

Wind waves are mechanical waves that propagate along the interface between water and air. The restoring force is provided by gravity, and so they are often referred to as surface gravity waves. As the wind blows, pressure and friction forces perturb the equilibrium of the water surface. These forces transfer energy from the air to the water and the waves are formed. Water waves are considered oscillatory or nearly oscillatory if the motion described by the water particles is circular orbits that are closed or nearly closed for each wave period. The linear theory represents pure oscillatory waves. Waves defined by finite-amplitude wave theories are not pure oscillatory waves (CEM, 2006), but still periodic since the fluid is moved in the direction of wave advance by each successive wave. This motion is termed mass transport of the waves. When water particles advance with the wave and do not return to their original position, the wave is called a wave of translation. A solitary wave is an example of a wave of translation.

3.2.1 Breaking and non-breaking wave

Wave height is limited by both depth and wavelength. For a given water depth and wave period, there is a maximum height limit above which the wave becomes unstable and breaks. The breaking wave height in deep water is a function of the wavelength. In shallow and transitional water it is a function of both depth and wavelength. Wave breaking is a complex phenomenon and it is one of the areas in wave mechanics that has been investigated extensively both experimentally and

numerically (CEM, 2006). As a solitary wave moves into shoaling water it eventually becomes unstable and breaks. A solitary wave breaks when the water particle velocity at the wave crest becomes equal to the wave celerity. According to Miles (1980, 1981), this occurs when

$$\left(\frac{H}{h}\right)_{max} = 0.78 \tag{3.6}$$

Laboratory studies have shown that the value of $(H/h)_{max} = 0.78$ agrees better with observations for oscillatory waves than for solitary waves and that the near-shore slope has a substantial effect on this ratios (SPM, 1984). Other factors such as bottom roughness may also be involved. Tests of periodic waves with periods from 1 to 6 sec on slopes m = 0.0, 0.05, 0.10, and 0.20 have shown (SPM, 1984) that H_b/h_b ratios are approximately equal to 0.83, 1.05, 1.19, and 1.32, respectively. Tests of single solitary waves on slopes from m = 0.01 to m = 0.20 (SPM, 1984) indicate an empirical relationship between the slope and the breaker height to water depth ratio given by

$$\frac{H_b}{h_b} = 0.75 + 25m - 112m^2 + 3780m^3 \tag{3.7}$$

Researchers have made some progress over the last three decades in the numerical modeling of waves close to breaking. Studies suggests that the limiting wave steepness to be H/L = 0.141 in deep water and H/h = 0.83 for solitary waves in shallow water with a corresponding solitary wave celerity of $c/(gh)^{1/2} = 1.29$ for wave breaking (CEM, 2006).

3.3 Basic Equation of Wave Motion

The basic equation of wave motion has been developed by assuming that a propagating wave propagates in water with uniform depth *h* in the direction of x-axis and y-axis is vertically upward (Fig. 3.2.1). The waves have been considered to be generated by a certain action from the still water state and fluid viscosity has been

ignored to develop the formula. The velocity potential $\emptyset$ is defined with the velocity component *u* and *v* in x and y direction respectively.

$$u = \frac{\partial \emptyset}{\partial x}, \qquad v = \frac{\partial \emptyset}{\partial y} \tag{3.8}$$

Water has been considered as an incompressible fluid, hence the continuity equation becomes

$$\frac{\partial u}{\partial x} + \frac{\partial v}{\partial y} = 0 \tag{3.9}$$

Combining Eq. 3.8 and 3.9

$$\frac{\partial^2 \emptyset}{\partial x^2} + \frac{\partial^2 \emptyset}{\partial y^2} = 0 \tag{3.10}$$

This equation has been satisfied in the region $-h \leq y \leq \eta, -\infty < x < \infty$, where η the water surface elevation measured above the still water level. The boundary condition on the impermeable sea bottom can be expressed as:

$$(v)_{y=-h} = \left(\frac{\partial \emptyset}{\partial y}\right)_{y=-h} = 0 \tag{3.11}$$

Hence, the vertical velocity component at the sea bottom is zero. By considering the integral form of the equation of motion for an irrotational fluid the pressure equation can be expressed as:

$$\frac{\partial \emptyset}{\partial t} + \frac{1}{2}\left[\left(\frac{\partial \emptyset}{\partial x}\right)^2 + \left(\frac{\partial \emptyset}{\partial y}\right)^2\right] + \frac{P}{\rho} + gy = 0 \tag{3.12}$$

Taking P_0 as the pressure at the free surface $y = \eta$ Eq. 3.12 becomes

$$\left(\frac{\partial \emptyset}{\partial t}\right)_{y=\eta} + \frac{1}{2}\left[\left(\frac{\partial \emptyset}{\partial x}\right)^2 + \left(\frac{\partial \emptyset}{\partial y}\right)^2\right]_{y=\eta} + \frac{P_0}{\rho} + gy = 0 \tag{3.13}$$

This is a boundary condition at the free surface. When the free surface is expressed by the equation $F(x, y, z, t) = 0$ the boundary condition is in general given by *DF/Dt* =0,

where $\frac{D}{Dt} = \frac{\partial}{\partial t} + \frac{u\partial}{\partial x} + \frac{v\partial}{\partial y} + \frac{w\partial}{\partial z}$ an operator. Here, the function *F* is dependent on *z* and given by $F(x, y, z, t) = \eta(x, t) - y = 0$.

Therefore,

$$\left(\frac{DF}{Dt}\right)_{y=\eta} = \left(\frac{\partial \eta}{\partial t} + u\frac{\partial}{\partial x} - v\right)_{y=\eta} = 0 \tag{3.14}$$

Or,

$$\frac{\partial \eta}{\partial t} + \frac{\partial \eta}{\partial x}\left(\frac{\partial \phi}{\partial x}\right)_{y=\eta} = \left(\frac{\partial \phi}{\partial y}\right)_{y=\eta} \tag{3.15}$$

This condition indicates that a water particle on the free surface should always remain in the future stage.

3.3.1 Small Amplitude Wave Theory

In linear wave theories, the free surface boundary conditions are linearized on the assumption that the wave amplitude is small in comparison with the wave length. Among various waves, progressive waves in water of uniform depth are of fundamental importance. These waves propagate without deformation and the surface profile as well as the variation of the water particle velocity is sinusoidal. The boundary condition at the free surface for Eq. 3.13 and 3.15 are non-linear. So, the fundamental assumptions underlying this equation to form it a linear equation are:

- The fluid is homogeneous and incompressible; therefore, the density ρ is a constant.
- Surface tension can be neglected.
- Coriolis effect due to the earth's rotation can be neglected.
- Pressure at the free surface is uniform and constant.
- The fluid is ideal or inviscid (lacks viscosity).
- The particular wave being considered does not interact with any other water motions. The flow is irrotational so that water particles do not rotate (only normal forces are important and shearing forces are negligible).

- The bed is a horizontal, fixed, impermeable boundary, which implies that the vertical velocity at the bed is zero.
- The wave amplitude is small and the waveform is invariant in time and space.
- Waves are plane or long-crested (two-dimensional).

Therefore, in order to eliminate the non-linearity only waves with very small wave heights has been considered. This is called the small amplitude wave theory or linear wave theory. So, the basic equation of waves can be expressed as:

$$\frac{\partial^2 \emptyset}{\partial x^2} + \frac{\partial^2 \emptyset}{\partial y^2} = 0 - h \leq y \leq \eta, -\infty < x < \infty \tag{3.16}$$

$$\left(\frac{\partial \phi}{\partial y}\right)_{y=-h} = 0 \tag{3.17}$$

$$\left(\frac{\partial \phi}{\partial t}\right)_{y=0} + g\eta = 0 \tag{3.18}$$

$$\frac{\partial \phi}{\partial t} = \left(\frac{\partial \phi}{\partial y}\right)_{y=0} \tag{3.19}$$

3.4 Boundary Conditions for model development

Wave motion is a boundary-value problem and its solution requires specifying realistic boundary conditions. These boundary conditions are usually imposed at the free surface and sea bottom. Since the seabed is often impermeable, flow rate through the sea bottom must be zero. Therefore, the bottom boundary condition (BBC) may be stated in terms of ϕ as $\phi(x, -h)$ at $z = -h$.

Two boundary conditions, kinematic and dynamic, are needed at the free surface. The kinematic condition states that water particles on the free surface remain there and consequently flow rate through the surface boundary must be zero. The net flow Q between the sea surface and seabed may be specified as $\phi(x, \eta)$ at $z = \eta$. The dynamic free-surface boundary condition is an expression to specify the pressure at the free surface which is termed as atmospheric pressure.

In determining the two-dimensional integrated conservation of mass and momentum equations the kinematic boundary conditions are required. For the free surface boundary condition (FSBC) equivalence is required between the vertical velocity at the free surface and the total rate of change of the instantaneous water surface elevation, η (Fig. 3.2.1). Hence, the expression can be arranged as:

$$w_\eta = \frac{\delta\eta}{\delta t} + u_\eta \frac{\delta\eta}{\delta x} + v_\eta \frac{\delta\eta}{\delta y} \tag{3.20}$$

The expression for the bottom boundary condition can be written as:

$$\frac{\delta\eta}{\delta t} + u_{-h} \frac{\delta h}{\delta x} + v_{-h} \frac{\delta h}{\delta y} + w_{-h} = 0 \tag{3.21}$$

The subscript η and –h represents the location of a specific quantity at the free surface or at the bottom respectively. The velocity components in the x, y and z directions are u, v and w respectively.

3.5 Equation for Calculating Wave Height and Wave Length

It is desirable to know how fast wave energy is moving. One way to determine this is to look at the speed of wave groups that represents propagation of wave energy in space and time. The speed a group of waves or a wave train travels is generally not identical to the speed with which individual waves within the group travel. The group speed is termed the group velocity C_g. The individual wave speed is the phase velocity or wave celerity. The wave celerity is calculated by using Eq. 3.2 and 3.3. Where, unknown parameter is the shallow water wave length and it is calculated by the trial and error method using Eq. 3.4. Finally the group velocity is calculated by using the following formula:

$$C_g = \frac{1}{2}\frac{L}{T}\left[1 + \frac{\frac{4\pi h}{L}}{sinh\left(\frac{4\pi h}{L}\right)}\right] \tag{3.22}$$

For calculating the wave height at different position the wave angles at those positions are calculated first with the following equation:

$$cos\theta_1 = \cos(\pi - \theta) \tag{3.23}$$

Where, θ and θ_1 the initial and location angle of wave at the point of interest respectively in radian. By using this value the coefficient K_r and K_s can be calculated as:

$$K_r = (cos\theta_0/cos\theta_1) \text{ and } K_s = \left(C_{g0}/C_{g1}\right) \tag{3.24}$$

From Eq. 3.24 using the values of coefficients the Wave Height at different locations are calculated.

$$H_s = \mathrm{H} * K_r * K_s \tag{3.25}$$

Where, H is the initial deep water wave height.

3.6 Equation of Conservation of Mass

The net mass of fluid flowing across the boundaries into a small element in a certain time Δt be equal to the amount by which the mass of the element has increased in the same time interval Δt (Ippen, 1966). The general form of the three dimensional conservation of mass equation for incompressible fluid is:

$$\frac{\delta\rho}{\delta t} + \frac{\delta(\rho u)}{\delta x} + \frac{\delta(\rho v)}{\delta y} + \frac{\delta(\rho w)}{\delta z} = 0 \tag{3.26}$$

ρ is the density of the fluid. Integrating over the depth and using Leibnitz Rule Eq. 3.26 becomes:

$$\begin{aligned}\frac{\delta}{\delta t}\int_{-h}^{\eta}\rho dz - \rho_\eta\frac{\delta\eta}{\delta t} + \rho_{-h}\frac{\delta(-h)}{\delta t} + \frac{\delta}{\delta x}\int_{-h}^{\eta}\rho u dz - \rho_\eta u_\eta\frac{\delta\eta}{\delta x} + \rho_{-h}u_{-h}\frac{\delta(-h)}{\delta x} \\ + \frac{\delta}{\delta y}\int_{-h}^{\eta}\rho v dz - \rho_\eta v_\eta\frac{\delta\eta}{\delta y} + \rho_{-h}v_{-h}\frac{\delta(-h)}{\delta y} - \rho_\eta w_\eta \\ - \rho_{-h}w_{-h} = 0\end{aligned} \tag{3.27}$$

Using the FSBC and BBC Eq. 3.20, 3.21 and 3.23 can be simplified as:

$$\frac{\delta}{\delta t}\int_{-h}^{\eta}\rho dz+\frac{\delta}{\delta x}\int_{-h}^{\eta}\rho u dz+\frac{\delta}{\delta y}\int_{-h}^{\eta}\rho v dz=0 \tag{3.28}$$

If the velocities u and v consist of a time independent mean flow $(\bar{U},\bar{V})$ a wave induced flow $(\hat{u},\hat{v})$ and an arbitrarily fluctuating component (u',v') respectively then the velocity term can be expressed by:

$$u=\bar{U}+\hat{u}+u'$$
$$v=\bar{V}+\hat{v}+v'$$

Substituting u and v in Eq. 3.24 it gives:

$$\frac{\delta}{\delta t}\int_{-h}^{\eta}\rho dz+\frac{\delta}{\delta x}\int_{-h}^{\eta}\rho\bar{U}dz+\frac{\delta}{\delta y}\int_{-h}^{\eta}\rho\bar{V}dz+\frac{\delta}{\delta x}\int_{-h}^{\eta}\rho\hat{u}dz + \frac{\delta}{\delta y}\int_{-h}^{\eta}\rho\hat{v}dz+\frac{\delta}{\delta x}\int_{-h}^{\eta}\rho u'dz+\frac{\delta}{\delta y}\int_{-h}^{\eta}\rho v'dz=0 \tag{3.29}$$

The time average of a function is defined by:

$F=\frac{1}{T}\int_0^T Fdt$ (F is the functional form of any differential equations)

Where, T is wave period. If the Eq. 3.29 is time averaged and integration is performed modify the equation, it becomes:

$$\frac{\delta}{\delta t}\{\rho(h+\bar{\eta})\}+\frac{\delta}{\delta x}\{\rho\bar{U}(h+\bar{\eta})\}+\frac{\delta}{\delta y}\{\rho\bar{V}(h+\bar{\eta})\}+\frac{\delta}{\delta x}\overline{\int_{-h}^{\eta}\rho\hat{u}dz} + \frac{\delta}{\delta y}\overline{\int_{-h}^{\eta}\rho\hat{v}dz}+\frac{\delta}{\delta x}\overline{\int_{-h}^{\eta}\rho u'dz}+\frac{\delta}{\delta y}\overline{\int_{-h}^{\eta}\rho v'dz}=0 \tag{3.30}$$

Where, $\bar{\eta}$ time independent mean free surface displacement. The turbulence fluctuations u' and v' are of very high frequency and by definition their averages are identically zero. Then:

$$\frac{1}{T}\int_0^T u'dt\equiv 0$$

$$\frac{1}{T}\int_0^{-T} v'dt \equiv 0$$

Using the above identities Eq. 3.26 becomes:

$$\frac{\delta}{\delta t}\{\rho(h+\bar{\eta})\} + \frac{\delta}{\delta x}\{\rho\bar{U}(h+\bar{\eta})\} + \frac{\delta}{\delta y}\{\rho\bar{V}(h+\bar{\eta})\} + \frac{\delta}{\delta x}\overline{\int_{-h}^{\eta}\rho\hat{u}dz} + \frac{\delta}{\delta y}\overline{\int_{-h}^{\eta}\rho\hat{v}dz} = 0 \tag{3.31}$$

It is seen that the time average of the vertically integrated wave induced velocities in $\hat{u}$ and $\hat{v}$ are not zero. Defining:

$$u \equiv \bar{U} + \tilde{u} \tag{3.32}$$

$$v \equiv \bar{V} + \tilde{v}$$

Then

$$\tilde{u} = \frac{\overline{\int_{-h}^{\eta}\rho\hat{u}dz}}{\rho(h+\bar{\eta})}$$

$$\tilde{v} = \frac{\overline{\int_{-h}^{\eta}\rho\hat{v}dz}}{\rho(h+\bar{\eta})} \tag{3.33}$$

Are the mass transport velocities. The total depth of water is found to be:

$$D \equiv h + \bar{\eta}$$

Substituting the above definitions in Eq. 3.31 and assuming that the location of the bottom is constant with time and that the density is constant in space and time:

$$\frac{\delta\bar{\eta}}{\delta t} + \frac{\delta}{\delta x}(uD) + \frac{\delta}{\delta y}(vD) = 0 \tag{3.34}$$

3.7 Equation of Conservation of Momentum

The equations of horizontal motion with the assumption that the fluid is inviscid, incompressible and internally source-free fluid, becomes a well known equation when the rotation of the earth is neglected is called Navier-Stokes equation.

In the x-direction

$$\frac{\delta u}{\delta t}+\frac{\delta u^2}{\delta x}+\frac{\delta uv}{\delta z}+\frac{\delta uw}{\delta z}=-\frac{1}{\rho}\frac{\delta P}{\delta x}+\frac{1}{\rho}\left(\frac{\delta \tau_{xx}}{\delta x}+\frac{\delta \tau_{yy}}{\delta y}+\frac{\delta \tau_{zz}}{\delta z}\right) \tag{3.35}$$

In the y-direction

$$\frac{\delta v}{\delta t}+\frac{\delta uv}{\delta x}+\frac{\delta v^2}{\delta y}+\frac{\delta uw}{\delta z}=-\frac{1}{\rho}\frac{\delta P}{\delta y}+\frac{1}{\rho}\left(\frac{\delta \tau_{xy}}{\delta x}+\frac{\delta \tau_{yy}}{\delta y}+\frac{\delta \tau_{zy}}{\delta z}\right) \tag{3.36}$$

Where, P is the absolute pressure and $\tau_{xx}, \tau_{xy}, \tau_{yx}, \tau_{yy}, \tau_{zx}, \tau_{zy}$ are directional stresses. Integrating these two equations over depth and time averaging over a wave period, the x-direction solution is given as follows with y-direction solution being of the same form. Integrating over depth and using Leibnitz Rule, the left hand side (LHS) term is given by:

$$\int_{-h}^{\eta}\frac{\delta u}{\delta t}dz=\frac{\delta}{\delta t}\int_{-h}^{\eta}udz-u_\eta\frac{\delta \eta}{\delta t}+u_{-h}\frac{\delta(-h)}{\delta t}$$

$$\int_{-h}^{\eta}\frac{\delta u^2}{\delta t}dz=\frac{\delta}{\delta x}\int_{-h}^{\eta}u^2dz-{u_\eta}^2\frac{\delta \eta}{\delta x}+{u_{-h}}^2\frac{\delta(-h)}{\delta x}$$

$$\int_{-h}^{\eta}\frac{\delta uv}{\delta y}dz=\frac{\delta}{\delta y}\int_{-h}^{\eta}uvdz-u_\eta v_\eta\frac{\delta \eta}{\delta y}+u_{-h}v_{-h}\frac{\delta(-h)}{\delta y}$$

$$\int_{-h}^{\eta}\frac{\delta uw}{\delta z}dz=u_\eta w_\eta-u_{-h}w_{-h}$$

Adding the above terms and rearranging the LHS becomes:

$$\frac{\delta}{\delta t}\int_{-h}^{\eta}udz+\frac{\delta}{\delta x}\int_{-h}^{\eta}u^2dz+\frac{\delta}{\delta y}\int_{-h}^{\eta}uvdz-u_\eta\left(\frac{\delta \eta}{\delta t}+u_\eta\frac{\delta \eta}{\delta x}+v_\eta\frac{\delta \eta}{\delta y}-w_\eta\right)$$
$$-u_{-h}\left(\frac{\delta h}{\delta t}+u_{-h}\frac{\delta h}{\delta x}+v_{-h}\frac{\delta h}{\delta y}+w_{-h}\right)$$

After using the kinematic boundary conditions these two equations become:

$$\frac{\delta}{\delta t}\int_{-h}^{\eta}udz+\frac{\delta}{\delta x}\int_{-h}^{\eta}u^2dz+\frac{\delta}{\delta y}\int_{-h}^{\eta}uvdz$$

Substituting the total velocities u and v by their components and averaging over a wave period, the LHS becomes term by term:

$$\frac{\delta}{\delta t}\overline{\int_{-h}^{\eta} u dz} = \frac{\delta}{\delta t}\overline{\int_{-h}^{\eta} \bar{U} dz} + \frac{\delta}{\delta t}\overline{\int_{-h}^{\eta} \hat{u} dz} + \frac{\delta}{\delta t}\overline{\int_{-h}^{\eta} u' dz}$$

$$\frac{\delta}{\delta x}\overline{\int_{-h}^{\eta} u^2 dz} = \frac{\delta}{\delta x}\overline{\int_{-h}^{\eta} \bar{U}^2 dz} + \frac{\delta}{\delta x}\overline{\int_{-h}^{\eta} \hat{u}^2 dz} + \frac{\delta}{\delta x}\overline{\int_{-h}^{\eta} u'^2 dz} + \frac{\delta}{\delta x}\overline{\int_{-h}^{\eta} 2\bar{U}\hat{u} dz}$$
$$+ \frac{\delta}{\delta x}\overline{\int_{-h}^{\eta} 2\bar{U}u' dz} + \frac{\delta}{\delta x}\overline{\int_{-h}^{\eta} 2\hat{u}u' dz}$$

$$\frac{\delta}{\delta y}\overline{\int_{-h}^{\eta} uv dz} = \frac{\delta}{\delta y}\overline{\int_{-h}^{\eta} \bar{U}\bar{V} dz} + \frac{\delta}{\delta y}\overline{\int_{-h}^{\eta} \bar{U}\hat{v} dz} + \frac{\delta}{\delta y}\overline{\int_{-h}^{\eta} \bar{U}u' dz}$$
$$+ \frac{\delta}{\delta y}\overline{\int_{-h}^{\eta} \hat{u}\bar{V} dz} + \frac{\delta}{\delta y}\overline{\int_{-h}^{\eta} \hat{u}\hat{v} dz} + \frac{\delta}{\delta y}\overline{\int_{-h}^{\eta} \hat{u}v' dz}$$
$$+ \frac{\delta}{\delta y}\overline{\int_{-h}^{\eta} u'\bar{V} dz} + \frac{\delta}{\delta y}\overline{\int_{-h}^{\eta} u'\hat{v} dz} + \frac{\delta}{\delta y}\overline{\int_{-h}^{\eta} u'v' dz}$$

The wave induced velocity is essentially constant relative to the turbulent fluctuations since the frequency of this later is much greater than the wave frequency. Therefore, integrals involving products of a turbulent component and a wave induced component are zero in the time average. Making use of this result and the fact that the time average of the turbulent component is identically zero, each term of the LHS reduces to:

$$\frac{\delta}{\delta t}\overline{\int_{-h}^{\eta} u dz} = \frac{\delta}{\delta t}\overline{\int_{-h}^{\eta} \bar{U} dz} + \frac{\delta}{\delta t}\overline{\int_{-h}^{\eta} \hat{u} dz}$$

$$\frac{\delta}{\delta x}\overline{\int_{-h}^{\eta} u^2 dz} = \frac{\delta}{\delta x}\overline{\int_{-h}^{\eta} \bar{U}^2 dz} + \frac{\delta}{\delta x}\overline{\int_{-h}^{\eta} \hat{u}^2 dz} + \frac{\delta}{\delta x}\overline{\int_{-h}^{\eta} u'^2 dz} + \frac{\delta}{\delta x}\overline{\int_{-h}^{\eta} 2\bar{U}\hat{u} dz}$$

$$\frac{\delta}{\delta y}\overline{\int_{-h}^{\eta} uv dz} = \frac{\delta}{\delta y}\overline{\int_{-h}^{\eta} \bar{U}\bar{V} dz} + \frac{\delta}{\delta y}\overline{\int_{-h}^{\eta} \bar{U}\hat{v} dz} + + \frac{\delta}{\delta y}\overline{\int_{-h}^{\eta} \hat{u}\bar{V} dz}$$
$$+ \frac{\delta}{\delta y}\overline{\int_{-h}^{\eta} \hat{u}\hat{v} dz} + + \frac{\delta}{\delta y}\overline{\int_{-h}^{\eta} u'v' dz}$$

Assuming that the density is constant in space and time and integrating over the depth, the right hand side (RHS) of Eq. 3.35 becomes:

$$-\frac{1}{\rho}\int_{-h}^{\eta} \frac{\delta P}{\delta x} dz + \frac{1}{\rho}\int_{-h}^{\eta} \frac{\delta \tau_{xx}}{\delta x} dz + \frac{1}{\rho}\int_{-h}^{\eta} \frac{\delta \tau_{yx}}{\delta y} dz + \frac{1}{\rho}\int_{-h}^{\eta} \frac{\delta \tau_{zx}}{\delta z} dz$$

Also assuming an inviscid fluid such that no horizontal viscous stress exists, then τ_{xx} and τ_{yx} become zero. The RHS simplifies to:

$$-\frac{1}{\rho}\int_{-h}^{\eta}\frac{\delta P}{\delta x}dz+\frac{1}{\rho}\int_{-h}^{\eta}\frac{\delta \tau_{zx}}{\delta z}dz$$

Time averaging the above terms, expanding the pressure by the use of Leibnitz Rule and performing the integration of the last term, the RHS becomes

$$\frac{1}{\rho}\frac{\delta}{\delta x}\int_{-h}^{\eta}Pdz+\frac{1}{\rho}\overline{P_{\eta}\frac{\delta \eta}{\delta x}}+\frac{1}{\rho}\overline{P_{-h}\frac{\delta h}{\delta x}}+\frac{1}{\rho}\overline{\tau_{zx_{\eta}}}-\frac{1}{\rho}\overline{\tau_{zx_{-h}}}$$

Assuming now that the pressure at the free surface P_{η} is zero and realizing that $\overline{\tau_{zx_{\eta}}}$ and $\overline{\tau_{zx_{-h}}}$ are respectively, the time averaged surface and bottom shear stresses, the RHS can be rewriting as:

$$-\frac{1}{\rho}\frac{\delta}{\delta x}\int_{-h}^{\eta}Pdz+\frac{1}{\rho}\overline{P_{-h}}\frac{\delta h}{\delta x}+\frac{1}{\rho}\overline{P_{-h}\frac{\delta h}{\delta x}}+\frac{1}{\rho}\overline{\tau_{sx}}-\frac{1}{\rho}\overline{\tau_{bx}}$$

At the bottom, the mean pressure can be defined as the sum of the dynamic pressure and the hydrostatic pressure:

$$\overline{P_{-h}}=\overline{P_{dyn_{-h}}}+\rho g(h+\bar{\eta})$$

Substituting this expression in $\overline{P_{-h}}\frac{\delta h}{\delta x}$ it comes

$$\overline{P_{-h}}\frac{\delta h}{\delta x}=\overline{P_{dyn_{-h}}}\frac{\delta h}{\delta x}+\rho g(h+\bar{\eta})\frac{\delta h}{\delta x}$$

Alternatively

$$\frac{1}{\rho}\overline{P_{-h}}\frac{\delta h}{\delta x}=\frac{1}{\rho}\overline{P_{dyn_{-h}}}\frac{\delta h}{\delta x}+\frac{1}{2}\frac{\delta}{\delta x}\{g(h+\bar{\eta})^2\}-g(h+\bar{\eta})\frac{\delta \bar{\eta}}{\delta x}$$

After using this result, the RHS is:

$$-\frac{1}{\rho}\frac{\delta}{\delta x}\overline{\int_{-h}^{\eta} P dz} + \frac{1}{\rho}\overline{P_{dyn}}_{-h}\frac{\delta h}{\delta x} + \frac{1}{2}\frac{\delta}{\delta x}\{g(h+\bar{\eta})^2\} - g(h+\bar{\eta})\frac{\delta\bar{\eta}}{\delta x} + \frac{1}{\rho}\overline{\tau_{sx}} - \frac{1}{\rho}\overline{\tau_{bx}}$$

The time averaged depth integrated x-momentum equation is give by

$$\begin{aligned}
&\frac{\delta}{\delta t}\left\{\bar{U}(h+\bar{\eta}) + \overline{\int_{-h}^{\eta}\hat{u}dz}\right\} \\
&\quad + \frac{\delta}{\delta x}\left\{\bar{U}^2(h+\bar{\eta}) + 2\bar{U}\overline{\int_{-h}^{\eta}\hat{u}dz} + \overline{\int_{-h}^{\eta}\hat{u}^2dz} + \frac{1}{\rho}\overline{\int_{-h}^{\eta}Pdz}\right. \\
&\quad \left. - \frac{1}{2}g(h+\bar{\eta})^2\right\} \\
&\quad + \frac{\delta}{\delta y}\left\{\bar{U}\bar{V}(h+\bar{\eta}) + \bar{U}\overline{\int_{-h}^{\eta}\hat{v}dz} + \bar{V}\overline{\int_{-h}^{\eta}\hat{u}dz} + \int_{-h}^{\eta}\hat{u}\hat{v}dz\right\} \\
&\quad = \frac{1}{\rho}\overline{P_{dyn}}_{-h}\frac{\delta h}{\delta x} - g(h+\bar{\eta})\frac{\delta\bar{\eta}}{\delta x} + \frac{1}{\rho}\overline{\tau_{sx}} - \frac{1}{\rho}\overline{\tau_{bx}} \\
&\quad - \frac{\delta}{\delta x}\overline{\int_{-h}^{\eta}u'^2dz} - \frac{\delta}{\delta y}\overline{\int_{-h}^{\eta}u'v'dz}
\end{aligned} \tag{3.37}$$

The radiation stresses the moment fluxes due to the presence of waves are defined as:

$$S_{xx} \equiv \overline{\int_{-h}^{\eta}(P+\rho\hat{u}^2)dz} + \frac{1}{2}\rho g(h+\bar{\eta})^2 - \frac{1}{\rho(h+\bar{\eta})}\overline{\left\{\int_{-h}^{\eta}\rho\hat{u}dz\right\}^2} \tag{3.38}$$

$$S_{xy} \equiv \overline{\int_{-h}^{\eta}\rho\hat{u}\hat{v}dz} - \frac{1}{\rho(h+\bar{\eta})}\overline{\int_{-h}^{\eta}\rho\,\hat{v}dz}\,\overline{\int_{-h}^{\eta}\rho\,\hat{u}dz} \tag{3.39}$$

$$S_{yy} \equiv \overline{\int_{-h}^{\eta}(P+\rho\hat{v}^2)dz} - \frac{1}{2}\rho g(h+\bar{\eta})^2 - \frac{1}{\rho(h+\bar{\eta})}\overline{\left\{\int_{-h}^{\eta}\rho\hat{v}dz\right\}^2} \tag{3.40}$$

In order to achieve the final x-momentum equation the following further assumptions are also made:

(a) The product of the wave induced pressure at the bottom and the bottom slope is assumed negligible:

$$\left(\frac{1}{\rho}\overline{P_{dyn}}_{-h}\frac{\delta h}{\delta x} \simeq 0\right)$$

(b) The gradient of the pressure due to turbulent fluctuations is neglected:

$$\left(-\frac{\delta}{\delta x}\overline{\int_{-h}^{\eta} u'^2 dz} \simeq 0\right)$$

(c) The lateral friction caused by momentum fluxes due to turbulent fluctuation is assumed to be independent of depth.

This last assumption is not as reasonable as the former two since physical observations reveal the existence of the concentration of turbulence to the upper layer. In the surf zone this is the case of spilling breakers, Huntley (1976).

The lateral friction is defined as $\overline{\tau_l} = -\rho\overline{u'v'}$ and the total depth of water as $D \equiv h + \bar{\eta}$. Using the velocities u and v as defined previously, the final form of the conservation of momentum equation in x-direction is:

$$\frac{\delta}{\delta t}(uD) + \frac{\delta}{\delta x}(u^2 D) + \frac{\delta}{\delta y}(uvD) = -gD\frac{\delta\bar{\eta}}{\delta x} - \frac{1}{\rho}\frac{\delta S_{xx}}{\delta x} - \frac{1}{\rho}\frac{\delta S_{xy}}{\delta x} + \frac{1}{\rho}\overline{\tau_{sx}} - \frac{1}{\rho}\overline{\tau_{bx}} - \frac{D}{\rho}\frac{\delta\overline{\tau_l}}{\delta y} \tag{3.41}$$

Similarly, the final form of the conservation of momentum equation in the y-direction can be found to be:

$$\frac{\delta}{\delta t}(vD) + \frac{\delta}{\delta x}(uvD) + \frac{\delta}{\delta y}(v^2 D) = -gD\frac{\delta\bar{\eta}}{\delta y} - \frac{1}{\rho}\frac{\delta S_{xy}}{\delta x} - \frac{1}{\rho}\frac{\delta S_{yy}}{\delta y} + \frac{1}{\rho}\overline{\tau_{sy}} - \frac{1}{\rho}\overline{\tau_{by}} - \frac{D}{\rho}\frac{\delta\overline{\tau_l}}{\delta x} \tag{3.42}$$

3.8 Equation of Radiation Stress

Longuet-Higgins and Stewart (1966) have shown that the forms of the radiation stress terms S_{xx}, S_{xy} and S_{yy} as defined by Eq. 3.22 to 3.24 can be simplified to the following expressions which are correct to the second order of approximation:

$$S_{xx} = E\left[\left(2n - \frac{1}{2}\right)cos^2\Theta + n\left(n - \frac{1}{2}\right)sin^2\Theta\right] \tag{3.43}$$

$$S_{xy} = E\ n\ cos\Theta\ sin\Theta \tag{3.44}$$

$$S_{yy} = E\left[\left(2n - \frac{1}{2}\right)sin^2\Theta + n\left(n - \frac{1}{2}\right)cos^2\Theta\right] \tag{3.45}$$

Where, Θ wave angle, E the total wave energy and *n* is the ratio of group velocity to wave celerity, with E and n being defined according to linear wave theory as:

$$E = \frac{1}{8}\rho g H^2 \tag{3.46}$$

$$n = \frac{C_g}{C} = \frac{1}{2}\left[1 + \frac{2kh}{\sinh\,(2kh)}\right] \tag{3.47}$$

The wave celerity is given by:

$$C = \left[\frac{g}{\mathrm{k}}\tan\,(kh)\right]^{1/2} \tag{3.48}$$

3.9 Equation of Surface Stress

Von Dorn's method to determine the surface stress due to wind was utilized by Reid and Bodine (1968) and Pearce (1969) and suggested in the shore Protection Manual. This method assumes the wind to be a function of the wind speed such that:

$$\tau_{sx} = \rho K|W|W_x \tag{3.49}$$

$$\tau_{sy} = \rho K|W|W_y \tag{3.50}$$

Where, τ_{sx}, W_x and τ_{sx}, W_y are the mean surface stress term and wind velocity in the x and y directions respectively, ρ is the water density and *w* is the magnitude of the wind speed.

The empirically determined wind stress coefficient K is given by

$$K = K_1 \quad \text{for } W \leq W_{cr} \qquad (3.51)$$
$$K = K_1 + K_2\left(1 - \frac{W_{cr}}{W}\right) \quad \text{for } W \geq W_{cr}$$

W_{cr} is a critical wind speed taken as 14 knots (7.19 m/sec) and the coefficients K_1 and K_2 are taken as 1.1×10^{-6} and 2.5×10^{-6} respectively.

3.10 Equation of Bottom Stress

Longuet-Higgins (1970a) assumed that the bottom friction stress due to waves and currents would be adequately represented by Chezy Law:

$$\tau_b = \rho C_f |u_t| u_t \qquad (3.52)$$

Where, C_f is a friction coefficient dependent on the type of bottom and u_t is the instantaneous total velocity vector near bottom.

For the case of near-normal incident waves on a plane beach Longuet-Higgins arrived at the following time-averaged bottom stress form by assuming that the longshore velocity is much smaller than the wave orbital velocity:

$$\bar{\tau}_b = \rho C_f \overline{|\hat{u}_w|} V \qquad (3.53)$$

Where, $\hat{u}_w$ is the wave induced velocity and V is the mean longshore velocity both at bottom.

If $\hat{u}_w$ is sinusoidally periodic, it can be shown that:

$$\overline{|\hat{u}_w|} = \frac{2}{\pi}\hat{u}_{max} \qquad (3.54)$$

Where, $\hat{u}_{max}$ is the maximum orbital velocity given by linear wave theory as:

$$\hat{u}_{max} = \frac{\pi H}{T \sinh(kh)} \qquad (3.55)$$

Substituting Eq. 3.49 into 3.50, Longuet-Higgins linear approximation for the mean bottom friction stress is found to be:

$$\bar{\tau}_b = \frac{2}{\pi}\rho C_f \hat{u}_{max} V \tag{3.56}$$

Based on Chezy's Law in 1970 Thornton proposed a bottom friction stress formula for wave and current components. The bottom friction component due to the wave motion was given by:

$$\bar{\tau}_{bw} = \rho \frac{f_w}{2} \overline{|\hat{u}_w|} \overline{\hat{u}_w} \tag{3.57}$$

The wave friction factor can be expressed approximately by Jonsson (1966) as:

$$\frac{1}{4\sqrt{f_w}} + \log\frac{1}{4\sqrt{f_w}} = -0.08 + \log\frac{\xi_{-h}}{N_r} \tag{3.58}$$

where, N_r is the Nikuradse roughness parameter and ξ_{-h} is the maximum particle excursion at the bottom as predicted by linear wave theory.

$$\xi_{-h} = \frac{H}{2}\frac{1}{\sinh(kh)} \tag{3.59}$$

3.11 Summary

The understanding of sediment transport requires the fundamental knowledge on wave generation, wave propagation and other wave parameters in a detail and comprehensive manner. In this chapter all the important parameters that are responsible to produce the wave generated current has been studied. Especially the Small Amplitude Wave theory is the basic for developing any further study in this filed. In this chapter, these types of wave theory and related boundary conditions for solving differential equations on wave propagation have been discussed in a elaborative manner.

CHAPTER 4

Experimental Setup and Data Collection

4.1 General

From the literature review it has been observed that wave parameters have significant physical effect on cross-shore sediment transport process. Along with different wave parameters such as wave period, wave height and wave length, water depth and wave direction also plays important role to sediment transport process in the cross-shore direction. All these parameters are important to predict the type of beach response due to wave attack on the normal beach slope. An experiment was conducted in the laboratory with experimental beach slope of 1:15. Though the natural beach slopes are much milder than the experimental set-up but the experimental setup is very much necessary to understand the sediment transport process in the cross-shore direction with varying wave parameters and water depth. This is why three different water depths (50 cm, 40 cm and 35 cm) were used with three different wave periods (1 sec, 2 sec and 2.5 sec) for observing the response of sediment transport.

In the River Engineering and Hydraulics Laboratory of Water Resources Engineering Department of Bangladesh University of Engineering and Technology this experiment was carried out. In the laboratory flume different experimental runs have been carried out by varying the water depth and wave period.

4.2 Laboratory Equipments

For carrying out the experiment and collecting necessary data the following equipments were used:

- Laboratory flume
- Wave Generator
- Water Reservoir

- Artificial Beach Slope
- Breakwaters
- Point Gage

Other necessary accessories used to conduct the experiment were wire screens, concrete blocks, water supply pipes etc. In the following section overviews of the physical model components have been discussed in brief.

4.2.1 Laboratory Flume

The experiment has been carried out in a 70 ft (21.34 m) long, 2.5 ft (0.762 m) wide and 2.5 ft (0.762 m) deep rectangular tilting flume in the Hydraulics and River Engineering Laboratory (Photograph 4.2.1).

Photograph 4.2.1: Laboratory Flume

The side walls of the flume are vertical and they are made of clear glass and the bed is painted by water resistance color to avoid any development of unnecessary bed friction. In this flume wave generator is located at the downstream end with a tail gate. In the upstream end a 1:15 slope was placed to conduct the experiment and the length of the slope was 9.14 m. The stilling chamber with approximately 3.0 m length is located behind the wave generator. On the slope a 3.0 cm sand layer with d_{50} value between 0.11 mm to 0.24 mm was used.

Flume bed has been kept horizontal and it is supported on an elevated steel truss. Rubber pads have been attached to prohibit the flush out of wave from the flume for

the case of highest wave height generation. In the flume water was supplied by external pipes and the depth was kept to desired level. For avoiding any unnecessary leakage in the flume, necessary steps were taken.

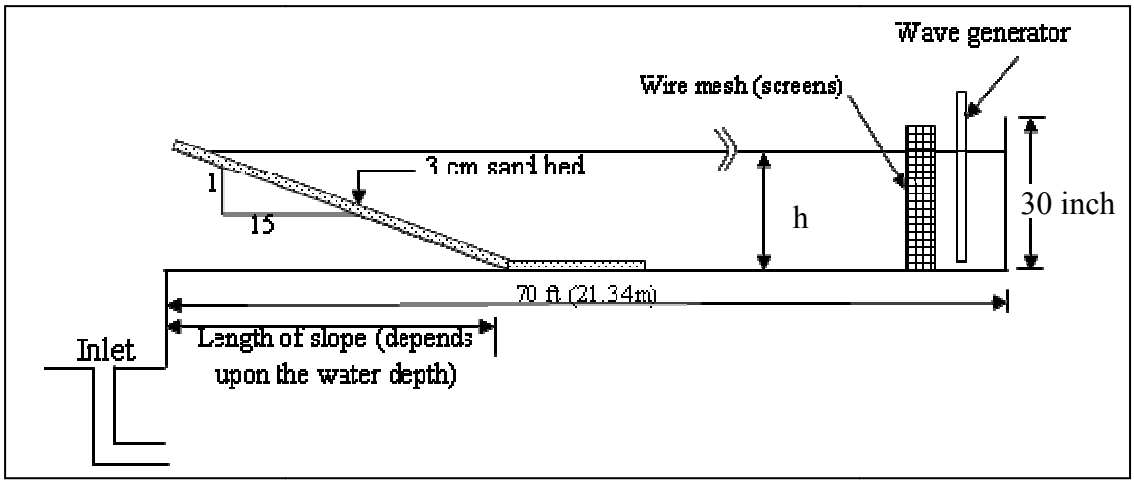

Figure 4.2.1: Sketch of Laboratory Flume

4.2.2 Wave Generator

Wave generator consists of a motor and wave making paddle, which is connected with two vertical limbs (Photograph 4.2.2). Waves are generated by rotating the wave paddle with different frequency as per the requirement. Displacement of wave paddle can be controlled by a crank which is connected to the wave paddle by a connecting rod. Radius of rotation of the crank can be controlled by screw adjustment. The wave paddle is allowed to move horizontally to a distance equal to the radius of rotation of the rotating crank. Therefore, the displacement of the wave paddle can be adjusted by changing the radius of rotation of the crank. The wave period and wave height for different run conditions and water depth has been set by altering the rotational speed the arm of paddle. Rotational speed can be altered between 20 rpm to 120 rpm and the paddle arm can be altered by 25 mm to 320 mm. Hence the required values can be set from the wave generator.

Two displacements have been observed during the movement of wave paddle of the wave generator; firstly the rotational displacement and secondly the vertical

displacement. These two types of adjustments can be adjusted by adjusting the vertical limbs of the wave generator.

Photograph 4.2.2: Wave Generator

4.2.3 Wire screens to reduce wave reflections

In the flume several screens were set to the upstream of the wave generator to reduce wave reflections.

Photograph 4.2.3: Weir Mesh (Screen)

Screens were made of coarse wire mesh (Photograph 4.2.3). Screens were kept at approximately 5 cm apart from each other. In this study finally 20 screens have been used to reduce reflections. The number and spacing were selected by trial and error

method. The wave reflection was considered minimum, when the crests of generated waves in the flume were seen in a straight line from a side view.

4.2.4 Water Reservoir

The water reservoir used in the flume is a steel structure. Water is stored in the reservoir during the time of conducting the experiment. In the reservoir the water supply can be controlled by the existing facilities in the reservoir.

4.2.5 Bank Slope Preparation

In the laboratory flume a steel frame with height of 2 ft and length of 30 ft (slope 1:15) was used to conduct the experiment. The slope was fixed for the entire experimental study. Over the steel frame steel sheet was placed and they were screwed with the frame with the help of screws (Photograph 4.2.4).

Photograph 4.2.4: Construction stage of artificial slope

Cotton net was placed over the steel sheet to create artificial frictional surface for holding sands over the slope. Then the sides of the slope were made water tight by using sanitary putting to this reduced the probability of sand loss from slope to the bottom of the flume. This was obligatory to obtain reliable data during the experiment time. After completing all these process sand was placed over the slope with a thickness of 3.0 cm and the d_{50} value of the sand was between 0.11 mm to 0.20 mm to represent the actual bed material. From the study of Sekiguchi et al. (2004) it has been found that for monochromatic wave action in the laboratory flume, 3.0 cm thick sand

layer exhibits good result for 1 hr and 15 minutes wave action. Therefore, in this study the sand layer has been chosen as 3.0 cm.

The sediment size of natural beaches varies from region to region depending on the geological formation of that location. Matin (1995) conducted a study to investigate the soil sample size (d_{50}) in the major beaches of Bangladesh. From the study it has been found that the representative soil sample size (d_{50}) varies between 0.11mm to 0.2 mm. Therefore, in this study representative soil sample with d_{50} value 0f 0.125 mm was used to conduct the study.

Photograph 4.2.5: Construction stage of artificial slope

4.2.6 Breakwaters

In this study two types of Breakwaters were used. The size of the rectangular breakwater was 75 cm x 35 cm x 16 cm both for floating and submerged condition (Photograph 4.2.6). It had three equal hollow parts to resist the vertical and horizontal pressure of water in the flume and it was made with plastic. The weight of the empty Breakwater was about 10 pounds.

The breakwater was placed at the end of the artificial slope for both the floating and submerged condition.

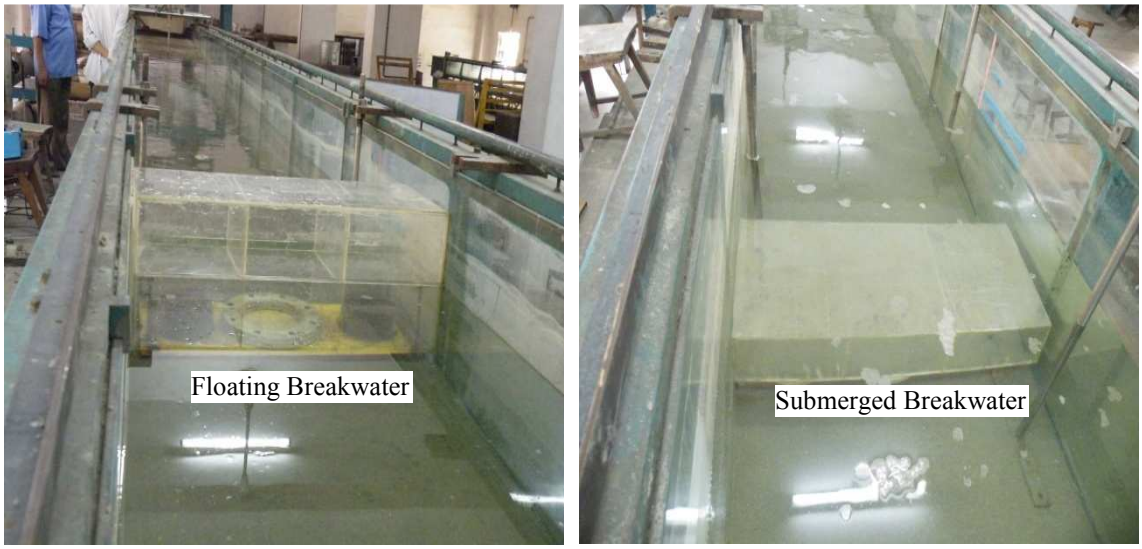

Photograph 4.2.6: Placement of Breakwater

Two flexible pipes were used to supply water in the flume water. For protecting the prepared slope, water was supplied to both the upstream and downstream end of the flume with a constant rate from the regular water supply line.

4.2.7 Point Gage

A Point gage was used to measure the bed profile after completing each run as stated in the test scenarios. The point gage was attached with a vertical scale and the bottom stand was placed from the top surface of the laboratory flume. The scale of the point gage

In addition to this, C.C Blocks with 3.5 cm X 3.5 cm X 2.5 cm size was used over the artificial sandy beach. In the Photograph 4.2.7 the placement of the C.C. Blocks has been shown. These blocks were used to investigate the response of sediment transport after completing the test run.

Photograph 4.2.7: Placement of C. C. Blocks

4.2.8 Electromagnetic Velocity Meter

For the measurement of velocity a programmable 2-D velocity meter was used. The type of the meter used in this study is E.M.S, ACM200-A of ALEC ELECTRONICS (Photograph 4.2.8). The velocity meter consists of three major basic parts: the probe, the control unit with analog display screen and the connection cable.

Photograph 4.2.8: Programmable velocity meter (E.M.S)

The E.M.S was attached with a vertical scale for placing the probe of E.M.S at desired water depth on the slope (half of still water depth) at each location (Photograph 4.2.9). The magnitude of velocity was found in cm/s. The dial was marked with both the negative and positive scale on the screen. At any location the dial shows the reading

of corresponding velocity in the x and y direction with two dials placed on the control unit.

Photograph 4.2.9: Placement of E.M.S at different depth

4.3 Measurement Techniques and Test Scenarios

In this study three different wave periods 1 second, 2 second and 2.5 second were fixed for observing the sediment transport process with three different water depths (50cm, 40cm and 35cm). At first the water depth was fixed and then for the three wave period the wave generator was fixed-up with necessary adjustment. Here, for each case the angular rotation ω, dimensionless parameter $\left(\frac{f+e}{f}\right)$ and rpm were calculated for wave generator set-up (Appendix A).

The RPM values of motor in the wave generator and the dimensionless parameters stated earlier are related with the water depth as well as the wave period. Hence, the following table was formulated for conducting the experiment to produce non-breaking wave in the laboratory flume by using the laboratory wave generator.

Table 4.3.1: Wave generator setup for experimental runs

h (cm)	T (sec)	$\omega = \frac{2\pi}{T}$	$\frac{\omega^2 h}{g}$	From Figure A.2		$\frac{f+e}{f}$	From Laboratory			rpm
				f	e		f	$e+f$	$\frac{f+e}{f}$	
50	1.0	6.28	2.01	0.09	0.81	10.0	0.62	6.2	10.0	18.5
	2.0	3.14	0.50	1.1	0.40	1.36	10	7.5	1.33	11.75
	2.5	2.51	0.32	1.6	0.31	1.19	8.3	10.2	1.22	10
40	1.0	6.28	1.61	0.73	0.23	1.315	1.4	1.8	1.29	19.1
	2.0	3.14	0.40	1.3	0.35	1.27	6	8.4	1.4	11.8
	2.5	2.51	0.26	1.76	0.28	1.16	8	1.8	1.2	10.2
35	1.0	6.28	1.41	0.3	0.69	3.3	1.3	3.1	3.38	18.70
	2.0	3.14	0.35	1.42	0.33	1.232	8.5	10.3	1.212	11.9
	2.5	2.51	0.22	1.88	0.26	1.138	8.9	10.4	1.168	10.1

The experimental run was carried out after completing all those necessary adjustments for non-breaking wave generation. The actual wave period was measured before taking the necessary data. When the actual wave period was seen quite close to the designated wave period by some minor adjustment in the wave generator, then the experiments was carried out and following measurements were taken for the test scenarios (Table 4.3.2):

- Wave period (T sec)
- Wave height (H cm)
- Actual velocity component (V_x and V_y in cm/sec)
- Measurement of bed profile

Table 4.3.2: Test Scenarios

Run No	Water Depth (cm)	Wave Period (Sec)	Remarks
1	50	1.0	3.0 cm sand bed on the slope
2		2.0	3.0 cm sand bed on the slope
3		2.5	3.0 cm sand bed on the slope
4	40	1.0	3.0 cm sand bed on the slope
5		2.0	3.0 cm sand bed on the slope
6		2.5	3.0 cm sand bed on the slope
7	35	1.0	3.0 cm sand bed on the slope
8		2.0	3.0 cm sand bed on the slope
9		2.5	3.0 cm sand bed on the slope
10	50	2.0	3.0 cm sand bed and Submerged Break-water
11		2.0	3.0 cm sand bed and Floating Break-water
12		2.0	3.0 cm sand bed and C. C. Blocks (3.5 cm X 3.5 cm X 2.5 cm)

4.3.1 Wave period measurement

Wave period is the time, usually measured in seconds, that it takes for a complete wave cycle (crest to crest or trough to trough) to pass a given fixed point. For measuring the wave period, a point on the flume side glass was pointed then the number of wave crests passing the point was counted for a minutes. Thus the wave period was measured by dividing the number with 60.

Table 4.3.3: Comparison of wave period

Water Depth (cm)	Run No	Setup wave period from wave generator (sec)	Measured Wave Period (sec)
50	1	1	1.06
	2	2	2.1
	3	2.5	2.6
40	4	1	1.1
	5	2	2.08
	6	2.5	2.56
35	7	1	1.05
	8	2	2.08
	9	2.5	2.48
50	10	2	2.06
	11	2	2.05
	12	2	2.1

4.3.2 Wave height measurement

The measurement of wave height was a significant and challenging part of the study as there was lack of sophisticated instrument. So, the wave height was measured by using different vertical scale attached with the vertical wall of the flume. The still water level was taken as reference level. The crest of the wave was measured with a scale and the trough of wave was measured by another scale. The total scale reading represented the actual wave height. For minimizing the errors, several measurements were taken at different locations and the average value was taken as the wave height (H) for the study.

4.3.3 Velocity component measurement

For the measurement of velocity a programmable 2-D velocity meter was used. The type of the meter is E.M.S, ACM200-A of ALEC ELECTRONICS. In this experiment wave orbital velocity was measured at different locations and the probe was placed at

half of the still water depth (van Rijn 1993). The depth along the slope at different positions was calculated from a vertical scale with which the velocity meter was attached. The width of the flume is 2.5 ft (0.762 m), so across the flume velocity was measured in three lines. From the left side of the flume wall, first measurement was taken at a distance of 19 cm; second one was 38cm and the final line was taken at a distance of 57cm. The velocity was measured along these three lines with a horizontal grid with a spacing of 10 cm. At any location the velocity meter gives the velocity component in V_x and V_y direction. The V_x velocity component was along the slope and the V_y component was across the flume width.

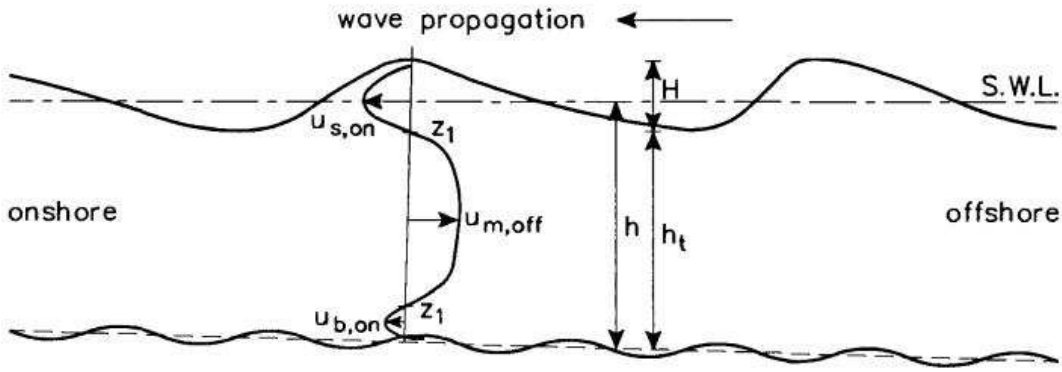

Figure 4.3.1: Net velocity profile due to nonlinear effects in shoaling wave (Source: van Rijn 1993)

4.3.4 Stepwise procedure for the experiment

A specific sequence of test procedure has been followed for every experimental run. These includes flume cleaning, wave generator set-up for maintaining a wave period, slope preparation, water depth maintain, data collection during and after experimental run and preparation for the next run. Methodology has been discussed briefly here:

Step-1

Straight flume was cleaned to make free from debris, moss and floating dirt before starting each experimental run. Cleaning has been done with pouring of water in the flume with very high velocity by using a pipe.

Step-2

In the next step, sand was placed above the slope with d_{50} varying from 0.11 mm to 0.24 mm (Matin, 1995) to form a natural beach condition in laboratory flume. Every time the thickness of the sand bed was taken 3.0 cm and the thickness was measured with a vertical scale carefully.

Step-3

In this experiment as the slope was fixed so, before operating wave generator, some adjustment was done between rotational and transitional movement that depends on wave period and water depth. Appendix- A gives rotational, *e* and transitional, *f* parameter to develop non-breaking harmonic waves. The stepwise procedure to generate regular waves without breaking at the paddle of wave generator has been presented in Appendix- A. This method is done before every wave period settlement when the flume is empty.

Step-4

A pipe was used to supply water into the flume to desire depth (50 cm, 40 cm and 35 cm).

Step-5

Total run time for the wave generator was taken as 1 hour and 15 minutes.

Step-6

Wave height, wave period and velocity components were taken from velocity meter in different location along and across the flume on the slope.

Step-7

Water was then drained out from the flume and the bed level on the slope was measured with the help of a point gage to predict the sediment transport rate with each run.

Step-8

During the last three runs (Run No 10, 11 and 12) runs with submerged and floating breakwaters and C.C. Blocks an extra step has to be added for the installation of it. For each case breakwater is set 100 cm. apart from the toe of the bank slope. For the case of C.C. Blocks, it was placed 50 cm upstream from the zero water depth and to the cross shore direction it was extended 100 cm.

4.4 Numerical Model Formation for Data Input

A part of this study is to compare different experimental result with Parabolic Wave Model (Navera, 2004). In this model for solving the wave propagation equation and calculating other parameters finite difference method has been adopted. In this method the Taylor series expansion has been taken into account to approximate the derivatives of other differential equations sated in the chapter 3. Here, first order terms of Taylor expansion has been considered.

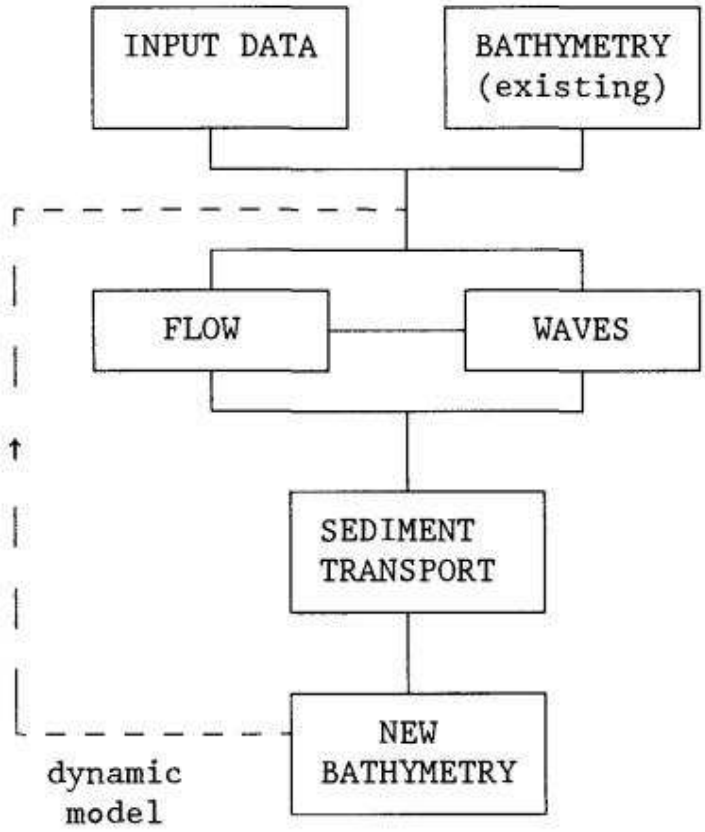

Figure 4.4.1: Flow Chart for Numerical Model operation

The model has adopted the explicit type solution technique for solving the differential equations at each mesh point. For explicit solution it requires the previous boundary values which may be calculated or initially given to the boundary condition. It requires some well-defined grid system for dealing with the transformation of the differential equations. Therefore, in this model the formation grid system is fundamental before getting the output solutions.

Grid Scheme

The model requires to form a rectangular grid mesh over the area of interest as shown in the Fig. 4.4.2, where x and y denote the offshore and longshore direction respectively. Thus the area is divided in a series of grid blocks with a characteristic depth and space increments Δx in the x direction and Δy in the y direction.

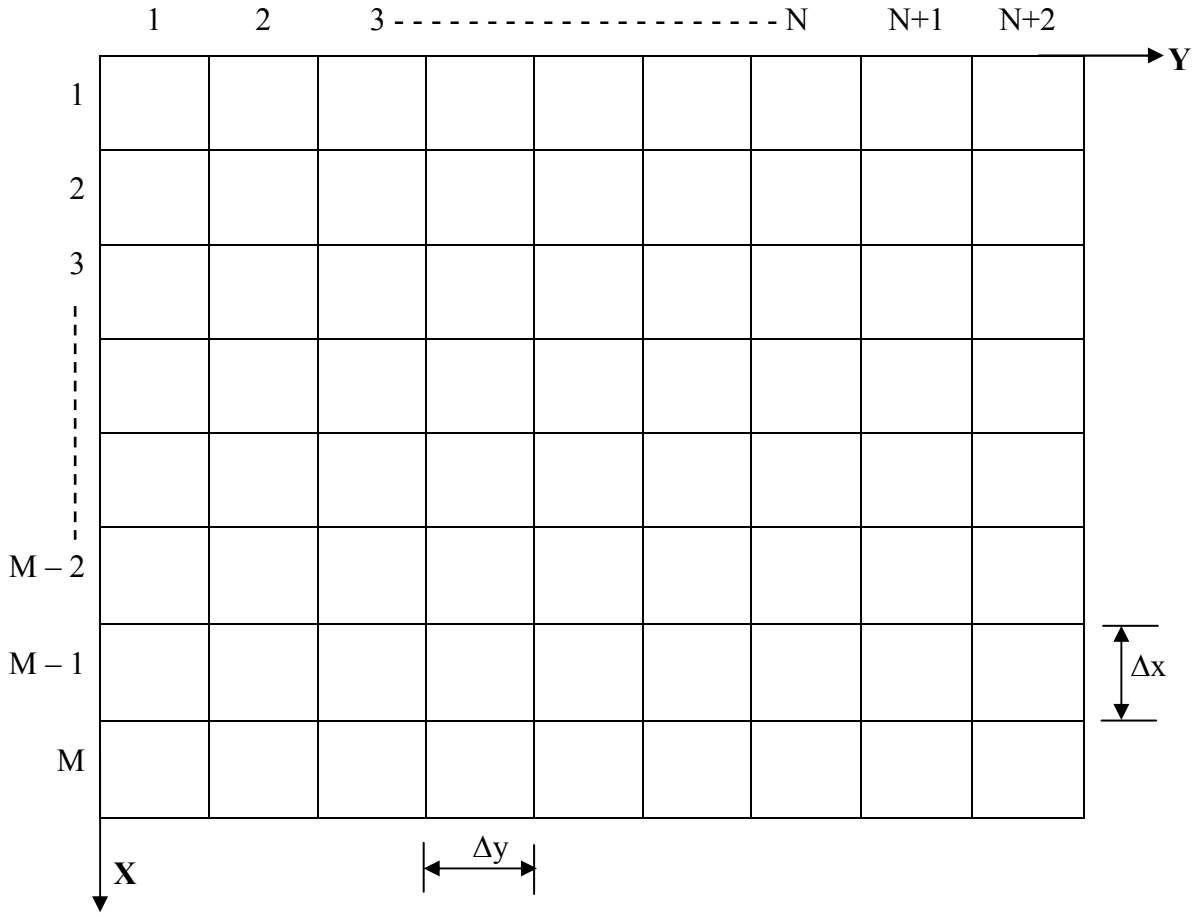

Figure 4.4.2: Grid mesh representation for model operation

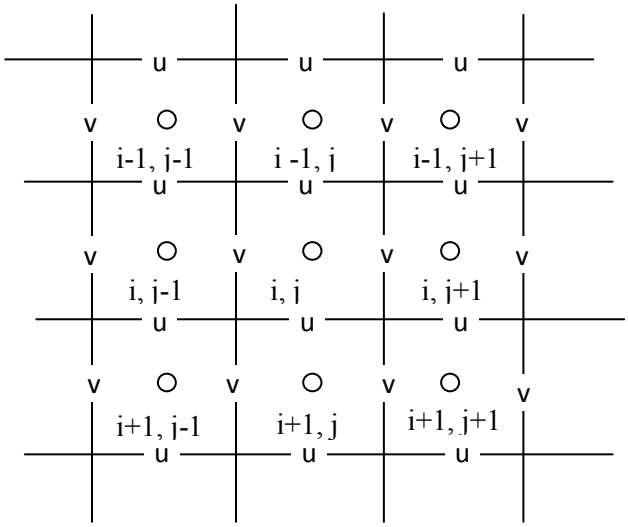

Figure 4.4.3: Grid block scheme differencing coordinate velocities for the model

The Fig. 4.4.3 illustrates the arrangement of variables on the finite difference grid. The velocities u and v are defined at the grid edges and all the other variables are defined at the grid center. The velocities $u_{i,j}$ and $v_{i,j}$ are defined as being positive if they enter the i,j grid block in the positive x and y directions.

Model Stability Criteria

For the full sets of equations used in the model, the exact stability criteria cannot be determined analytically. However, only when the computation is stable does the sequence of approximate solutions tend to the true solution as $\Delta t, \Delta x, \Delta y \rightarrow 0$. When the computation is unstable these solutions differ more and more as $\Delta t, \Delta x, \Delta y \rightarrow 0$ even though the truncation error tends to zero. The stability of the Parabolic Wave Model has been expressed in terms of wave propagation speed. The speed of propagation of some disturbance in the model must be less than or equal to the speed it takes the disturbance to cross a computational grid block in a time step. This is a model condition to detect the disturbance. The disturbance speed is in general the shallow water gravity wave celerity plus some time independent mean current. The stability criterion can generally be given by:

$$\frac{\sqrt{\Delta x^2 + \Delta y^2}}{\Delta t} \geq |u| + \sqrt{gh}$$

As the maximum shallow water wave celerity exceeds the right hand side of this equation, the criteria used in applications of this model are:

$$\frac{\sqrt{\Delta x^2 + \Delta y^2}}{\Delta t} \geq \sqrt{gh_{max}}$$ For two-dimensional case

$$\frac{\Delta x}{\Delta t} \geq \sqrt{gh_{max}}$$ For one dimensional case

Boundary Condition

The boundary condition used for the model has been described here. The area of interest is divided into M rows in the x-direction and into N+2 columns in the y-direction. At the offshore row i = M, a no flow boundary condition has been imposed. This condition simulates a wall at the offshore end of the grid mesh and is represented by $u_{M,j} = 0$. If the offshore boundary is sufficiently remote, then the offsets of rip currents and longshore currents at that boundary are negligible. However, a more correct boundary condition would be to let the mean free surface be zero in deep water. This would increase the number of grid blocks. In the inshore end of the grid mesh, a no flow boundary condition has been used although the location of the beach boundary is allowed to fluctuate through flooding or drying (Fig 4.4.4 and Fig. 4.4.5).

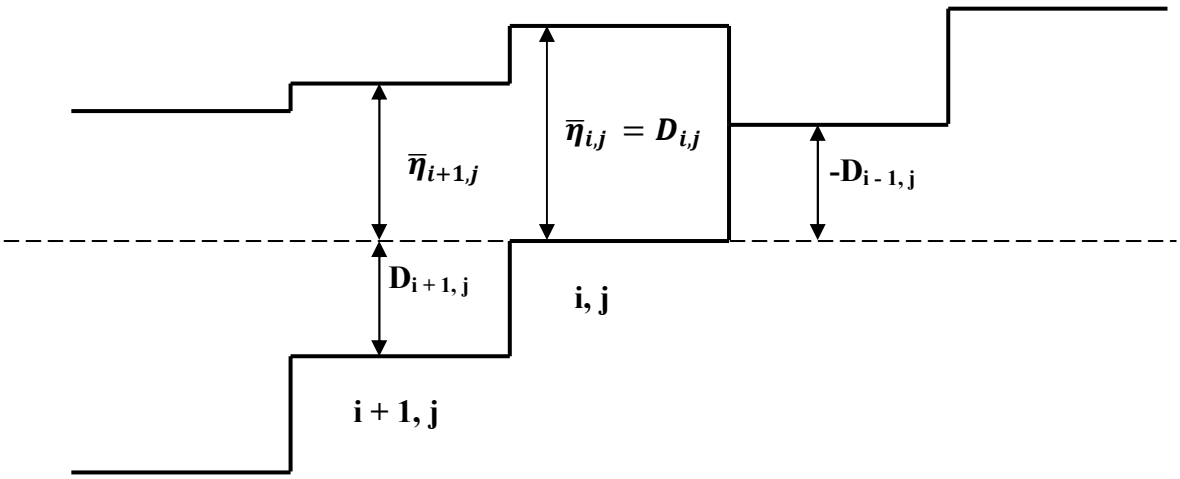

Figure 4.4.4: Before flooding condition of a grid mesh

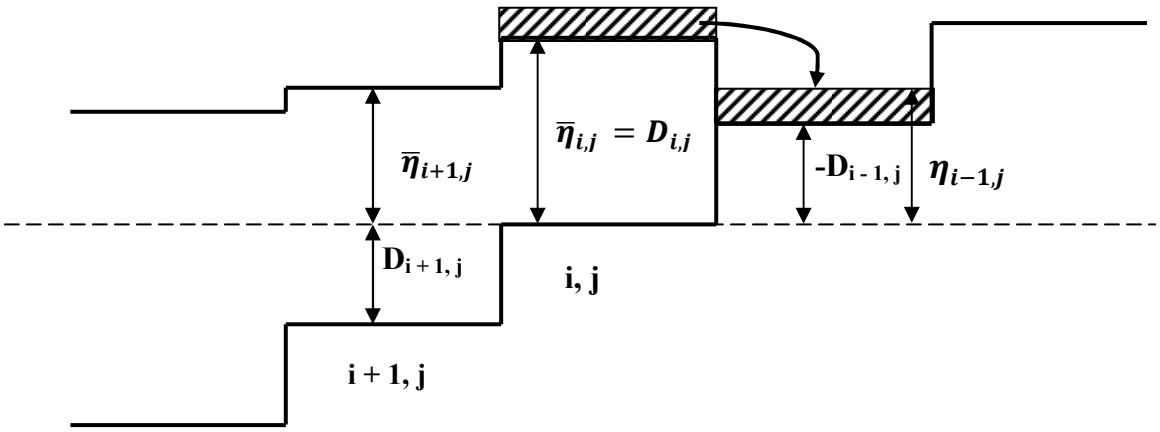

Figure 4.4.5: Grid mesh is flooded by a small volume of water form block (i, j) for model

From this model it has been found that the land ward most grid row remains dry. Considering the water depth at grid block (i, j) due to setup is greater than the water depth at grid block (i-1, j). In this case a small amount of the difference is moved from (i, j) to (i-1, j). This process is repeated until block (i-1, j) has a minimum depth of water which allows it to be included in the calculations and quickly be filled with water. If the depth at block (i-1, j) becomes less than the original amount placed in it, the block is dried by moving the remaining water to grid (i, j).

For the open coast cases the model boundary is different. Here, periodic boundary conditions have been imposed in the longshore direction because circulation patterns and bottom bathymetry along coastline often tend to have a periodicity associated with them. For any quantity, Q periodicity requires:

$$Q_{i,1} = Q_{i,N}$$
$$Q_{i,2} = Q_{i,N+1}$$
$$Q_{i,N+2} = Q_{i,3}$$

These boundary conditions can also be used for a beach without periodicity as long as these lateral boundaries are positioned far enough away from the area of interest. For lateral two dimensional wave basin case, the lateral no-flow conditions require $V_{i,2} = V_{i,N+2} = 0$. Therefore, the boundary conditions used are:

$$Q_{i,1} = Q_{i,2}$$
$$Q_{i,N+2} = Q_{i,N+1}$$

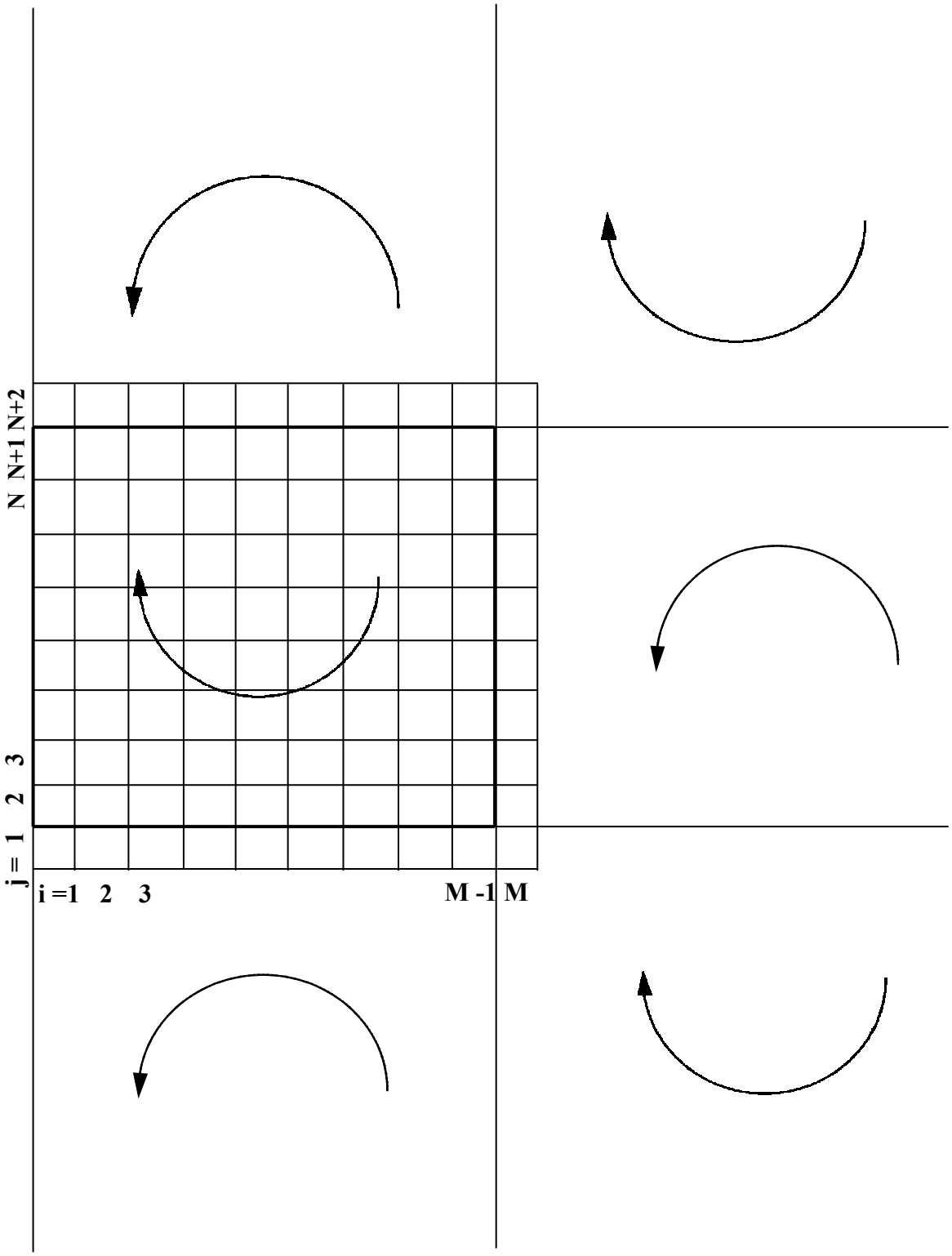

Figure 4.4.6: Wave basin showing the flow being reflected by the side and end walls for the model

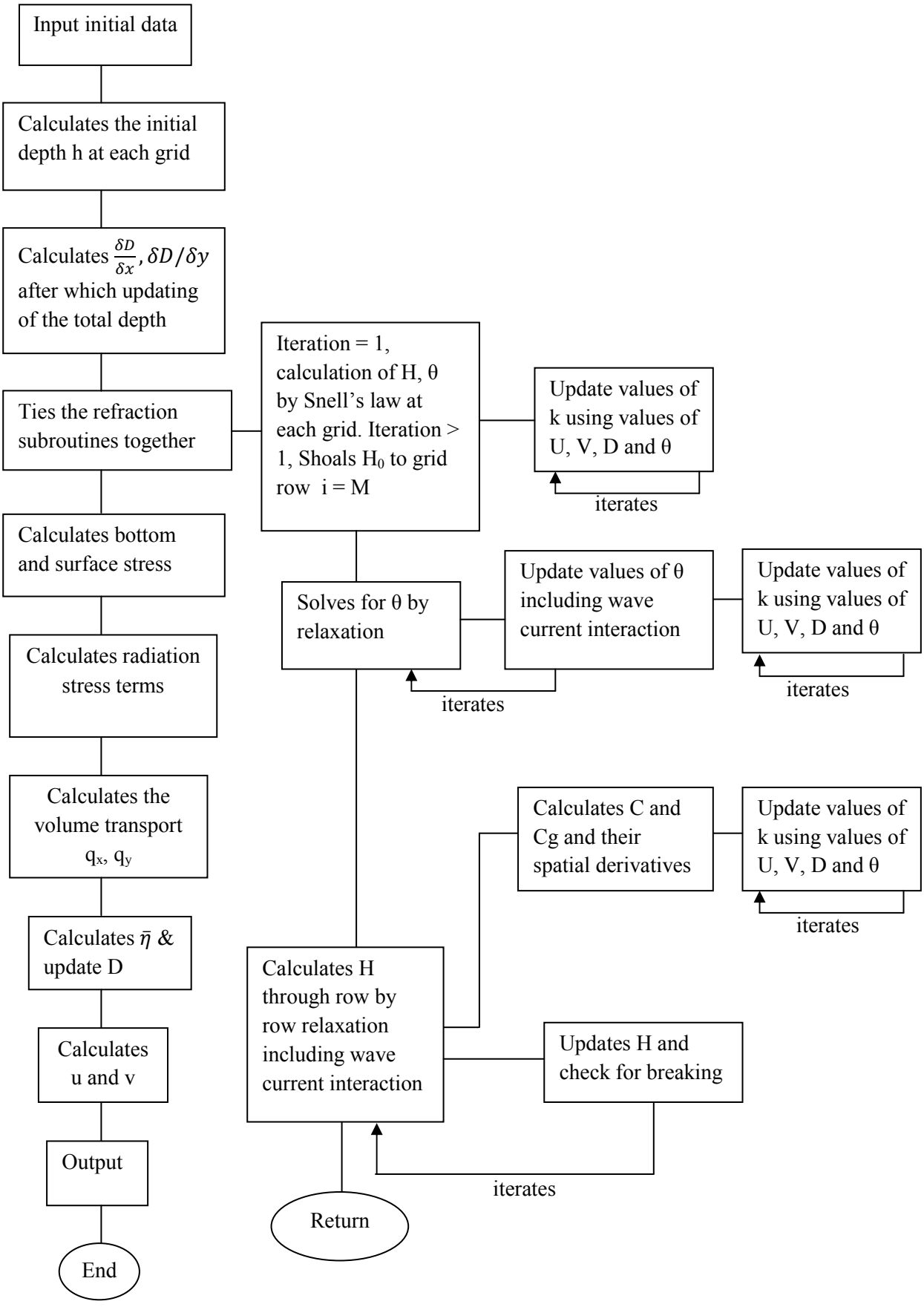

Figure 4.4.7: Simplified flow chart for model simulation

Method of Solution

The model computation starts from the state of rest for all applications. The velocity components u and v and the free surface displacement η have been set as zero in all grids. An initial depth field, together with the offshore wave characteristics was input in the model. Seaward of the offshore grid mesh row i = M, plane beaches were defined. Snell's law was used to calculate the wave characteristics boundary values at row i = M and their initial values in all the blocks.

In this model Newton-Raphson method has been used for solving the iteration process at different grid meshes. The wave height has been calculated by using this model. The wave height had to be build up from zero to its deep water value over a certain number of iterations in order to reduce the problem of the development of a high amplitude scheme due to no-flow boundary condition. In this model the Small Amplitude Wave theory has been used for calculating all the required wave parameters.

4.5 Summary

In this chapter, the detail experimental set up has been discussed. For this experimental study, the use of different laboratory equipments has been discussed with the process of setting. The detail slope preparation process has also been discussed for convenience. The data collection technique has also been discussed with the electromagnetic velocity meter. The total experimental scenarios been also presented here. For the validation of the study a Parabolic Wave Model has been used for this study. Here, the model formulation has been discussed. In this chapter, the detail model setup with solution technique of differential equations used in this model, boundary condition, grid mesh formulation and the solution process has been discussed.

CHAPTER 5

Results and Discussion

5.1 General

Wave is the governing parameter for sediment transport in the cross-shore direction. The process of sediment transport becomes more complicated when the current along with the wave comes as well as the sediment properties varies. Specially as the slope of natural beaches are mild, so waves are one of the responsible parameters for the erosion of beach. In sandy beaches, the fundamental parameters responsible for the morphological changes are necessary to understand the beach development process. Furthermore, the sediment transport processes are also important to the stability of the coastal structures that might be constructed in that region.

In Bangladesh, no extensive experiments have been carried out to investigate the cross-shore sediment transport. So, in this study an experiment has been carried out to investigate the sediment transport process due to non-breaking wave. This study has been carried out with different water depths and wave periods. In this study twelve (12) experimental runs have been conducted. For investigating the cross-shore sediment transport process bed level changes were also measured at the end of every experimental run along with the velocity and wave height.

5.2 Wave Breaking Criteria

As a solitary wave moves into shoaling water it eventually becomes unstable and breaks. A solitary wave breaks when the water particle velocity at the wave crest becomes equal to the wave celerity. According to Miles (1980, 1981) this occurs when

$$\frac{H}{h} \geq 0.78$$

Where, H is the wave height and h is the water depth.

Wave height is limited by both depth and wavelength. For a given water depth and wave period, there is a maximum height limit above which the wave becomes unstable and breaks. This upper limit of wave height is termed as breaking wave height and this is a function of wavelength in deep water. In shallow and transitional water it is a function of both depth and wavelength. Wave breaking is a complex phenomenon. To understand the process, extensive experimental and numerical investigations have been conducted to enrich this branch of wave mechanics.

Researchers have made some progress over the last three decades in the numerical modeling of waves close to breaking. Among all the past research works, the study of Dalrymple and Dean (1975) and Longuet-Higgins (1976) are two of them for defining the wave breaking criteria very well. These studies suggested that the limiting wave steepness to be H/L = 0.141 in deep water and H/h = 0.83 for solitary waves in shallow water with a corresponding solitary wave celerity of

$$\frac{C}{\sqrt{gh}} = 1.29$$

.Where, L is calculated by trial and error method by using the following formula:

$$L = \frac{gT^2}{2\pi} tanh\left(\frac{2\pi h}{L}\right) \tag{5.1}$$

Table: 5.2.1: Non-breaking wave parameter checking criteria

Water Depth, h cm	**Wave Height, H cm**	**Wave Period, T sec**	**Calculated Wave Length, L m**	**Celerity, C ms^{-1}**	$\frac{C}{\sqrt{gh}}$	$\frac{H}{h}$	**Remarks**
50	12	1	1.56	1.560	0.704	0.24	**Non-breaking**
	12.5	2	4.01	2.005	0.905	0.25	
	11.5	2.5	5.25	2.100	0.940	0.20	
40	11	1	1.51	1.510	0.706	0.275	**Non-breaking**
	11.2	2	3.70	1.850	0.930	0.280	
	10.5	2.5	4.75	1.900	0.960	0.263	
35	10	1	1.45	1.450	0.780	0.286	**Non-breaking**
	11	2	3.52	1.760	0.950	0.340	
	10	2.5	4.45	1.780	0.960	0.286	

From the Table 5.2.1 it can be seen that the propagating waves in the laboratory was non-breaking type. Therefore, the fundamental objective of the study for investigating sediment transport under non-breaking wave has been satisfied.

In the experiment, for calculating the wave length (L) wave period (T) has been taken as the value that was set from the wave generator. In the Chapter 4 it has been checked that the measured wave period and the fixed wave period set in wave generator was nearly equal. Therefore, it has been justified for the all these calculations.

5.3 Type of beach profile after wave action

Short term morphological change in the artificial laboratory beach is enhanced by the cross-shore sediment movement which is associated with the wave action. Different types of beaches are available in nature. Among them smooth beaches with steep and gentle slope, stepped beaches and barred beaches with single and multiple bars are three common types. According to the study of Mogi (1963), the barred beach or multi bar beach profile is common for both natural and artificial laboratory beaches. In this study, the type of beach with short term wave attack has been investigated. After completing every run it has been observed that the beach type barred beach with multi bar formation (Photograph 5.3.1)

Photograph 5.3.1: Bed profile Run No. 1 in the offshore region

The classification of beach has other criteria too. It can be classified into two main categories, accretion type and erosion type. Besides these two, another type named as stable beach also present in nature. For these types of beach formation, short term wave has major effect. Short term waves transport beach material to the offshore direction. Therefore, the beach erodes and different bars are formed. Johnson (1949) found from his wave flume experiments that wave steepness is an important factor for bar formation. Other laboratory studies conducted after Johnson's work indicates that sediment grain size is also a controlling factor. A wave tank study conducted by Sunamura and Horikawa (1974) showed that the bottom slope is another important factor affecting beach profile change. The proposed formula to predict the type of beach, whether it will erode or accrete is a function of three parameters, i.e. wave steepness, sediment grain size and bottom slope:

$$\frac{H_0}{L_0} = C_s(\tan\beta)^{-0.27}(d/L_0)^{0.67} \tag{5.2}$$

Where, H_0 and L_0 are the deep water wave height and length respectively, d is the sediment grain size and $tan\beta$ is the bottom slope, and C_s is a dimensionless constant. The values of C_s is 4~8 to demarcate erosion and accretion of laboratory beaches. If the left side of this equation is greater than the right side then an eroding beach will develop.

Table: 5.3.1: Determination of type of beach profile for the research

Run No	Wave Height H_0 (m)	Wave Length L_0 (m)	H_0/L_0	$(\tan\beta)^{-0.27}(d/L_0)^{0.67}$
1	0.120	1.56	0.0770	0.003740
2	0125	6.24	0.0200	0.001476
3	0.115	9.75	0.0118	0.001096
4	0.110	1.56	0.0705	0.003740
5	0.112	6.24	0.0180	0.001476
6	0.105	9.75	0.0108	0.001096
7	0.100	1.56	0.0640	0.003740
8	0.110	6.24	0.0192	0.001476
9	0.100	9.75	0.0100	0.001096

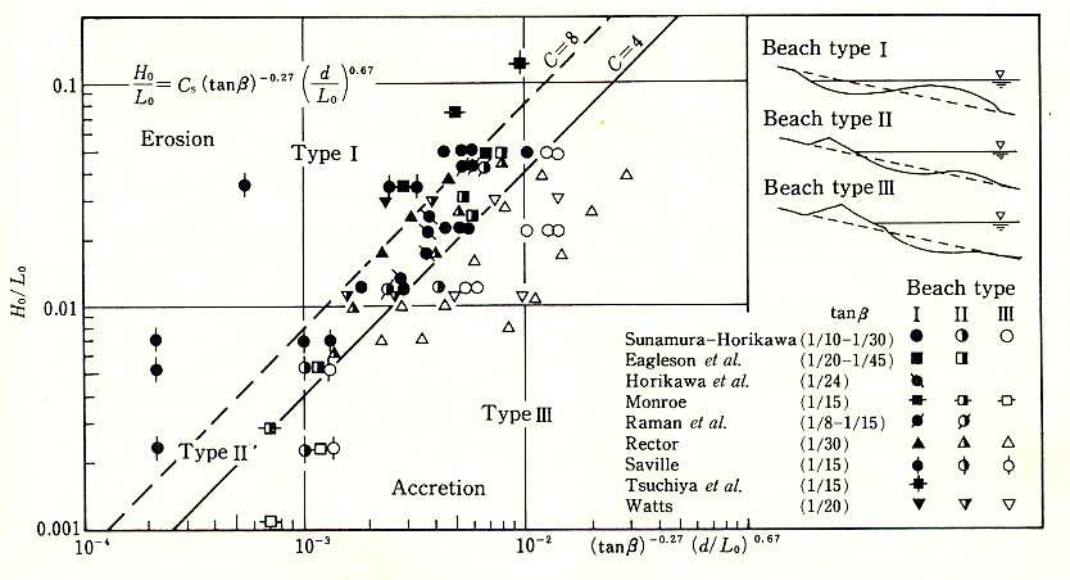

Figure 5.3.1: Classification of beach profile in laboratory (Source: Sunamura and Horikawa, 1974)

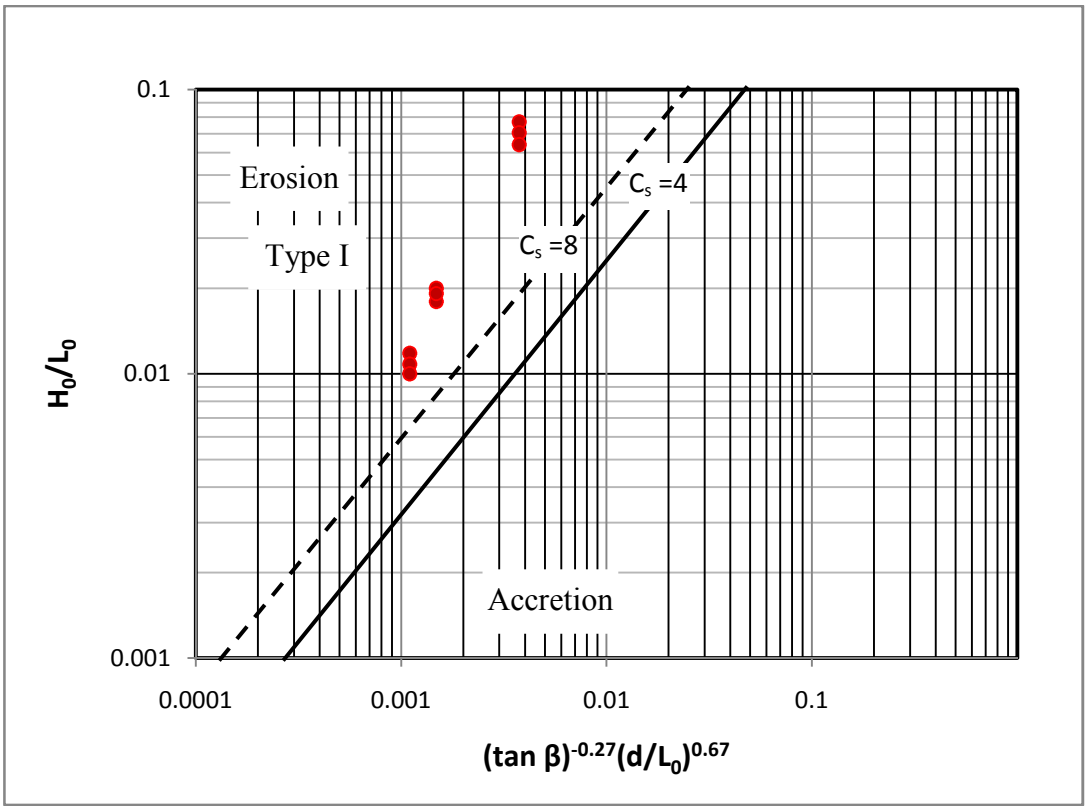

Figure 5.3.2: Laboratory data for beach profile classification

From this experiment it has been found that, all the data lies above the demarcating line (Fig. 5.3.2). Therefore, the artificial laboratory beach profile can be classified as an eroding Type I (Fig. 5.3.1) or barred beach of erosion type.

5.4 Volumetric Change in Sediment due to wave action

In this study, the bed elevation was measured with a point gage after completing every experimental run. The obtained data were then plotted to calculate the change of cohesion-less sediment volume for every case. Data were plotted in AutoCAD, where 270 cm length (Fig. 5.4.1) below the still water level (SWL) along the slope of artificial beach was taken as the area of interested.

For analyzing the data, total nine segments have been taken (Fig. 5.4.1) and the length of each segment has been taken as 30 cm. The first segment has been chosen from zero water depth (still water level) and it is extended towards the offshore direction on the slope.

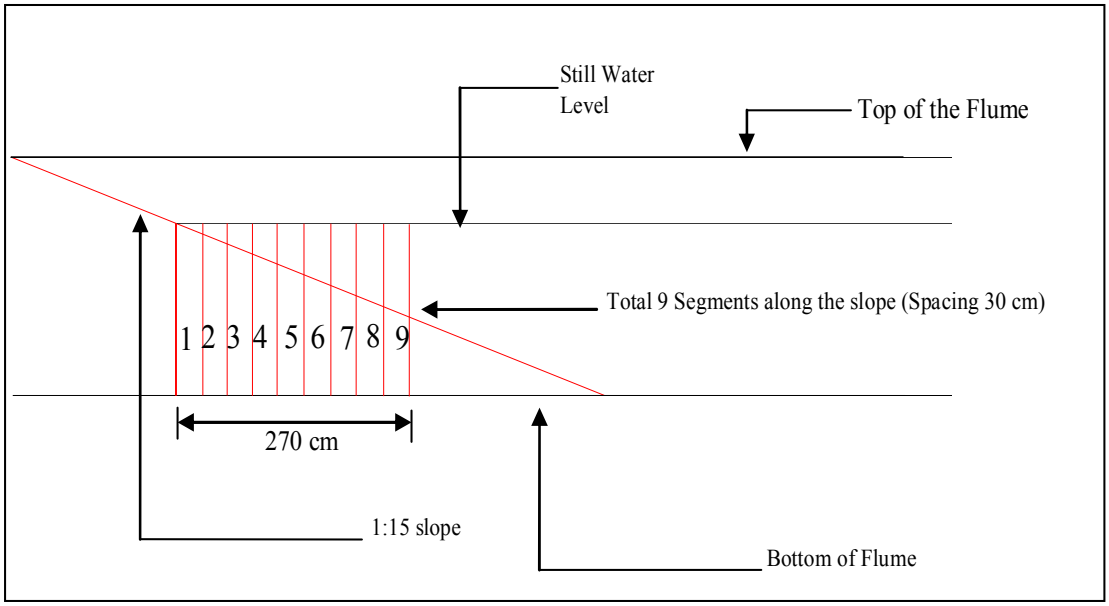

Figure 5.4.1: Study area on the slope

The wave run-up length has also been taken into consideration for calculating the volume change along the cross-shore direction. The bed profile in the wave run-up area (zero water depth to the end of wave run-up) was plotted by the same way and

total volume of sand was calculated per unit width of the flume. This analysis indicates that, along the cross-shore line (i.e. below the still water level) the movement of sediment volume is significant for both low and high water depth. It has been observed that, for higher wave period the movement of sediment volume towards the cross-shore direction is prominent (Table 5.4.1).

Table 5.4.1: Change in volume below SWL upto 270 cm along the slope

Water Depth (cm)	Wave Period (sec)	Actual sand Volume (cm^3/ unit width)	Final sand volume (cm^3/ unit width)	Change in volume (cm^3/ unit width)
50	1	810	860.05	+ 60.05
	2	810	936.90	+ 126.90
	2.5	810	956.67	+ 146.67
40	1	810	845.77	+ 35.77
	2	810	874.75	+ 64.75
	2.5	810	905.67	+ 95.67
35	1	810	793.48	+ 26.52
	2	810	835.48	+ 25.48
	2.5	810	845.67	+ 35.67

From the analysis it has been observed that (Table 5.4.2) in the wave run-up zone the rate of accumulation of bed material has been increased with the increase of wave period and water depth. In this zone the effect of wave period is a significant driving force for sediment transport. This study has been conducted with the fine cohesion-less sand so, the effect of cohesive and coarser material on the transport cannot be interpreted.

It has been observed from this study (Table 5.4.2) that wave run-up value has been changed with different wave period. This experiment suggests that for lower wave period the wave run-up value is lower and vice-versa. Therefore, the sediment movement for higher wave period and water depth above the SWL or near-shore zone is more.

Table 5.4.2: Change in volume above SWL

Water Depth (cm)	Wave Period (sec)	Distance of wave Run-up form initial water level (cm)	Actual sand Volume (cm^3/ unit width)	Final sand volume (cm^3/ unit width)	Change in volume (cm^3/ unit width)
50	1	50	150	156.05	6.046
	2	180	540	650.00	110.00
	2.5	130	390	510.00	120.00
40	1	64	192	224.56	32.56
	2	75	225	278.67	53.67
	2.5	80	240	327.68	87.68
35	1	60	180	202.80	22.80
	2	130	390	425.41	35.41
	2.5	140	420	467.40	47.40

With the increase of wave period, the time of incident wave in the surf zone also increases as well as the orbital velocity. Hence, the mixing period for sediment is increased and the volume suspended sediment is increased in that zone. This suspended sediment is carried towards the onshore zone by the wave induced current. In this study, similar phenomenon has been observed. But for the off-shore zone there is a great deal of variation.

Table 5.4.3: Total change of sediment volume

Water Depth (cm)	Wave Period (sec)	Actual sand Volume (cm^3/ unit width)	Final sand volume (cm^3/ unit width)	Change in volume (cm^3/ unit width)
50	1	960	1026.10	66.10
	2	1350	1556.90	206.90
	2.5	1200	1445.67	245.67
40	1	1002	1068.33	66.33
	2	1035	1163.32	128.32
	2.5	1050	1213.35	163.35
35	1	990	1039.32	49.32
	2	1200	1270.89	70.89
	2.5	1230	1328.07	93.07

Table 5.4.4: Net onshore off-shore movement of sediment volume

Water Depth (cm)	Wave Period (sec)	Movement below zero water depth (cm^3/ unit width)	Movement above zero water depth (cm^3/ unit width)	Change in volume (cm^3/ unit width)
50	1	60.05	6.046	+ 54.00
	2	126.90	110.00	+ 16.90
	2.5	146.67	120.00	+ 26.67
40	1	35.77	32.56	+ 3.210
	2	64.75	53.67	+ 11.08
	2.5	95.67	87.68	+ 7.99
35	1	26.52	22.80	+ 3.72
	2	25.48	35.41	- 9.93
	2.5	35.67	47.40	- 11.73

From the Table 5.4.4 it has been observed that the net movement of sediment volume is towards the offshore region is higher. But for lower water depth (35 cm) with wave period 2 sec and 2.5 sec the observation is different. For the two cases the net onshore movement of sediment volume is higher. Therefore, it can be concluded that with higher wave period when the water depth is low then accretion type beach is formed. Hence, sediment moves towards the onshore direction.

5.5 Classification of net cross-shore sediment transport direction

Cross-shore sediment transport produces the morphological and topographical changes in the coastal environment. Topographical changes on sandy coasts are produced by the net transport of sediment in the near-shore zone. A net transport is a result of the transport rates in opposite directions. The factors governing such difference in the onshore and offshore directions are:

- Asymmetric profile of waves due to shoaling and the resultant difference of water velocities in the onshore and offshore direction
- Asymmetric pattern of sand ripples and
- The total bottom slope

Sunamura (1982) suggested that the first two terms for classifying sediment transport direction as stated earlier, can be described the Ursell parameter. Hallermeier (1982)

formed a relationship between the Ursell parameter and flow intensity parameter to classify the direction of sediment transport.

$$Ur = \frac{HL^2}{h^3} \tag{5.3}$$

$$\Psi' = \frac{(d_o\sigma)^2}{sgd} \tag{5.4}$$

Where, *H* and *L* are wave height and wavelength, *h* is the water depth, $\sigma = {}^{2\pi}/_{T}$ (*T* is the wave period), *s* is sediment specific gravity in water, *d* is the sediment size and and d_0 is the excursion length of the near bottom orbital motion denoted by

$$d_0 = \frac{H}{\sinh\left(\frac{2\pi h}{L}\right)}$$

The Sunamura's experiment suggested that no transport occurs if the value of Ψ' is lower than 17 and for off-shore transport the condition $\Psi' \geq 0.048U_r^{1.5}$ must be satisfied.

In this study, to classify the sediment transport direction same sort of parameters has been considered to identify the transport process. All the relevant values have been calculated as shown in the Table 5.5.1.

Table 5.5.1: Experimental Ursell parameters and a flow intensity parameter

Water Depth, h (cm)	Wave Period, T (sec)	Calculated Wave Period (sec)	U_r	Ψ'
50	1	1.06	2.33	18.91
	2	2.1	10.50	36.75
	2.5	2.6	24.90	62.28
40	1	1.1	4.18	25.40
	2	2.06	18.37	52.00
	2.5	2.56	44.36	84.90
35	1	1.05	5.67	32.74
	2	2.08	26.93	68.55
	2.5	2.48	63.00	102.41

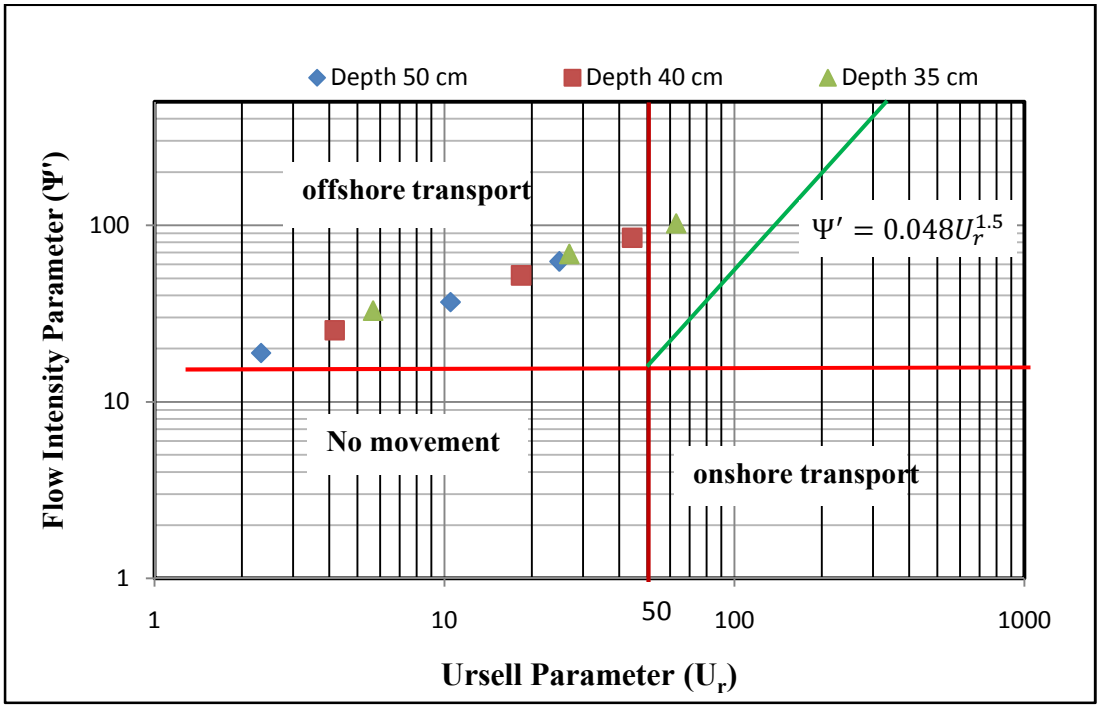

Figure: 5.5.1: Classification of net cross-shore transport direction

Figure 5.5.1 shows that the offshore sediment transport rate is dominating for this experiment which supports Sunamura (1982) result for sediment transport in the cross-shore direction. So, an erosion type beach profile was formed in this study as shown in the previous section. Hence, in the beach where this scenario prevails as created in the laboratory, the topographical changes in the beach will take place due to the beach erosion on the sandy coasts.

5.5.1 Quantification of Cross-Shore Transport

In the Fig. 5.5.3 and Fig. 5.5.4 the relationship between the amplitude of the Shields parameter, $\Psi_m = f_w \hat{U}_{bTrough}/2sgd$ for oscillating flow and the non-dimensional onshore and offshore transport rates, $\Phi = q_{net}/w_s d$ presented by Watanabe (1982) has been developed.

The Shields parameter is Ψ_m is an important useful descriptor for sediment transport in oscillating flow. The non-dimensional offshore and onshore transport is also an important indicator for the sediment transport in the cross-shore direction as stated by

researchers. Therefore, an attempt has been taken in this study to formulate same sort of functional correlation with Shields parameter and non-dimensional sediment transport rate.

Where, is Jonsson's (1960) wave friction factor, is the maximum value of the near bottom wave velocity, s is the sediment specific gravity, g is the gravitational acceleration and d is the sediment diameter. Critical Shields Parameter depends on

Where, sediment size d_{50} has been taken as 0.125 mm for this study from sieve analysis.

Madsen and Grant (1976) analyzed laboratory data of sediment transport under oscillatory flow and found that the Shields parameter was a useful descriptor (Fig. 5.5.2). The Shields parameter which is a non-dimensional bed shear stress and can be expressed in terms of the maximum value of the near bottom water particle velocity. The critical shields parameter is calculated from the Figure 5.5.2 as obtained by Madsen and Grant. According to them, sediment particle in natural beaches with specific gravity 2.65 the value of critical Shields parameter varies from 0.03 to 0.08.

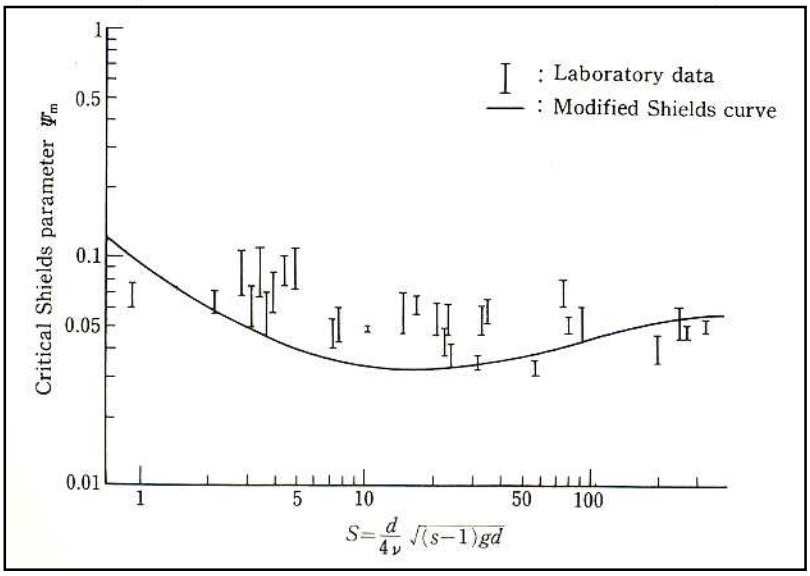

Figure 5.5.2: Critical condition for initiation of sediment movement (Source: Madsen and Grant, 1976).

For calculating the bottom friction f_w other parameters $\hat{A}_\delta, \hat{U}_\delta, k_s$ and υ are needed to calculate. Where, $\widehat{\mathrm{A}}_\delta = \frac{\mathrm{H}}{2\sinh(\mathrm{kh})}$ (the peak value near-bed orbital excursion), $\mathrm{k} = \frac{2\pi}{\mathrm{L}}$ (wave number) and $\widehat{\mathrm{U}}_\delta = \frac{\pi \mathrm{H}}{\mathrm{T}\sinh\left(\frac{2\pi \mathrm{h}}{\mathrm{L}}\right)}$ (peak value of near-bed orbital velocity).

The value of friction factor also dependent on some conditions:

- If $\frac{\hat{A}_\delta \hat{U}_\delta}{\upsilon} < 10^4$, then $f_w = 2\left(\frac{\hat{A}_\delta \hat{U}_\delta}{\upsilon}\right)^{-0.5}$
- If $10^4 < \frac{\hat{A}_\delta \hat{U}_\delta}{\upsilon} < 10^6$ then $f_w = 0.09\left(\frac{\hat{A}_\delta \hat{U}_\delta}{\upsilon}\right)^{-0.2}$
- Maximum f_w value is 0.3

Table 5.5.2: Calculation of cross-shore transport rate and Shields Parameter

h (cm)	T (Sec)	H (m)	$\hat{A}_\delta$	$\hat{U}_\delta$ (ms^{-1})	$\hat{U}_{bTrough}$	$\frac{\hat{A}_\delta \hat{U}_\delta}{\upsilon}$	f_w	Ψ_m	Ψ_c	Φ	Φ'
50	1	0.120	0.0163	0.1025	0.0946	1665	0.0850	0.117	0.075	0.1000	0.0200
	2	0.125	0.0554	0.1738	0.1623	9600	0.0200	0.081	0.075	0.0120	0.0066
	2.5	0.115	0.0896	0.2253	0.2100	20000	0.0124	0.084	0.075	0.0192	0.0074
40	1	0.110	0.0228	0.1438	0.1319	3268	0.0350	0.094	0.075	0.0410	0.0104
	2	0.112	0.0650	0.2054	0.1880	13311	0.0155	0.086	0.075	0.0228	0.0079
	2.5	0.105	0.1045	0.2620	0.2410	27300	0.0117	0.104	0.075	0.0661	0.0141
35	1	0.100	0.0260	0.1630	0.1490	4225	0.0300	0.105	0.075	0.0683	0.0145
	2	0.110	0.0750	0.2360	0.2137	17647	0.0127	0.089	0.075	0.0303	0.0089
	2.5	0.100	0.1148	0.2886	0.2638	33032	0.0112	0.120	0.075	0.1098	0.0216

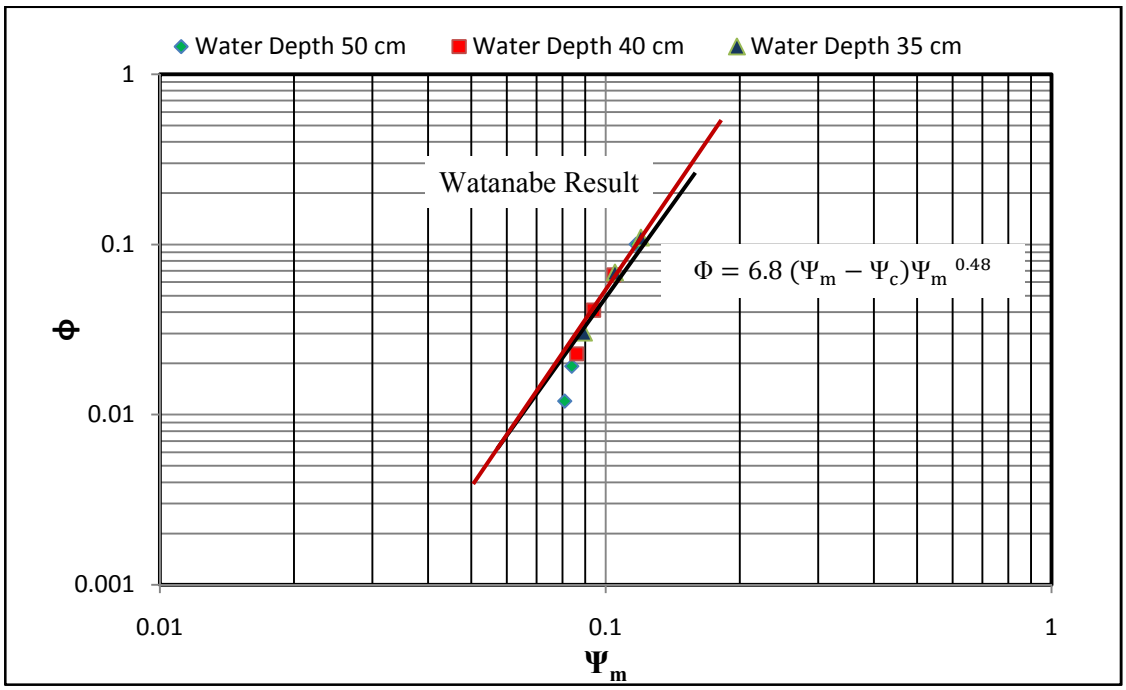

Figure 5.5.3: Correlation between non-dimensional cross-shore transport rate with Shields parameter.

This experimental result follows the Watanabe (1982) experiment for non-dimensional cross-shore transport. Form this data is evident that the non-dimensional transport rate follows this equation $\Phi = 6.8\,(\Psi_m - \Psi_c)\Psi_m^{\,0.48}$, which is very similar to the Watanable's proposed equation $\Phi = 7\,(\Psi_m - \Psi_c)\Psi_m^{\,0.5}$.

Fig. 5.5.4 also indicates same type of trend has been observed when the relationship is formed between Φ' and Shields parameter. Here, $\Phi' = \bar{q}/(w_0 d)$ and $\bar{q}$ denotes the mean value of sediment transport over one half wave cycle. From Watanabe experimental result, the co-relationship was found as $\Phi' = 12.5\Psi_m^{\,3}$. From this study it has been found as $\Phi' = 11.6\Psi_m^{\,2.8}$. So, this experimental result also follows same trend.

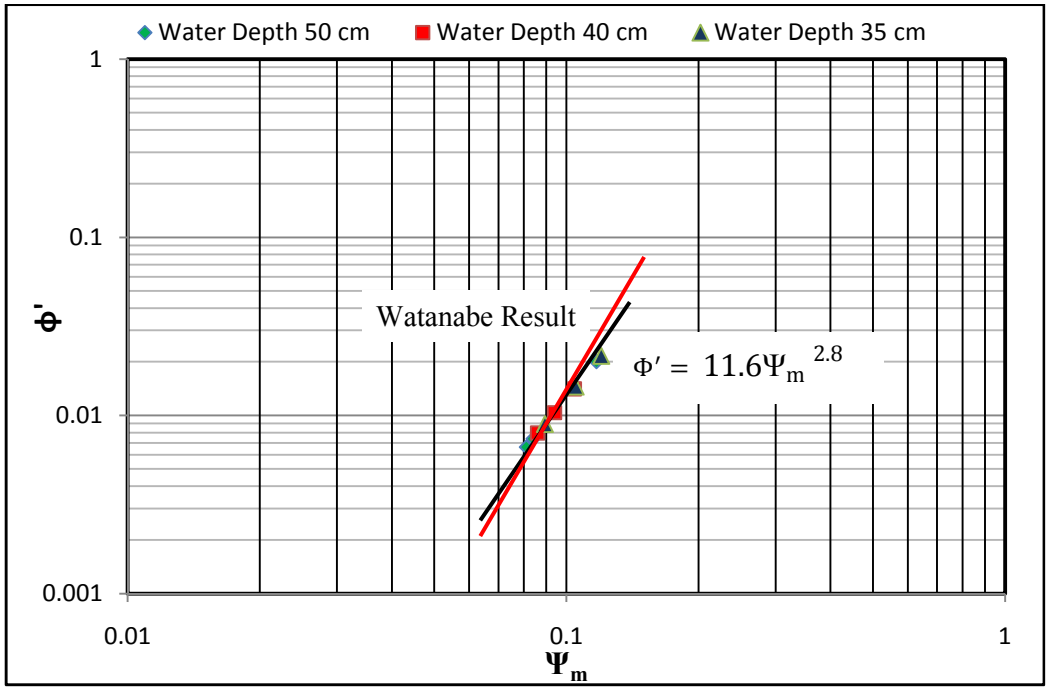

Figure 5.5.4: Correlation between non-dimensional cross-shore transport rate with Shields parameter.

Another important region of sediment transport in the cross-shore area is the swash zone. Swash zone is the sub-aerial beach landward of the surf zone where waves rush up and down. Sediment transport in this area is directly related to the onshore or offshore displacement of the shoreline. Different approaches had been carried out to develop reliable formulation of sediment transport in this region. Ogawa and Shuto (1981, 1982) had developed some correlation for sediment transport based on the field measurement of sediment transport.

The Ogawa and Shuto study formed the co-relationship between non-dimensional offshore and onshore transport rate Φ and flow intensity parameter Ψ'. The calculation procedures for these two terms are discussed in the earlier section.

Table 5.5.3: Calculation of cross-shore transport rate

Water Depth, h (cm)	Wave Period, T (Sec)	Φ	Ψ′
50	1	0.1000	18.91
	2	0.0120	36.75
	2.5	0.0192	62.28
40	1	0.0410	25.40
	2	0.0228	52.00
	2.5	0.0661	84.90
35	1	0.0683	32.74
	2	0.0303	68.55
	2.5	0.1098	102.41

Fig. 5.5.5 represents the relationship between non-dimensional sediment transport rate and the flow intensity parameter for swash zone. Ogawa and Shuto showed that a bore like advance turbulence, in the swash zone in the cross-shore direction is the principal cause for sediment transport.

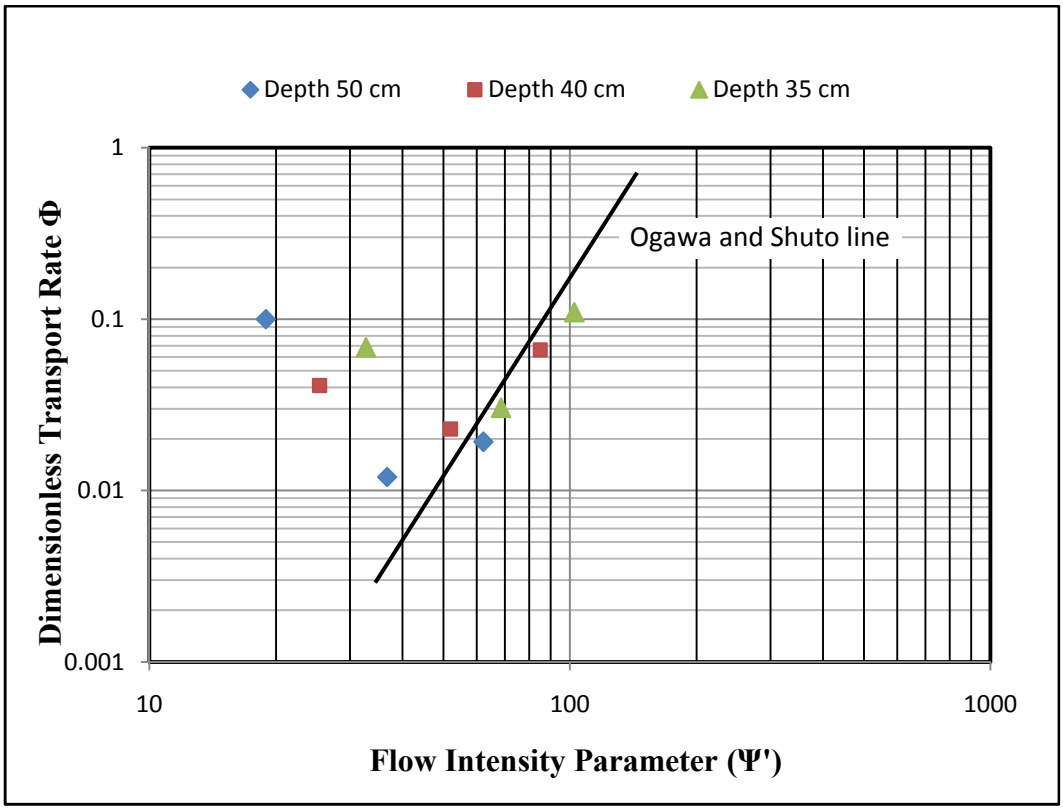

Figure 5.5.5: Sediment transport rate in the swash zone

The majority of the transport occurs in the first stage of wave propagation. For this approximation Ogawa stated that, both the grain size and beach slope are responsible for the sediment movement in the cross-shore direction. This experimental result also follows the same type of trend with minor deviation from Ogawa and Shuto experiment. From this study, it has been observed that the transport rate deviates when the wave period is 1 sec for all water depth. Hence, there might be formed some complex interaction between wave and receding wave for low wave periods.

From earlier research it has been found that sediment movement at the bottom of the slope occurs as a sheet flow in shallow water region. For this case, the bottom shear velocity is an important parameter that affects the sediment transport in the cross-shore direction. Hence, Yamashita, Sawamoto and Yokoyama (1984) conducted a study to obtain a reliable parameter for expressing sediment transport rate under sheet flow condition. From their study it was found that the dimensionless shear velocity due to wave (u_{*w}/w_0) is more suitable than the Shields parameter to express the sediment transport rate in the cross-shore direction. Here, w_0 is the fall velocity of sediment particle. Therefore, in this study (Fig. 5.5.6) same sort of parameters have been tested for the experimental data. In this study the dimensionless sediment transport rate Φ' has been plotted against the u_{*w}/w_0 value.

Where, $u_{*w} = (\tau_{bw}/\rho)^{0.5}$ and $\tau_{bw} = \left(\frac{1}{4}\right)\rho f_w\left(\widehat{U}_\delta\right)^2$

Table 5.5.4: Calculation of non-dimensional transport rate and u_{*w}/w_0

h (cm)	T (Sec)	H (m)	$\widehat{U}_\delta$ ms^{-1}	f_w	τ_{bw}	u_{*w} ms^{-1}	w_s ms^{-1}	u_{*w}/w_0	Φ'
50	1	0.120	0.1025	0.0850	0.223	0.0149	0.0140	1.064	0.0200
	2	0.125	0.1738	0.0200	0.151	0.0123	0.0140	0.879	0.0066
	2.5	0.115	0.2253	0.0124	0.157	0.0125	0.0140	0.893	0.0074
40	1	0.110	0.1438	0.0350	0.181	0.0135	0.0140	0.964	0.0104
	2	0.112	0.2054	0.0155	0.164	0.0128	0.0140	0.914	0.0079
	2.5	0.105	0.2620	0.0117	0.200	0.0142	0.0140	1.014	0.0141
35	1	0.100	0.1630	0.0300	0.199	0.0141	0.0140	1.007	0.0145
	2	0.110	0.2360	0.0127	0.177	0.0133	0.0140	0.950	0.0089
	2.5	0.100	0.2886	0.0112	0.233	0.0153	0.0140	1.093	0.0216

In this experiment, the correlation between non-dimensional transport rate non-dimensional shear velocity has been formed (Fig.5.5.6). From the experimental correlation formed by Yamashita et al. was found to be $\Phi' = 2.2\ (u_*/w_0)^3$. From the experimental result, the correlation has been found as $\Phi' = 2.0\ (u_*/w_0)^3$ which is very much similar to the Yamashita et al. result. Different researches suggested that this representation is more reliable than other non-dimensional correlations developed for understanding the sediment transport in the cross-shore direction due to non-breaking wave. Therefore, this representation is very much significant for cross-shore sediment transport.

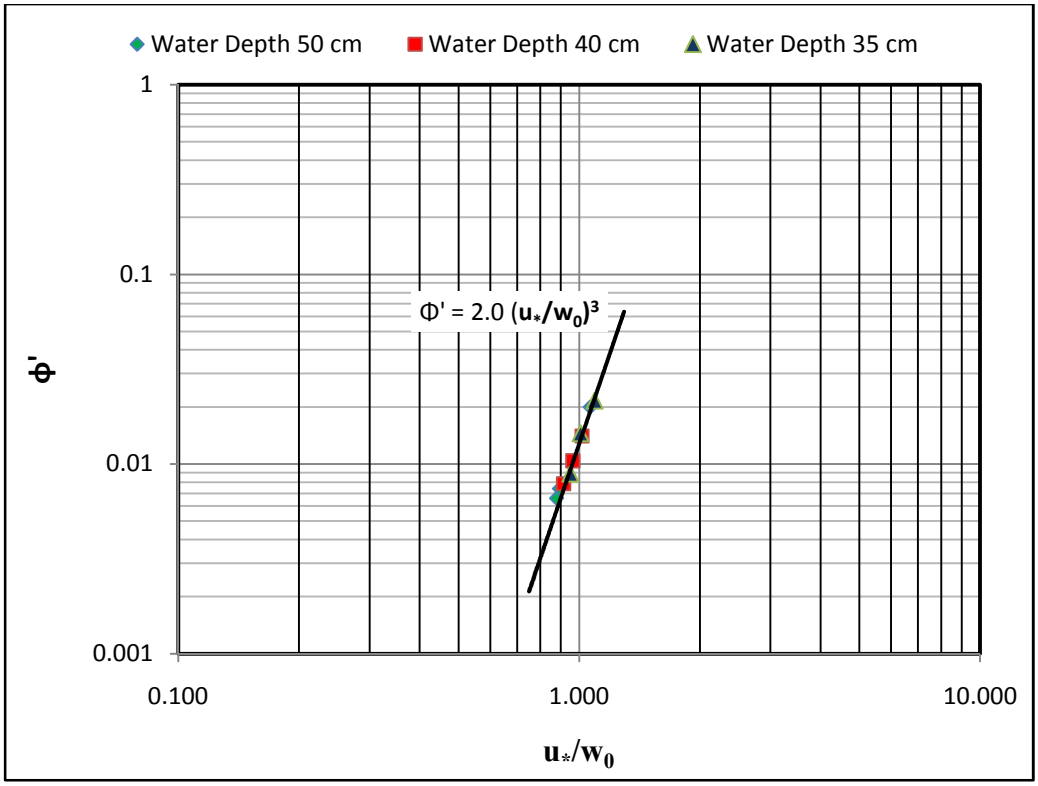

Figure 5.5.6: Correlation between Φ' and u_{*w}/w_0

5.5.2 Instantaneous sediment load transport

Instantaneous sediment load can be calculated by different formulas, which have been developed on some empirical concepts. In this study, the experimental data has been compared with some dominating and well known sediment transport formula to predict cross-shore transport due to non-breaking wave. In this study, two equations have been taken for consideration. The first consideration has been taken as the

Hallermeier (1982) formula. This formula consists least number of variables to calculate the sediment transport rate in the cross-shore direction. This formula has been developed to calculate the sediment transport rate for one cycle in oscillating flow.

$$q_{w,half} = \omega (d_{50})^2 (0.1\,\psi)^{1.5} \quad (5.5)$$

Where, $\psi = \frac{\hat{U}_\delta{}^2}{(s-1)gd_{50}}$ and $\omega = 2\pi/T$.

Table 5.5.5: Sediment load calculation by using Hallermeier (1982) formula

h (cm)	T (Sec)	H (m)	$\hat{U}_\delta$ (ms^{-1})	Ψ	$q_{w,half}$ (m^3/s/m)
50	1	0.120	0.1025	5.19	3.67x10^{-8}
	2	0.125	0.1738	14.92	8.95x10^{-8}
	2.5	0.115	0.2253	25.08	1.56x10^{-7}
40	1	0.110	0.1438	10.22	1.01x10^{-7}
	2	0.112	0.2054	20.85	1.48x10^{-7}
	2.5	0.105	0.2620	33.92	2.45x10^{-7}
35	1	0.100	0.1630	13.13	1.48x10^{-7}
	2	0.110	0.236	27.53	2.24x10^{-7}
	2.5	0.100	0.2886	41.16	3.28x10^{-7}

The second formula used for sediment transport is the van Rijn (1989) formula. This formula consist more variables. He proposed that, the transport rate due to asymmetric regular swell waves in the cross-shore area can be calculated by:

$$q_{w,net} = -0.00063\big((s-1)g\big)^{0.5}(d_{50})^{1.5}\left[\alpha_s(\Psi_{crest}-\Psi_{cr})^{1.7} - \alpha_s\big(\Psi_{trough}-\Psi_{cr}\big)^{1.7}\right] \quad (5.6)$$

Where, $\Psi_{crest} = \frac{(\hat{U}_{crest})^2}{(s-1)gd}$; $\Psi_{trough} = \frac{(\hat{U}_{trough})^2}{(s-1)gd}$ and $\Psi_{cr} = \frac{(\hat{U}_{cr})^2}{(s-1)gd}$

For shallow water, $\hat{U}_{crest} = \alpha\hat{U}_\delta$ and $\hat{U}_{trough} = (2-\alpha)\hat{U}_\delta$.

Where, $\alpha = 1 + 0.3(\frac{H_s}{h})$ and $\hat{U}_\delta = \frac{H}{2\sinh(kh)}$.

Table 5.5.6: Sediment load calculation by using van Rijn (1989) formula

h (cm)	T (Sec)	H (m)					$(m^3/s/m)$
50	1	0.120	0.1025	5.98	4.46	3.487	$1.20x10^{-8}$
	2	0.125	0.1738	17.25	12.81	3.487	$1.33x10^{-7}$
	2.5	0.115	0.2253	28.70	21.80	3.487	$3.32x10^{-7}$
40	1	0.110	0.1438	11.98	8.61	3.487	$6.96x10^{-8}$
	2	0.112	0.2054	24.58	17.47	3.487	$2.85x10^{-7}$
	2.5	0.105	0.2620	39.47	28.70	3.487	$6.38x10^{-7}$
35	1	0.100	0.1630	15.48	10.97	3.487	$1.20x10^{-7}$
	2	0.110	0.236	32.90	22.59	3.487	$5.19x10^{-7}$
	2.5	0.100	0.2886	48.51	34.45	3.487	$9.69x10^{-7}$

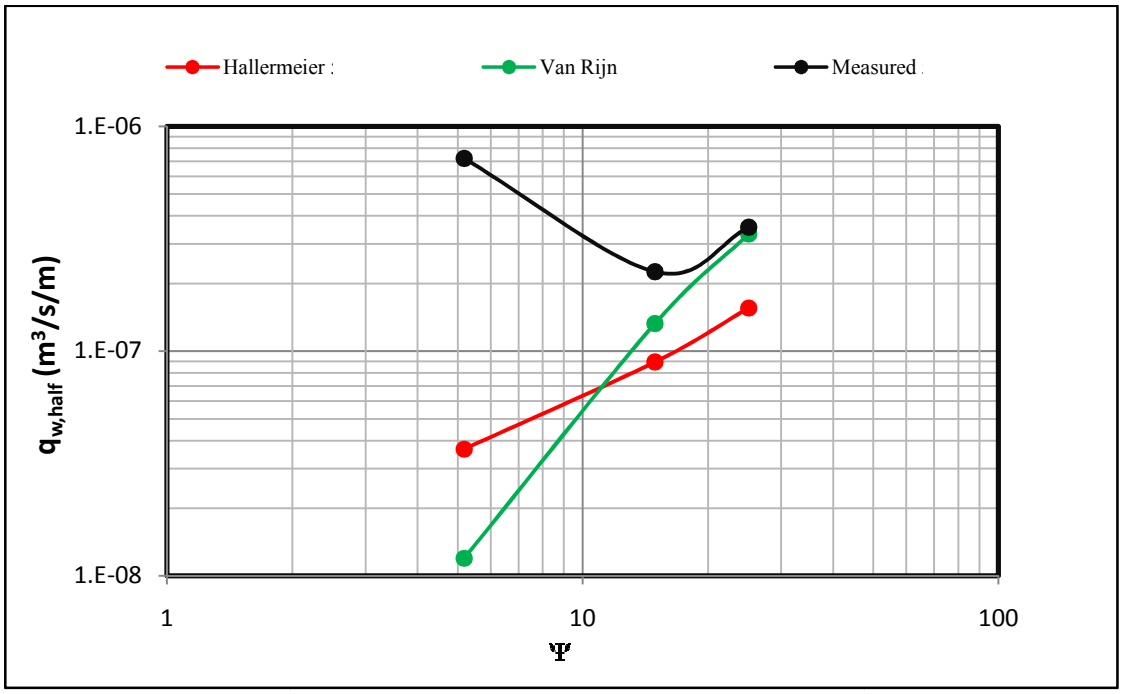

Figure 5.5.7: Comparison of sediment transport rate for 50 cm water depth

This comparison reveals that, the sediment transport rate does not varies too much by using these two formulas with the actual results obtained from the experiment. Therefore, it can be concluded that for small scale, these sediment transport formulae predict the rate of sediment transport with smaller variation. But in real practice the van Rijn formula is widely used. According to the study of Camenen et al. (2003) it has been observed that van Rijn formula gives good approximation for sediment transport.

Table 5.5.6: Sediment load comparison data

h (cm)	T (Sec)	H (m)	q_w (m^3/s/m) (van Rijn)	q_w (m^3/s/m) (Hallermeier)	Measured volume (cm^3/cm)	Measured transport rate (m^3/s/m)
50	1	0.120	$1.20x10^{-8}$	$3.67x10^{-8}$	54.00	$7.2x10^{-7}$
	2	0.125	$1.33x10^{-7}$	$8.95x10^{-8}$	16.90	$2.25x10^{-7}$
	2.5	0.115	$3.32x10^{-7}$	$1.56x10^{-7}$	26.67	$3.56x10^{-7}$
40	1	0.110	$6.96x10^{-8}$	$1.01x10^{-7}$	3.210	$4.28x10^{-8}$
	2	0.112	$2.85x10^{-7}$	$1.48x10^{-7}$	11.08	$1.48x10^{-7}$
	2.5	0.105	$6.38x10^{-7}$	$2.45x10^{-7}$	7.99	$1.07x10^{-7}$
35	1	0.100	$1.20x10^{-7}$	$1.48x10^{-7}$	3.72	$4.69x10^{-8}$
	2	0.110	$5.19x10^{-7}$	$2.24x10^{-7}$	9.93	$1.32x10^{-7}$
	2.5	0.100	$9.69x10^{-7}$	$3.28x10^{-7}$	11.73	$1.56x10^{-7}$

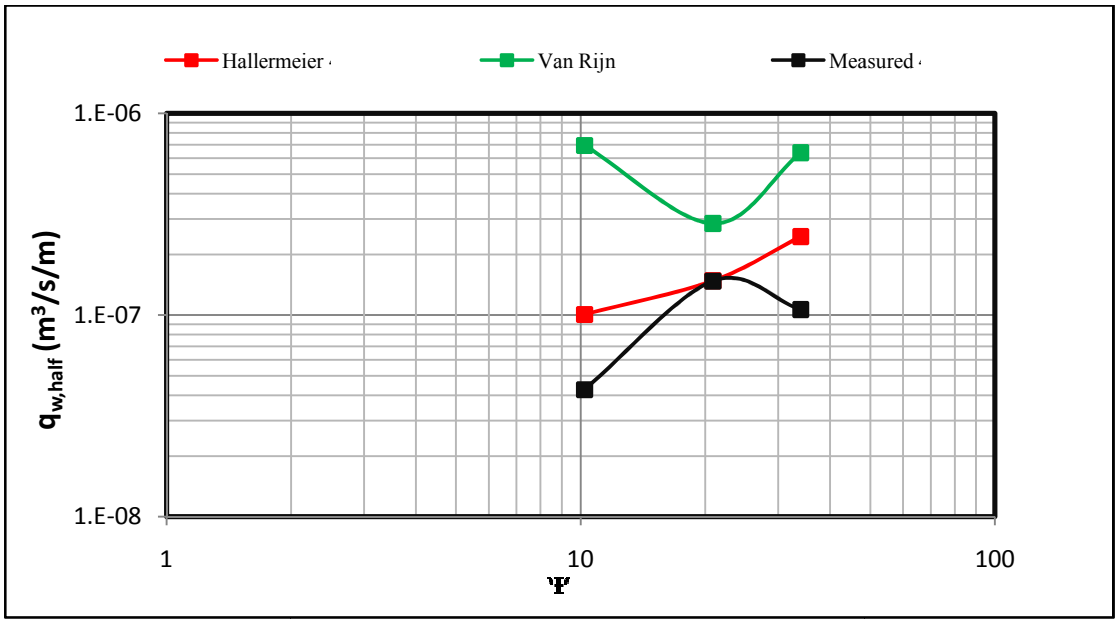

Figure 5.5.8: Comparison of sediment transport rate for 40 cm water depth

Form the analysis it has been found that, for 50 cm water depth, one data deviated much from the actual sediment volume. But for other two cases where water depth was 40 cm and 35 cm, the measured and calculated sediment transport rate was found to be quite close. Therefore, for small scale it can be concluded that the well known sediment transport rate formula calculates the transport rate with minor deviations from the actual measured transport rate. Furthermore, when the wave period was low, the calculated sediment transport rate by using these two formulas was deviated from the actual sediment volume movement. Therefore, for lower wave period as the

frequency of back-forth movement of wave is increased the calculated sediment transport rate shows some deviations.

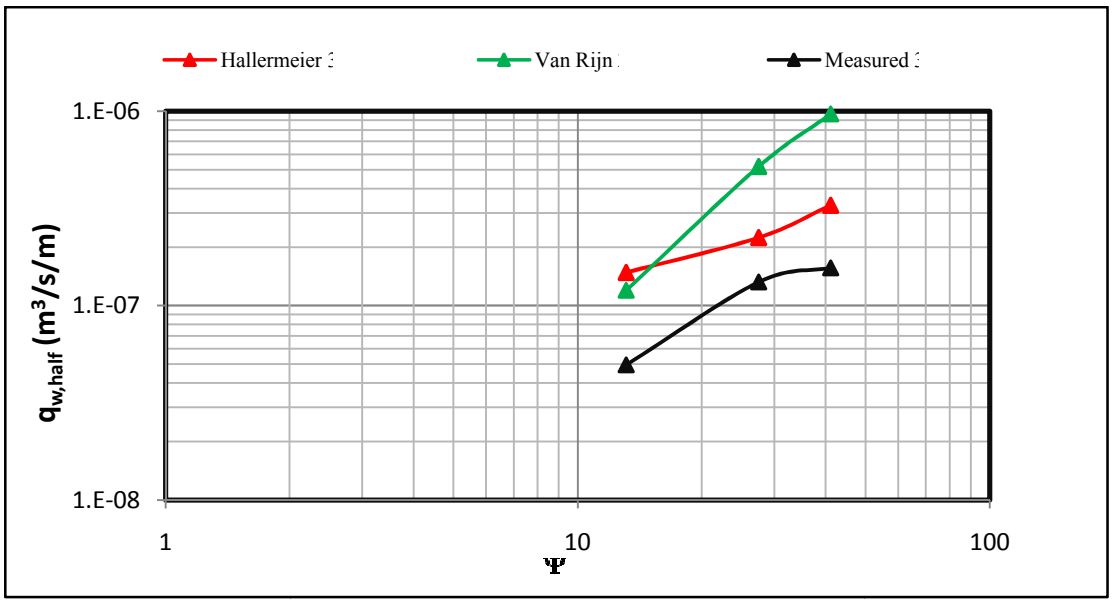

Figure 5.5.9: Comparison of sediment transport rate for 35 cm water depth

5.6 Comparison of bed profile due to non-breaking wave action

In this experiment, the bed profile data was measured after completing each experimental run with the help of point gage, and the values have been plotted. This bed profile gives the actual bed profile due to non-breaking wave. Then the experimental result has been compared with the Parabolic Wave Model output. In the model different wave parameter and sediment properties were incorporated and the final bathymetry was obtained.

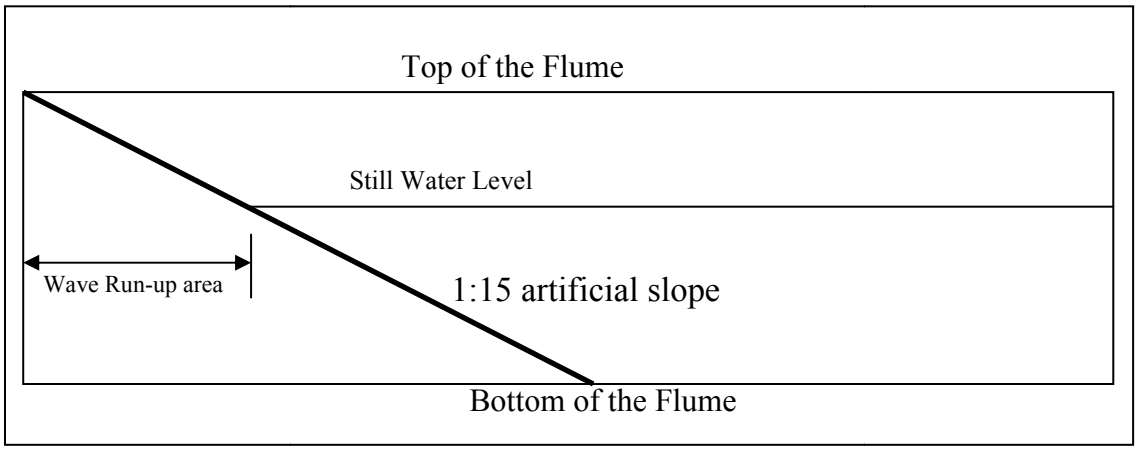

Figure 5.6.1: Schematic diagram of slope area along the centre line of the flume

Due to some limitations, the model cannot predict the bed profile above the still water level or in the wave run-up zone (Fig. 5.6.1). Wave run-up length is defined as the length where the effect of incident wave is active.

In the Fig. 5.6.2 to Fig. 5.6.10 the bed profile has been plotted at the end of each experimental run. In these figures, the initial bed, bed after completion of experimental run and model predicted bed are plotted along the center line of the flume. From these figures it can be observed that, the model prediction for bed profile was similar to that of experimental result except for the Run No 1, where a bar formation differs from the actual bed profile.

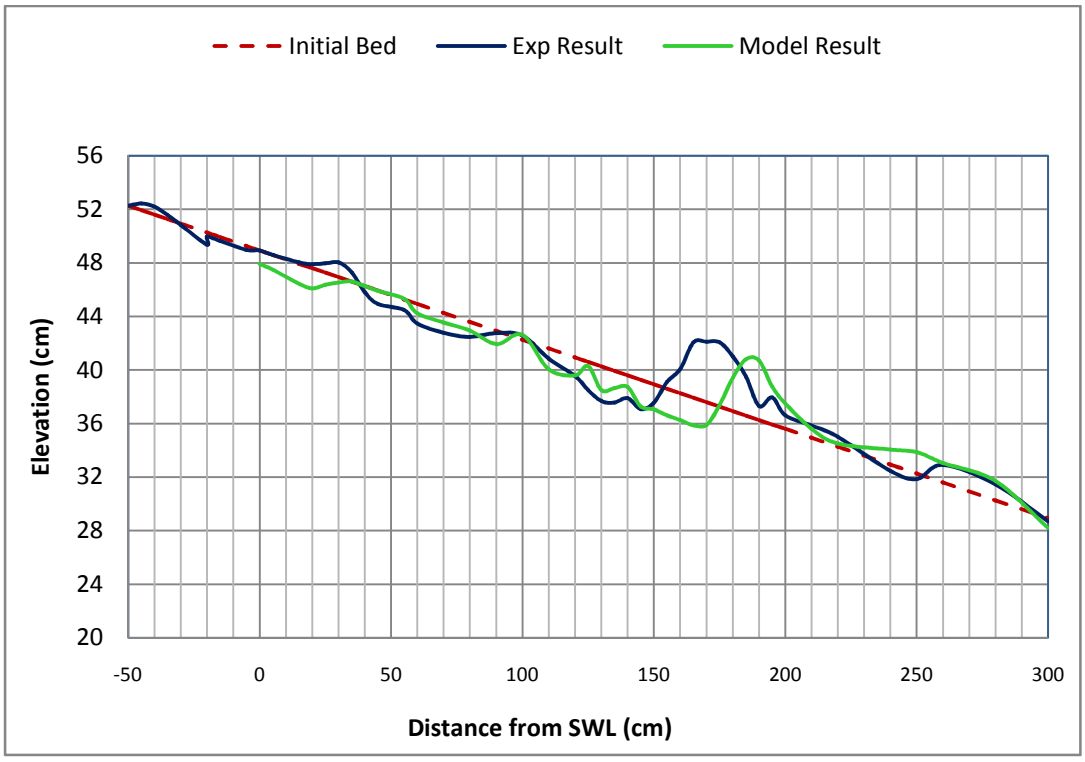

Figure 5.6.2: Bed profile for experimental run 1 (h = 50 cm, T = 1 sec)

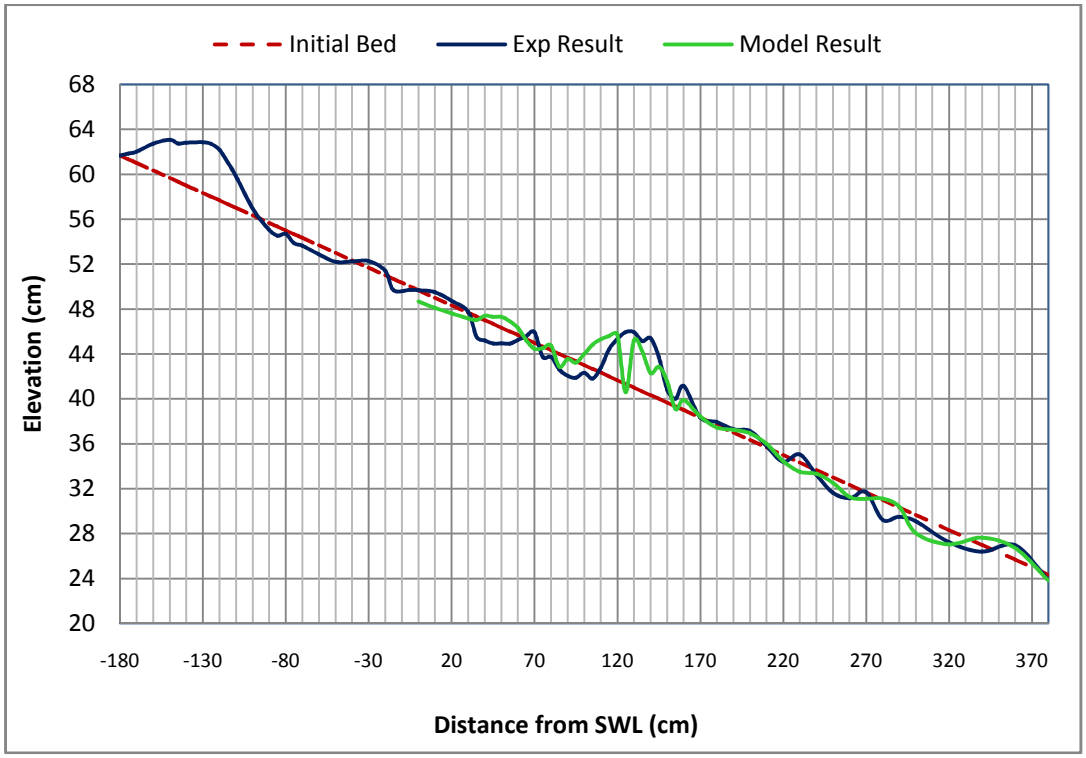

Figure 5.6.3: Bed profile for experimental run 2 (h = 50 cm, T = 2 sec)

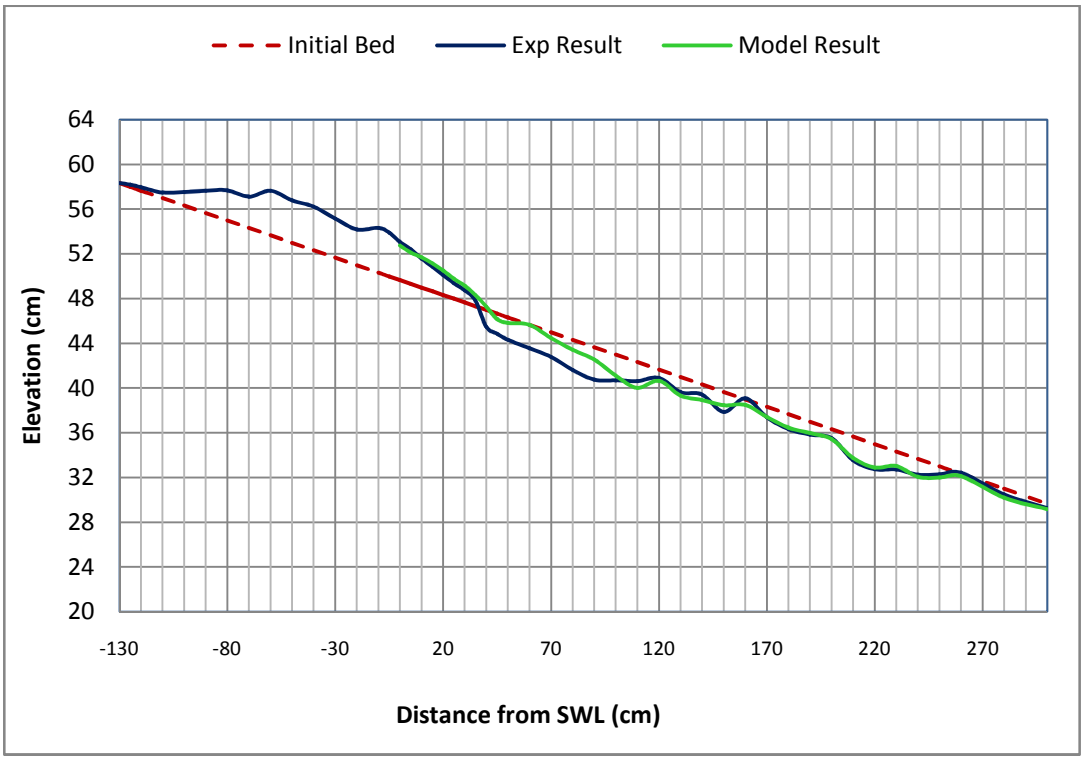

Figure 5.6.4: Bed profile for experimental run 3 (h = 50 cm, T = 2.5 sec)

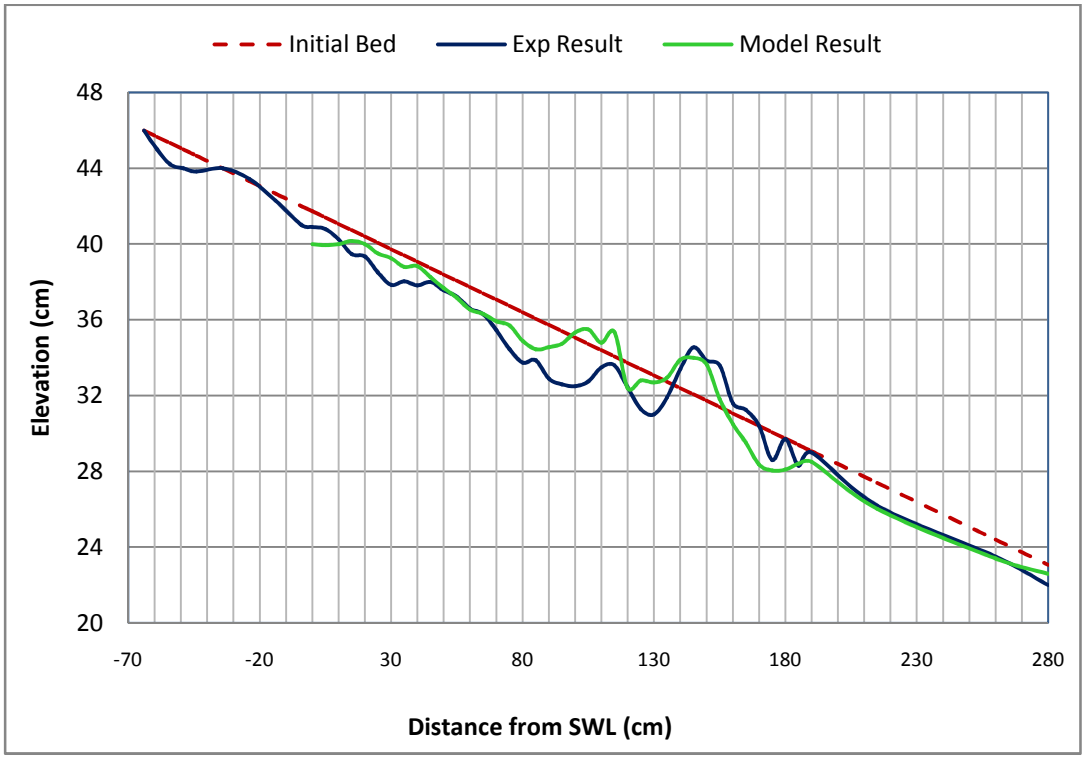

Figure 5.6.5: Bed profile for experimental run 4 (h = 40 cm, T = 1 sec)

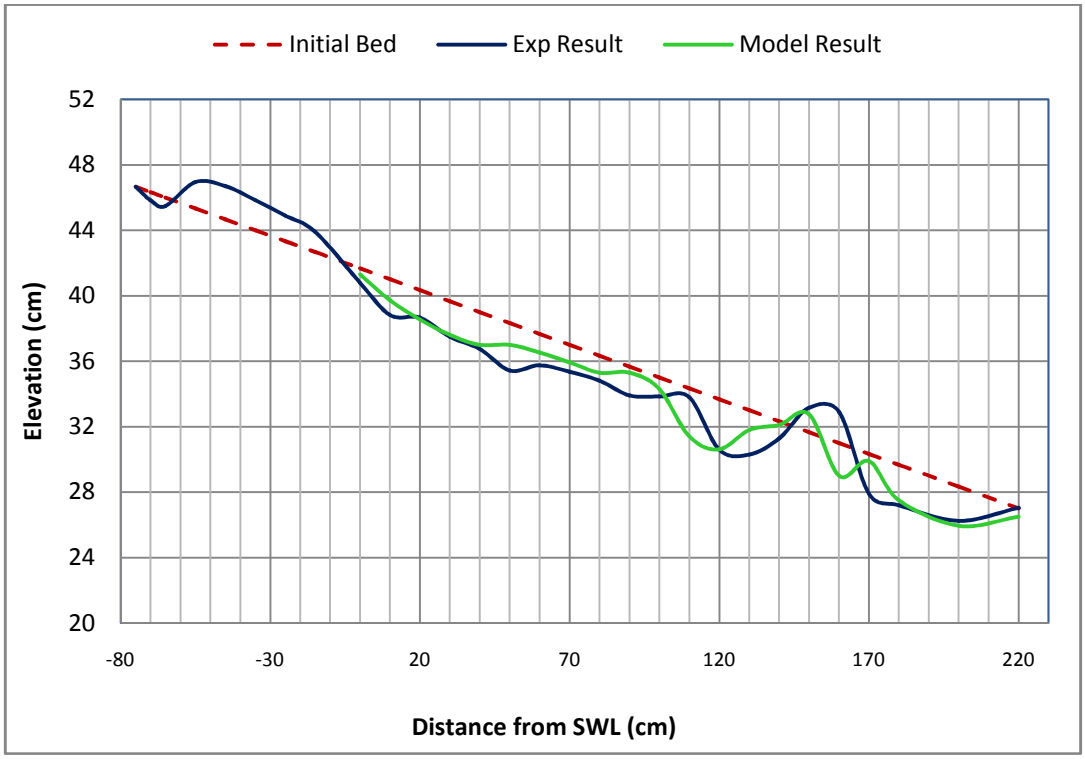

Figure 5.6.6: Bed profile for experimental run 5 (h = 40 cm, T = 2 sec)

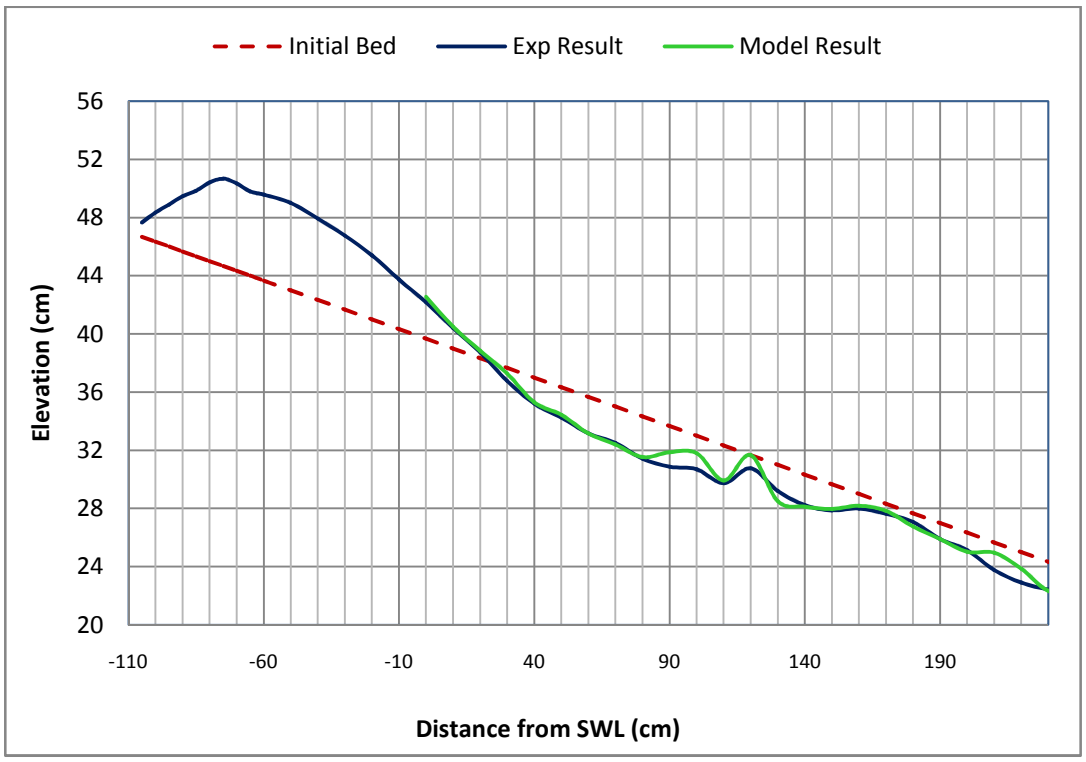

Figure 5.6.7: Bed profile for experimental run 6 (h = 40 cm, T = 2.5 sec)

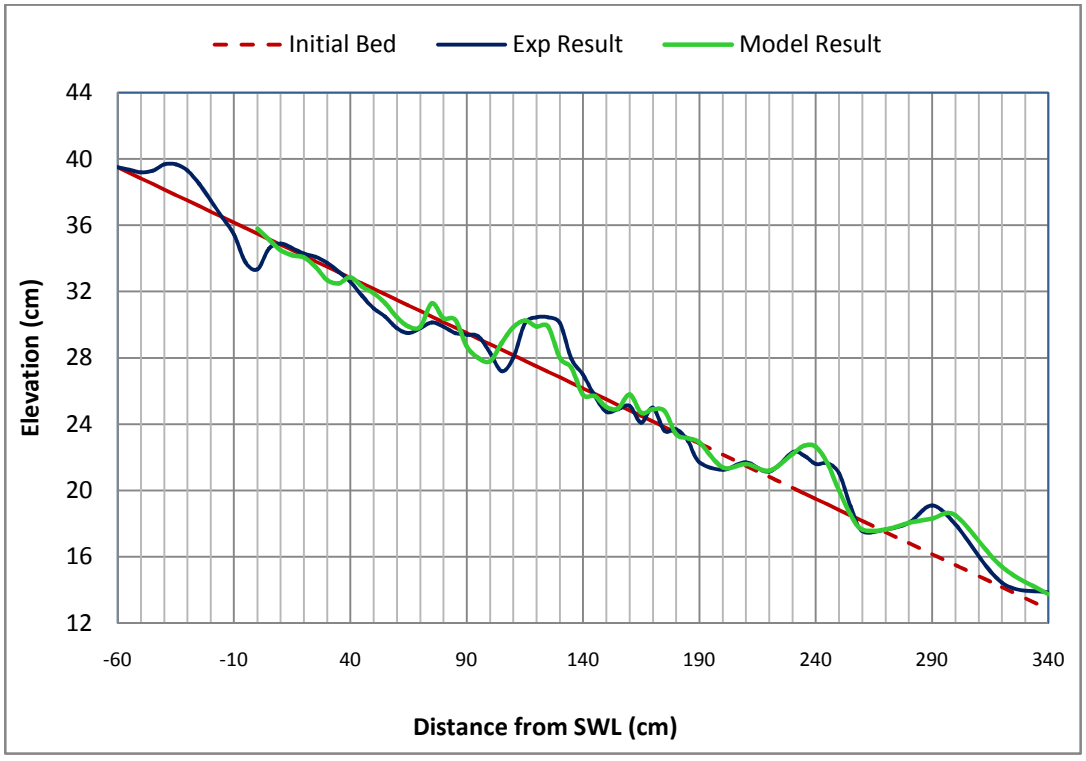

Figure 5.6.8: Bed profile for experimental run 7 (h = 35 cm, T = 1 sec)

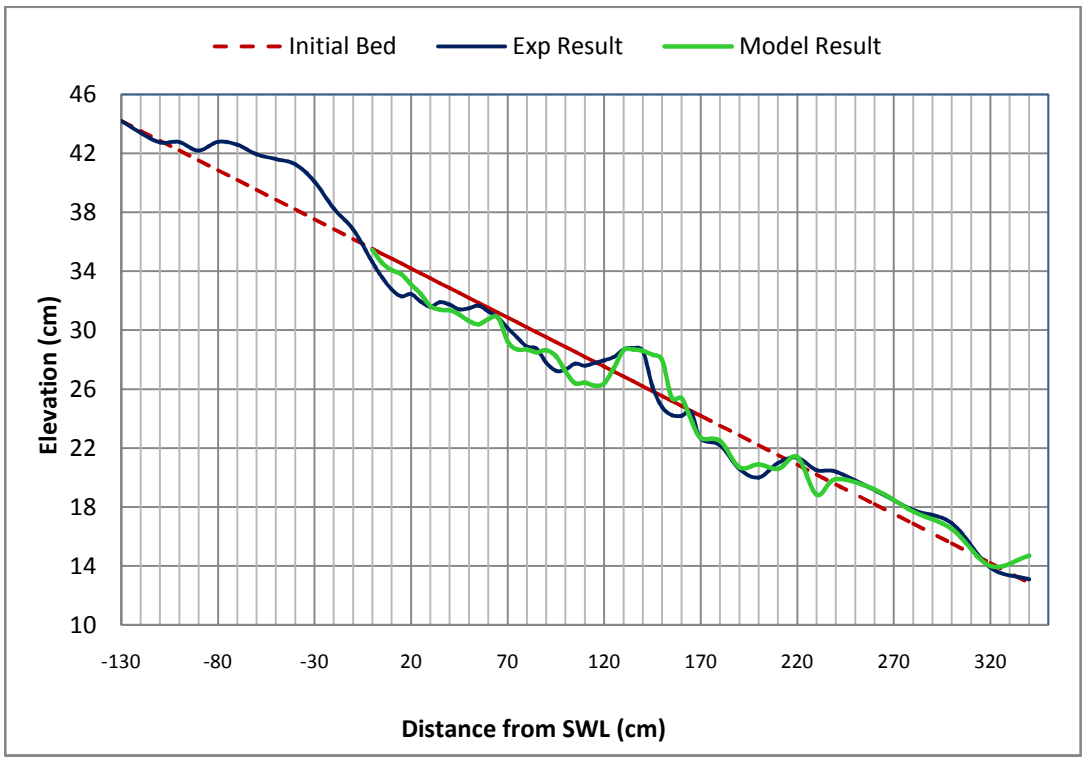

Figure 5.6.9: Bed profile for experimental run 8 (h = 35 cm, T = 2 sec)

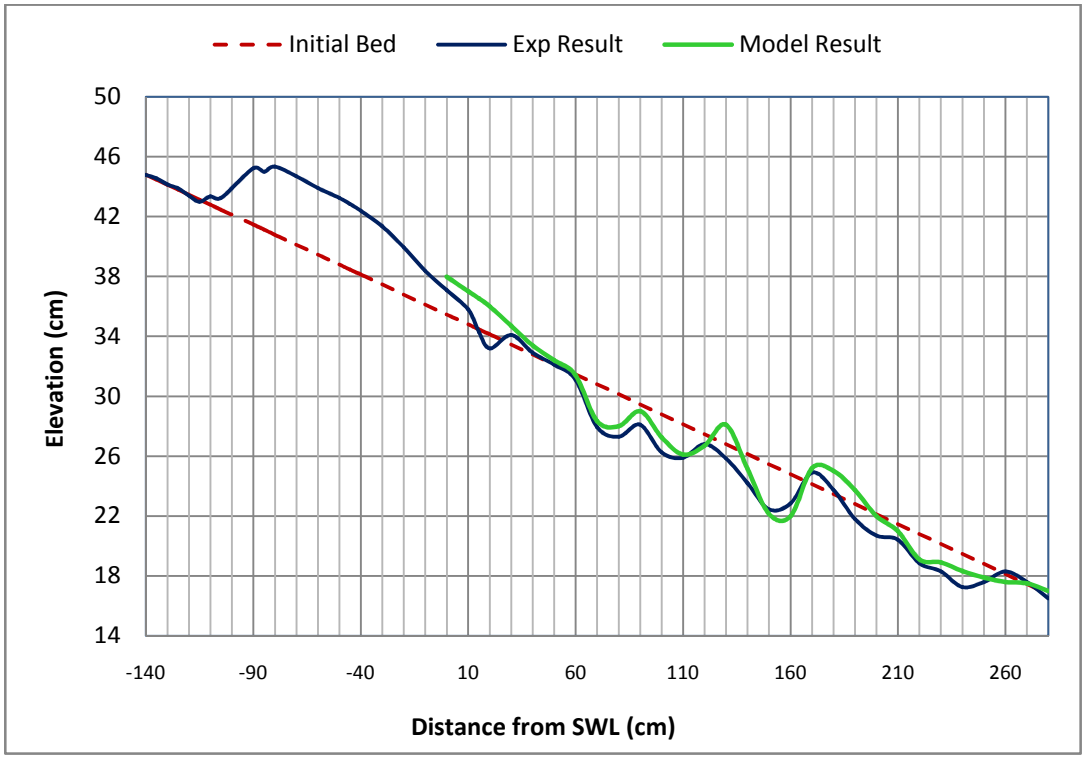

Figure 5.6.10: Bed profile for experimental run 9 (h = 35 cm, T = 2.5 sec)

In the flowing photographs (Photograph 5.6.1 to 5.6.3) some bed profiles are presented to visualize the effect of wave induced current in the experiment.

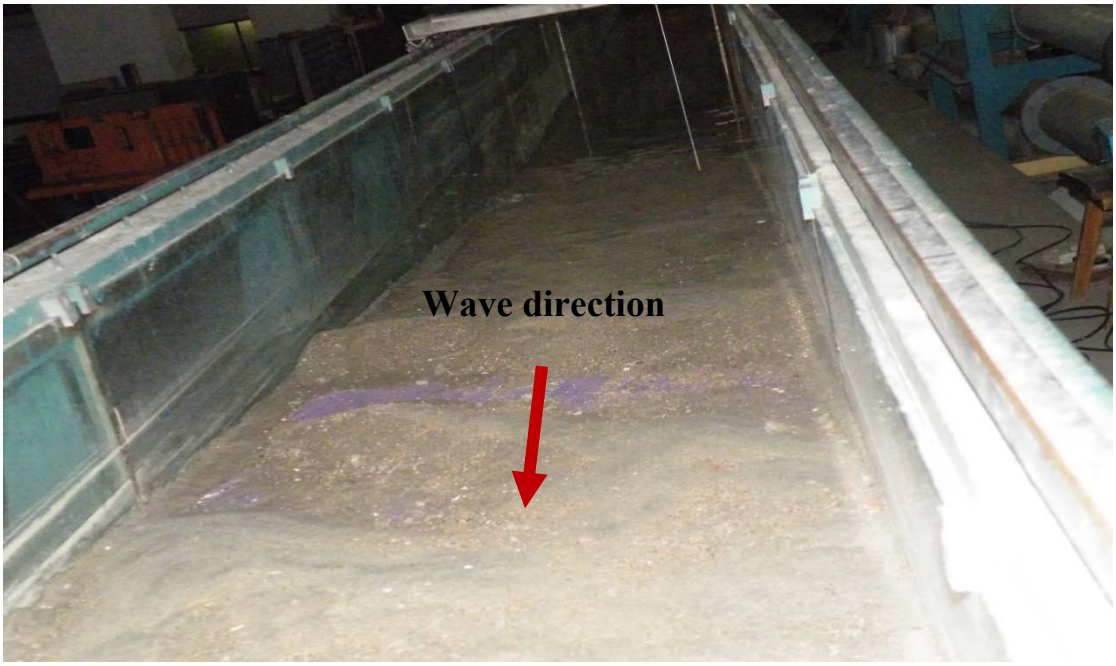

Photograph 5.6.1: Actual bed profile Run No. 1 (onshore area)

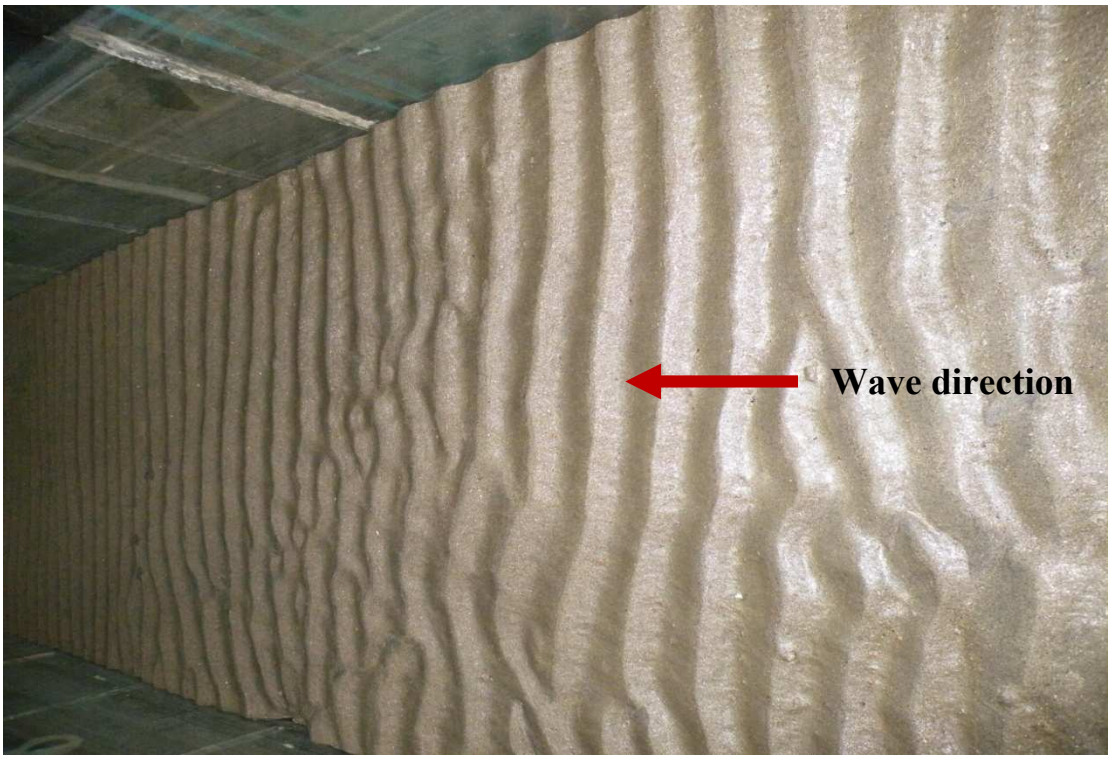

Photograph 5.6.2: Actual bed profile Run No. 4 (offshore area)

Photograph 5.6.3: Actual bed profile Run No. 4 (onshore area)

5.7 Comparison of velocity data

In this experiment, actual velocity was measured by using a programmable 2-D velocity meter. Type of the meter is E.M.S; ACM200-A of ALEC ELECTRONICS. In the Fig. 5.7.1 the positions for taking the velocity component has been shown. The distance between two consecutive locations for taking velocity was 10 cm. In the Fig. 5.7.2 to Fig.5.7.9 the x-component (V_x) of measured and simulated velocity by using Parabolic Wave Model has been plotted. These values are the centerline velocity on the slope. From the experiment it was found that the magnitudes of velocities in these three lines were similar for every case. These figures illustrate that, the actual and model predicted velocity data are almost same with minor deviation. In some cases, the actual data deviated from the model prediction. This deviation might be occurred due to the placement of velocity meter and the interference of flume glass sided wall. Overall the comparison is acceptable.

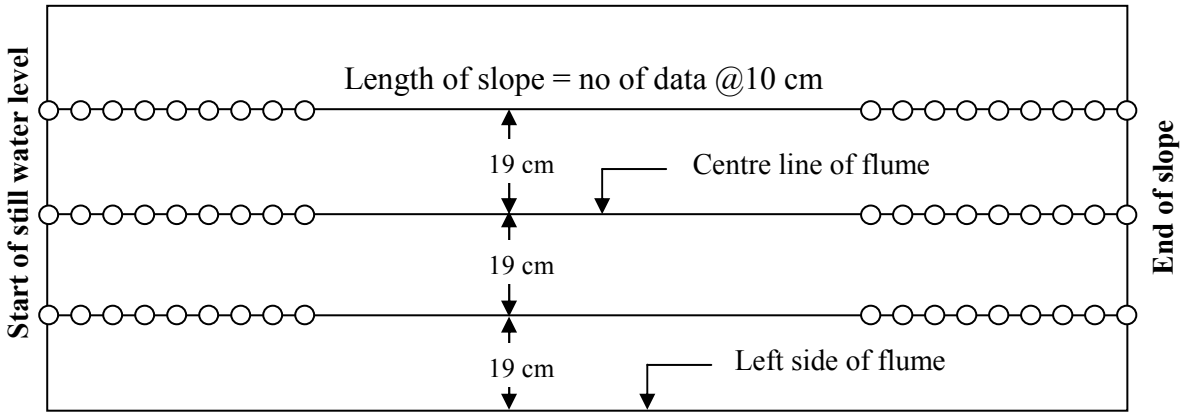

Figure 5.7.1: Plan view of the position for taking velocity data along the slope length

Fig.5.7.10 to Fig.5.7.11 shows the y-component (V_y) of the velocity that was measured and simulated by using the model. For this case, the deviation is also negligible. Therefore, the validation of the model is established to predict the bed profile as plotted in the earlier section.

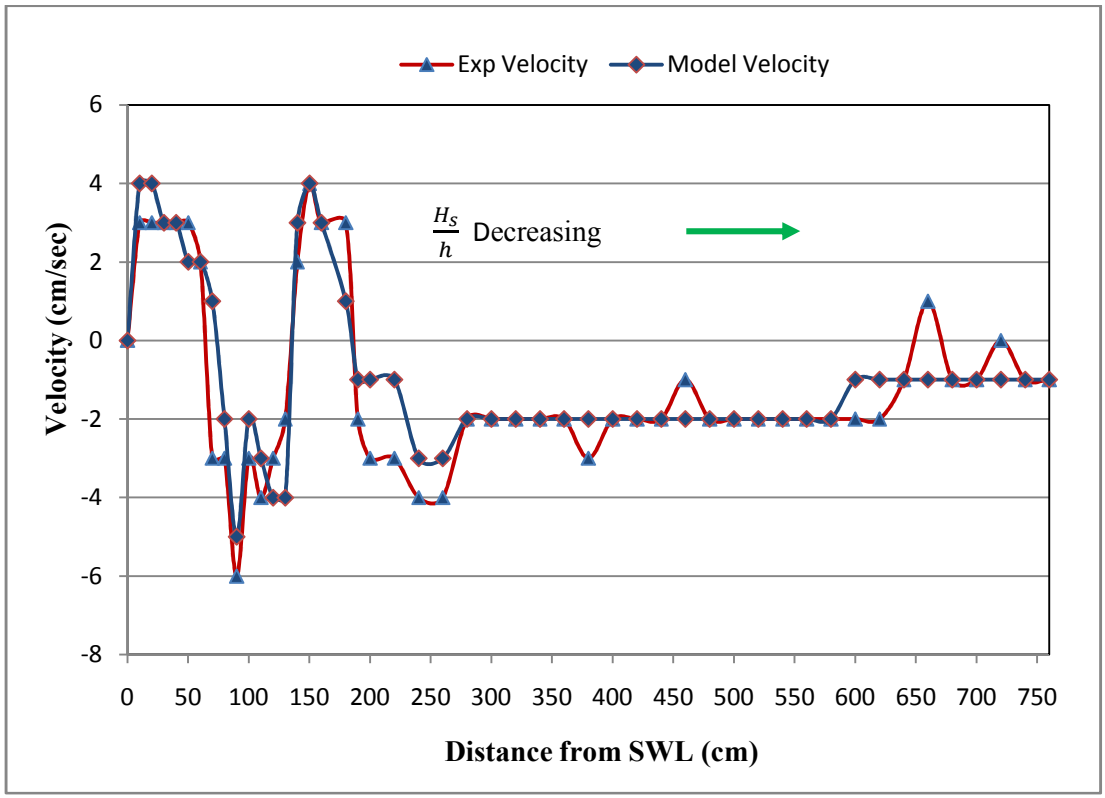

Figure 5.7.2: Velocity data (V_x) at centerline for experimental run no 1

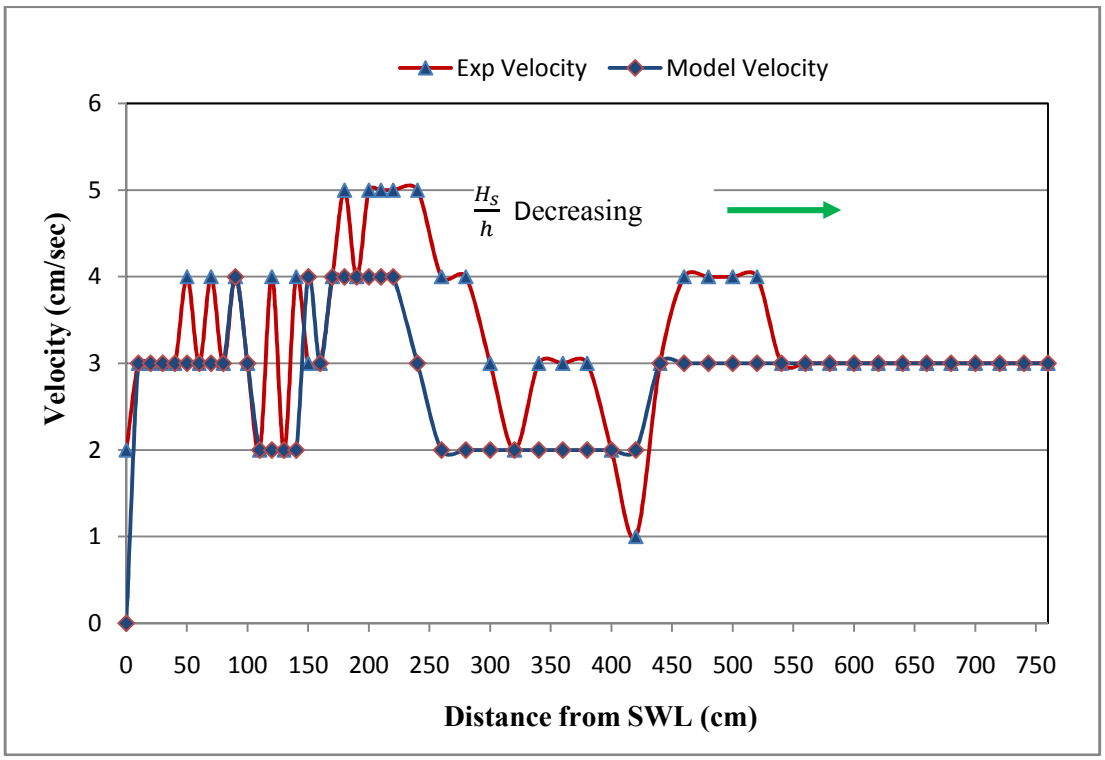

Figure 5.7.3: Velocity data (V_x) at centerline for experimental run no 2

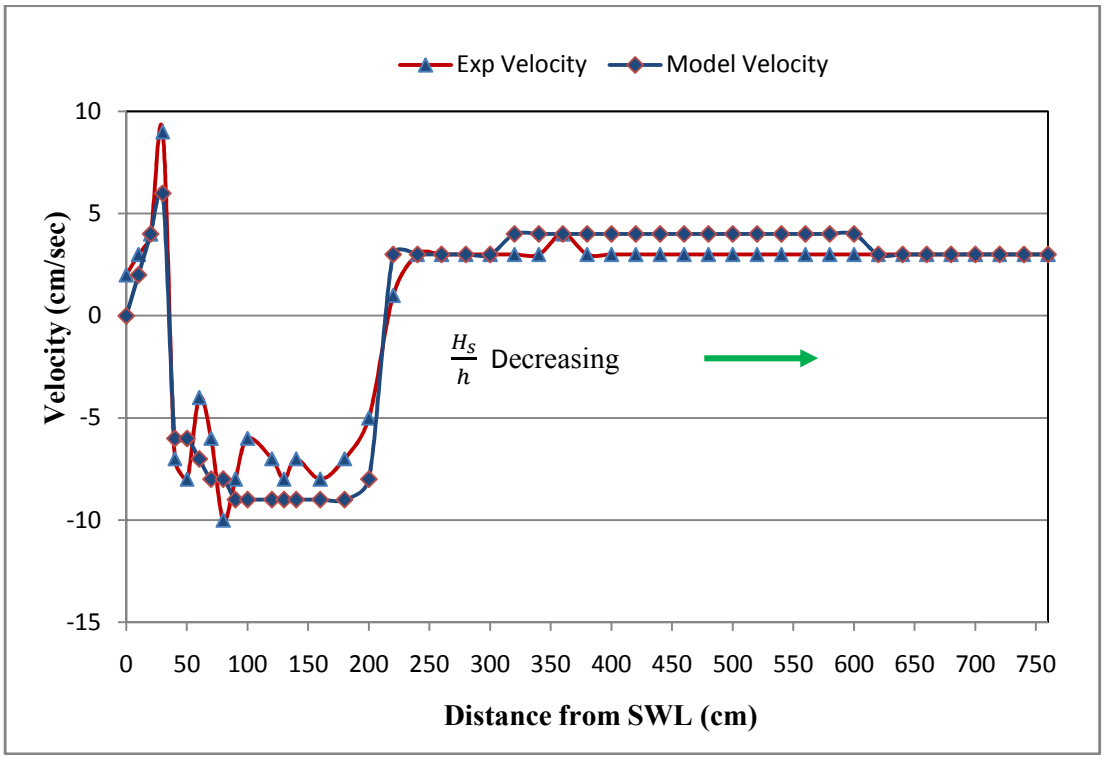

Figure 5.7.4: Velocity data (V_x) at centerline for experimental run no 3

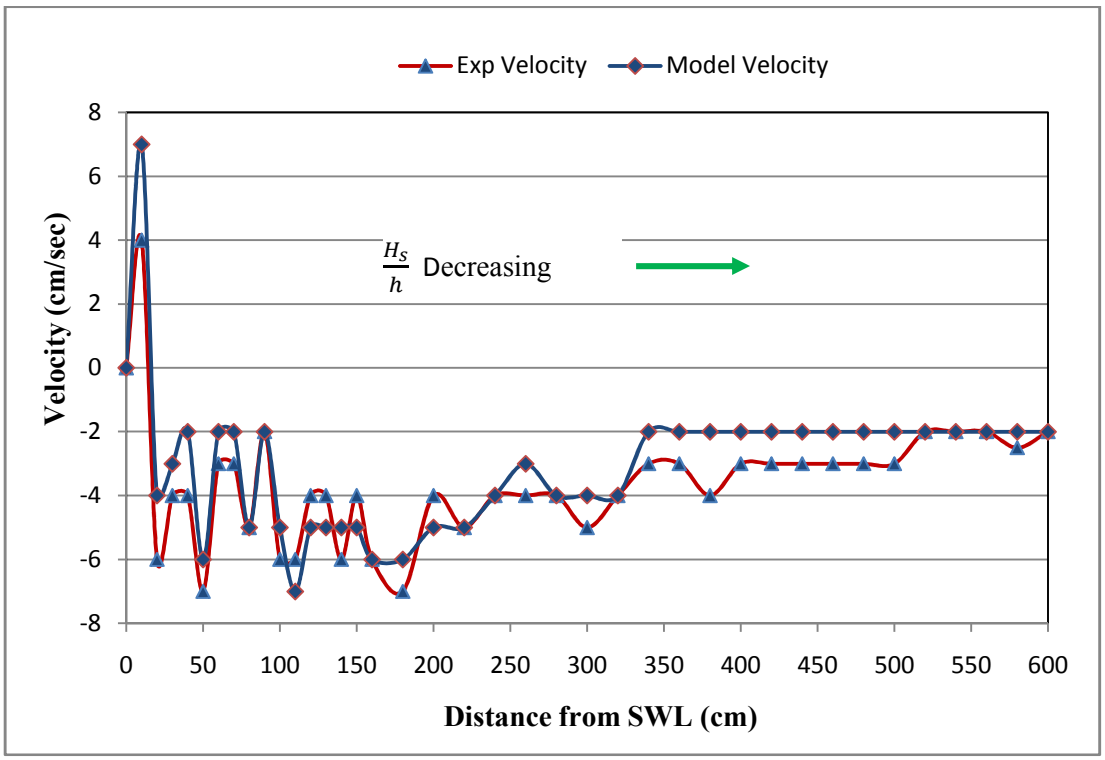

Figure 5.7.5: Velocity data (V_x) at centerline for experimental run no 4

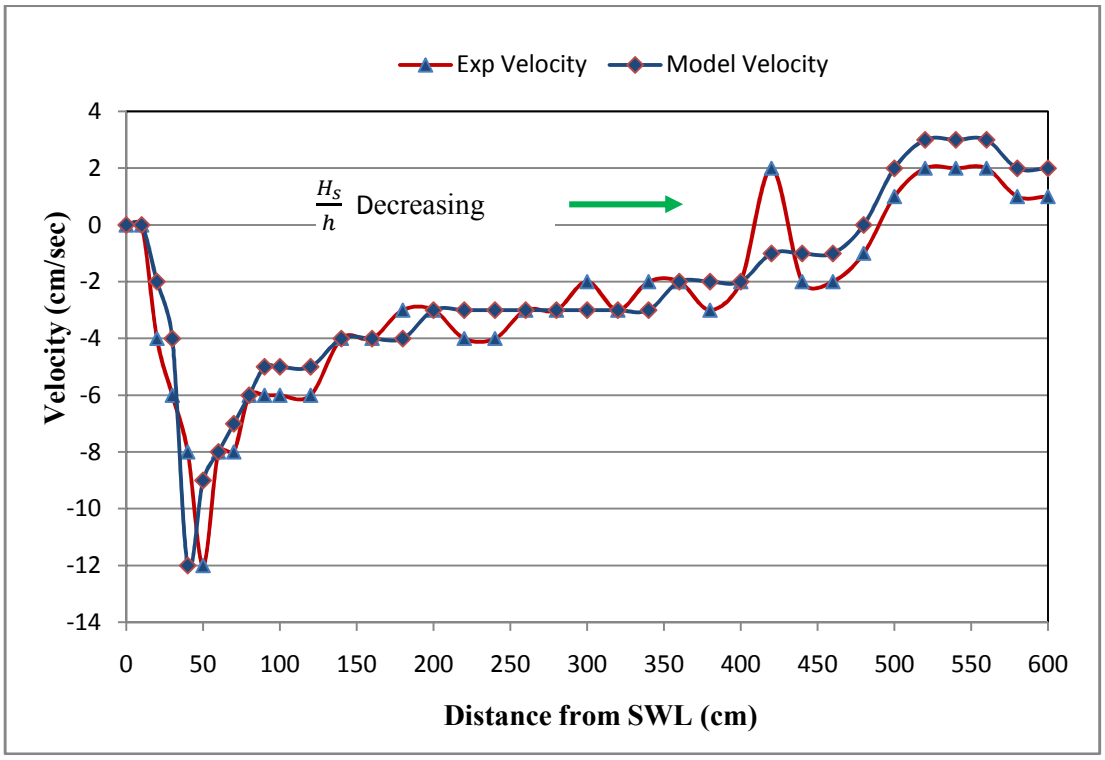

Figure 5.7.6: Velocity data (V_x) at centerline for experimental run no 6

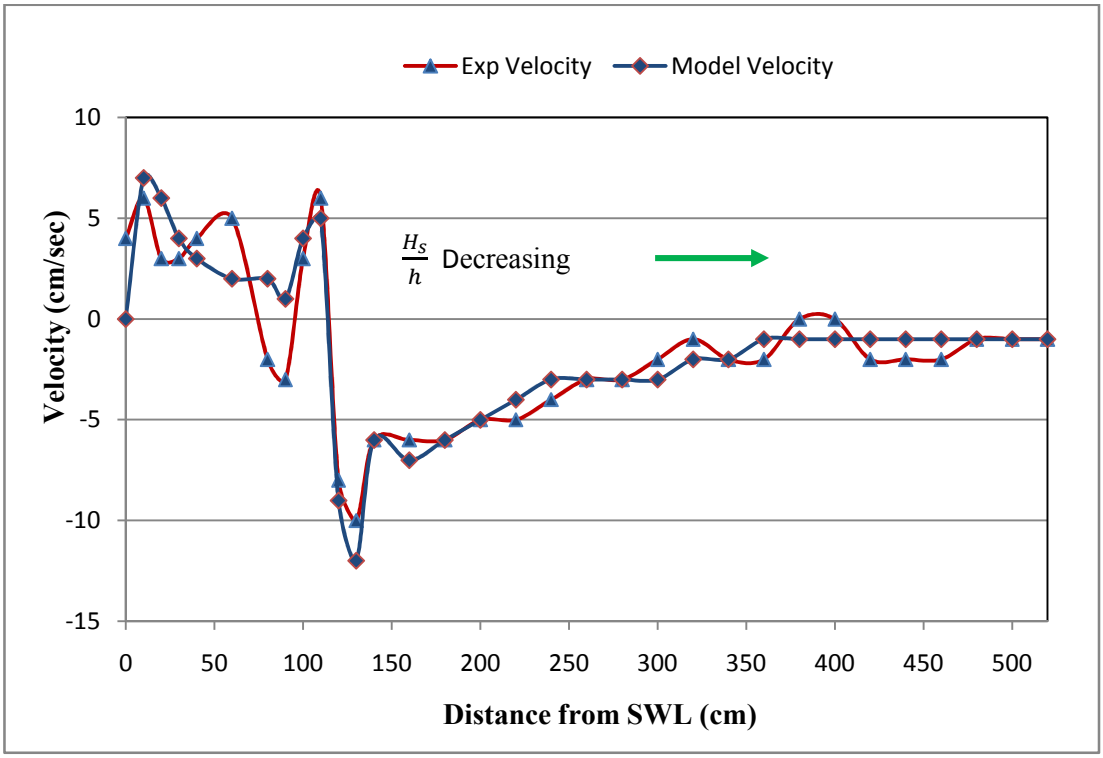

Figure 5.7.7: Velocity data (V_x) at centerline for experimental run no 7

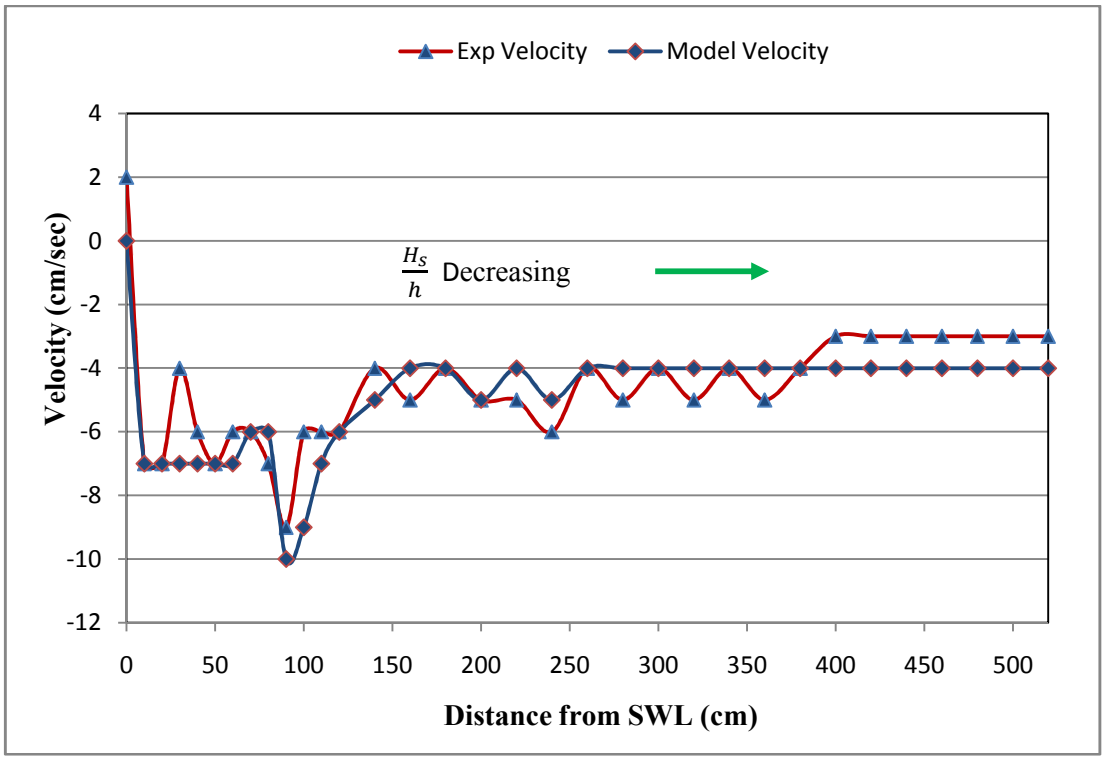

Figure 5.7.8: Velocity data (V_x) at centerline for experimental run no 8

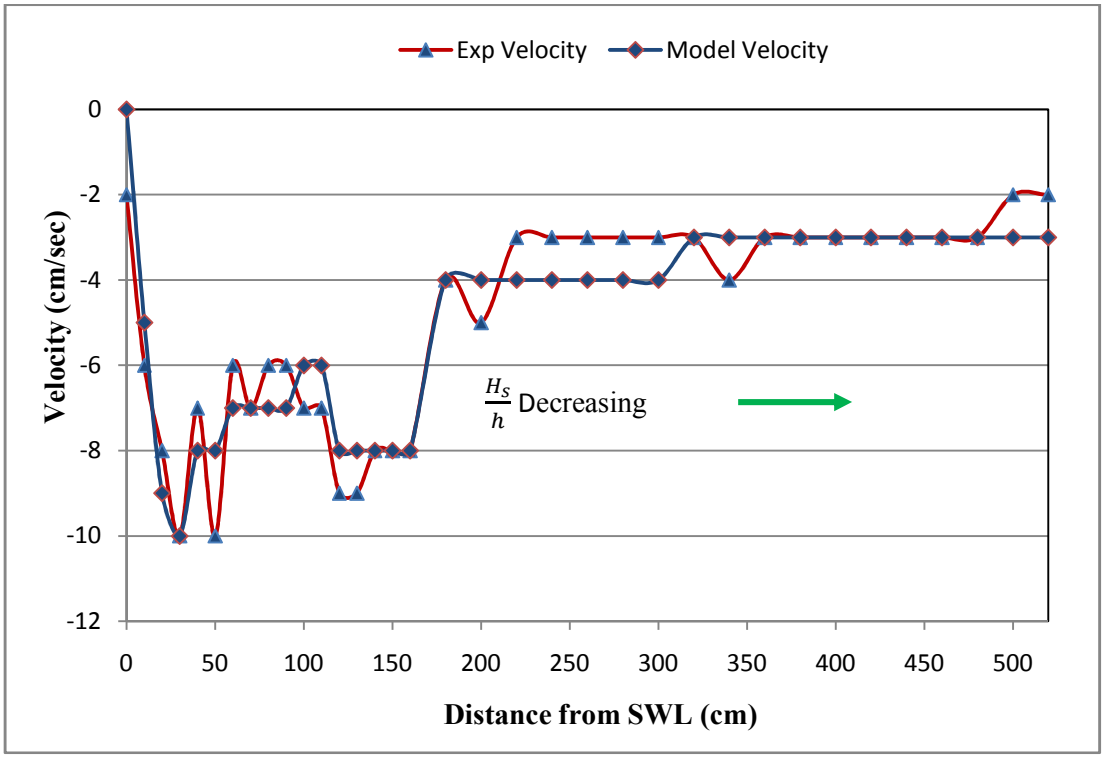

Figure 5.7.9: Velocity data (V_x) at centerline for experimental run no 9

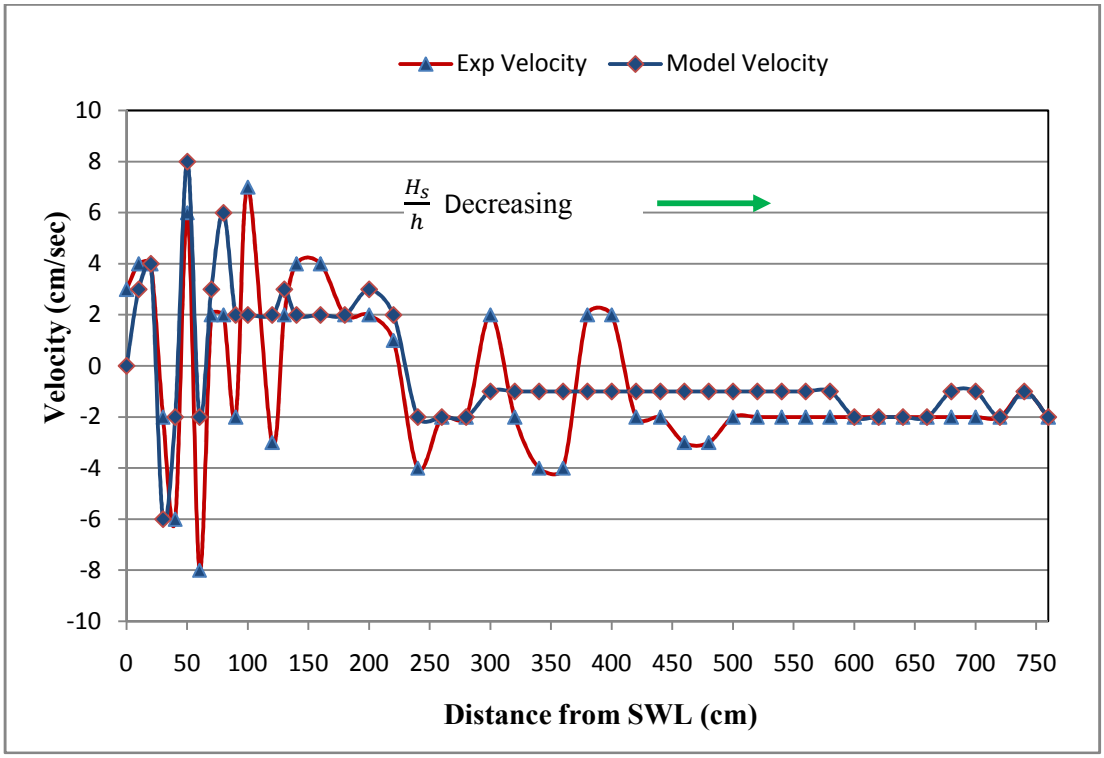

Figure 5.7.10: Velocity data (V_y) at centerline for experimental run no 3

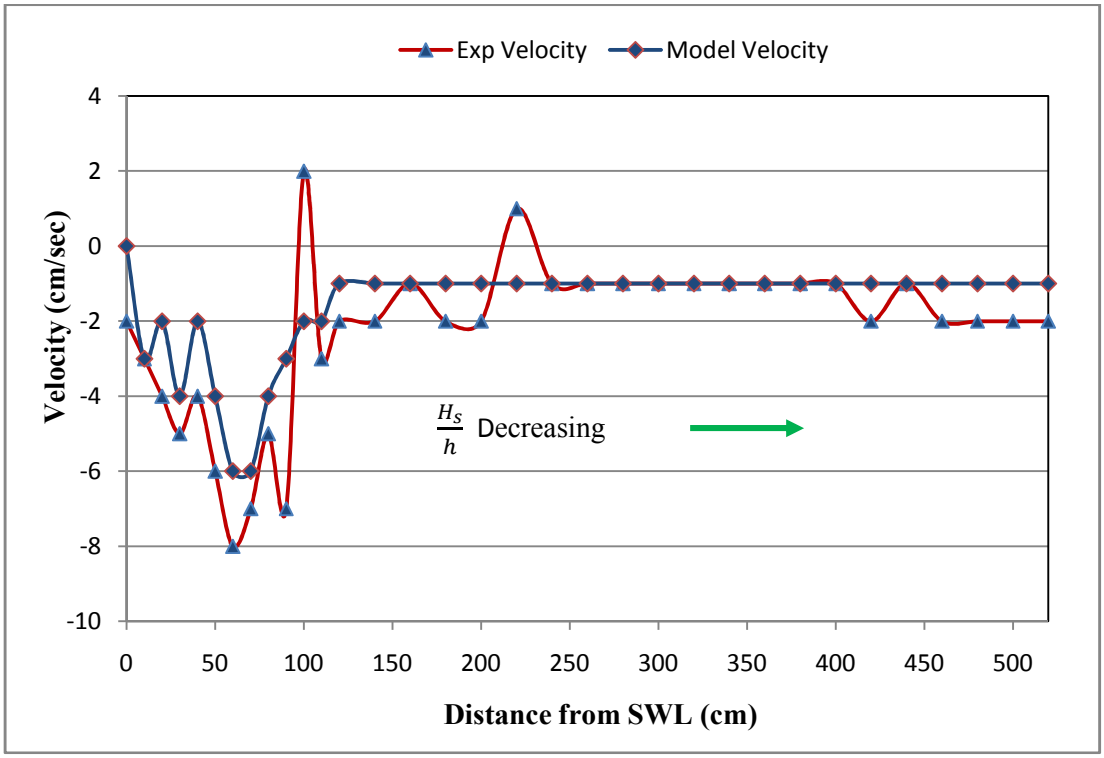

Figure 5.7.11: Velocity data (V_y) at centerline for experimental run no 8

5.8 Change of bed profile by using breakwater and CC Blocks

One of the objectives of this study was to investigate the bed profile change by using floating and submerged breakwater in the wave flume. Herein the same condition was also compared by using CC Block on the prepared slope.

The experimental result indicated that, for the submerged breakwater, the wave height was increased by 4 to 5 cm downstream of the breakwater compared to the upstream wave height of 12 cm. Hence the entire sand bed was disappeared after 20 minutes of the run (Photograph 5.8.1 to 5.8.3). As the wave height increases, so it requires more length for diminishing the effect of breakwater in the flume. In the experimental setup this condition was hard to attain and in nature this might be true. Therefore, the use of submerged breakwater in non-breaking wave did not exhibit any positive impact to minimize the beach erosion.

The study result for floating breakwater showed rather good response. In this case, it has been observed that, the wave height decreases to the downstream of breakwater so the bed elevation or the sediment volume was increased as it carried some sediment towards the near-shore zone (Fig. 5.8.1).

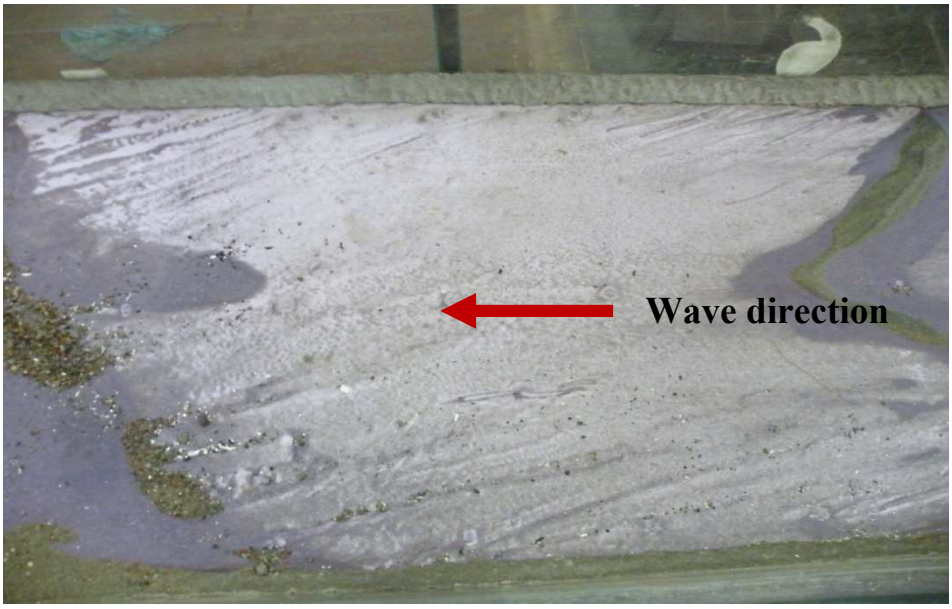

Photograph 5.8.1: Bed condition for Run No. 10 (onshore area)

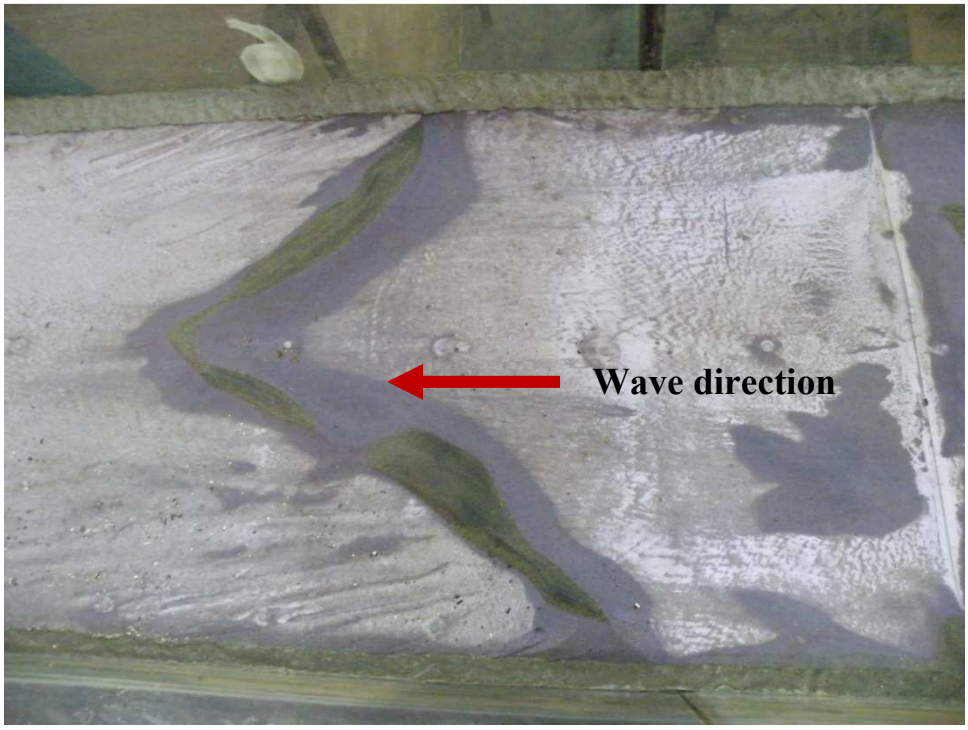

Photograph 5.8.2: Bed condition for Run No. 10 (onshore area)

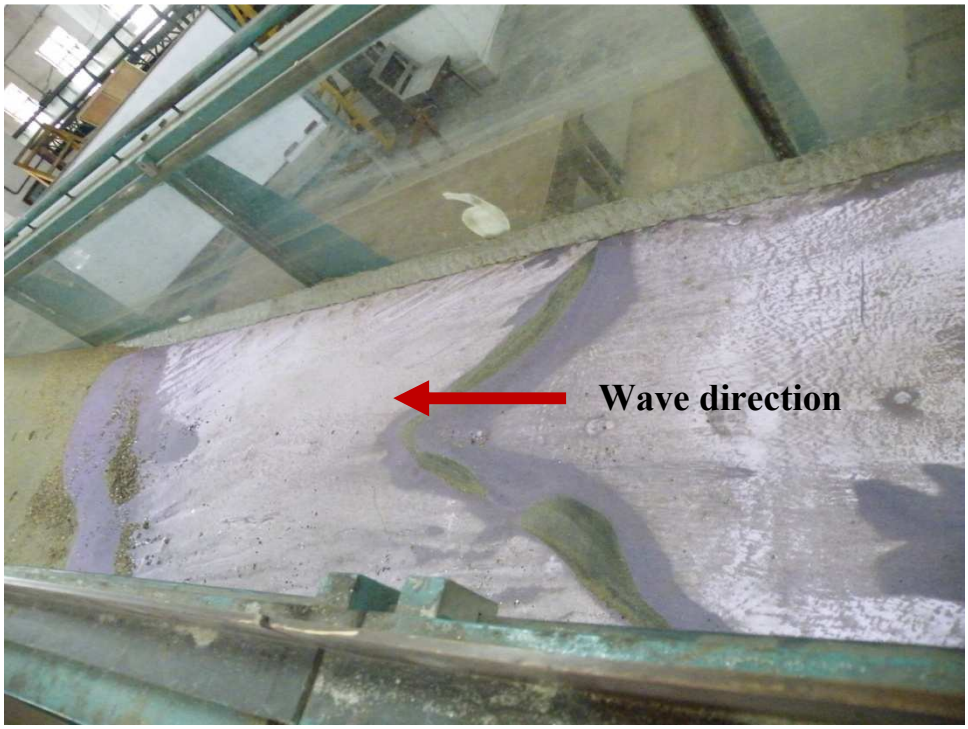

Photograph 5.8.3: Bed condition for Run No. 10 (onshore area)

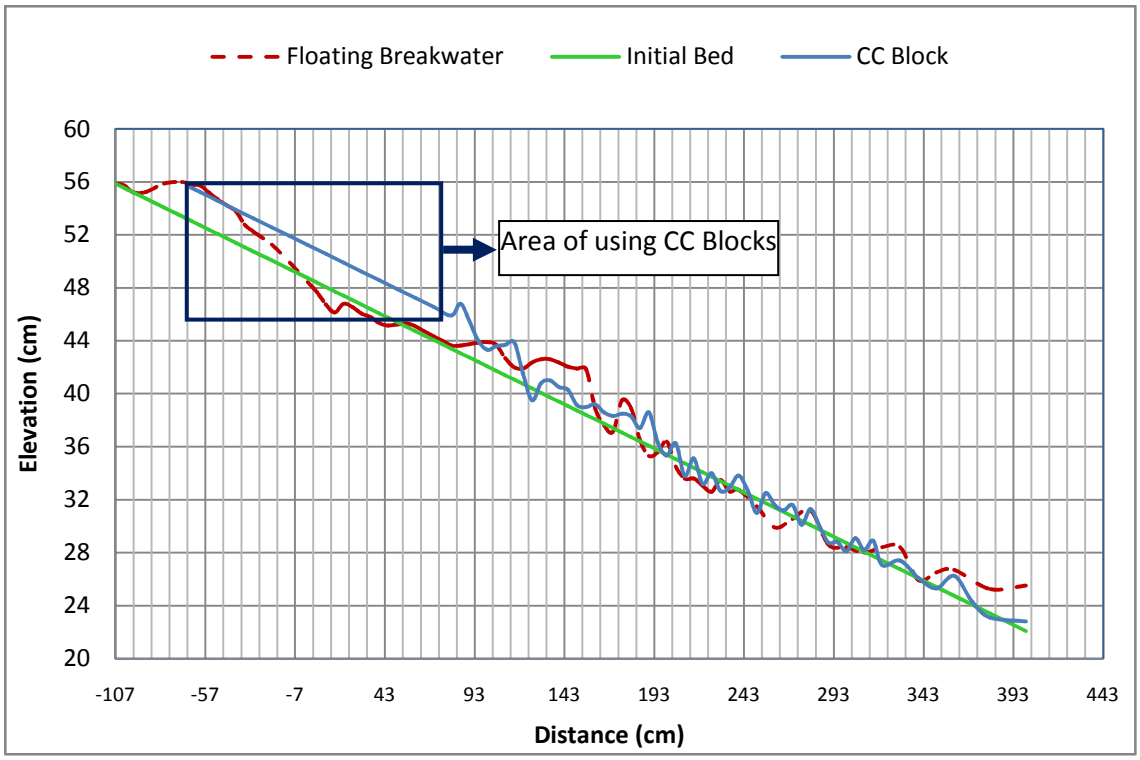

Figure 5.8.1: Bed profile by using CC block and breakwater

In this experiment, the effect of CC blocks (3.5cmX 3.5cm X 2.5cm) on the beach slope was also observed. Fig.5.8.1 represents the bed profile after the completing experimental run with CC blocks and floating breakwater. From this figure, it is evident that the bed elevation did not change too much when the CC blocks were used on the initial sandy beach slope.

So, the use of CC block for protecting the sand erosion or sediment erosion is effective to protect the coastal properties, though the cost of CC blocks is a major hindrance for adopting this. But it requires further elaborative and comparative study to make any concrete decision.

5.9 Change of Gradation of Bed Material Due to Wave Action

On natural beaches, sand sizes usually vary over a wide range. Fine and coarse sands in an initially well-mixed seabed can be sorted after sustained wave action. For ripples, the circulation is forced primarily by vortices over the uneven ripple profile (Sleath, 1974). Laboratory evidence of sand sorting in ripples has been confirmed by Foti and Blondeaux (1995). For sand bars, the circulation of a much larger length scale is dominated by the variation of wave amplitude. While sorting can be qualitatively anticipated from the theory of mass transport in the bottom boundary layer (Noda, 1968; Carteret et al., 1973), quantitative prediction requires more systematic and comprehensive data from experiments.

Theoretical modeling of sand bars of heterogeneous sand is difficult in view of our meager knowledge of resuspension (fluidization) and deposition in oscillatory boundary layers, and of the two-phase mechanics of turbulence. To observe the change of gradation of sediment particle under wave action, in this experiment sieve analysis has conducted for the bed material. In this study three representative runs (Run no 2, 4 and 9) were taken for observation. For these three runs the soil sample was collected before and after the completion of run for four locations (Fig. 5.9.1).

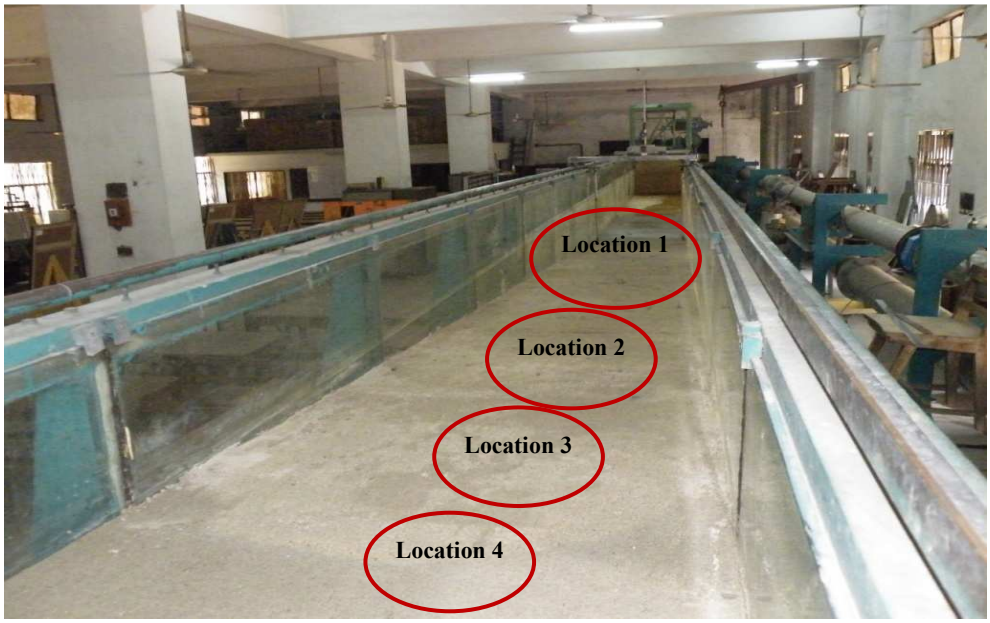

Figure 5.9.1: Location of sample collection on the slope

Samples were collected from four different locations on the slope. Location 1 was taken at the bottom part of the slope i.e. where the bottom of the flume is horizontal. Location 2 was selected on the slope of the artificial beach. Location 3 was selected on the slope where the wave strikes and Location 4 was taken on the slope in the area of wave run-up.

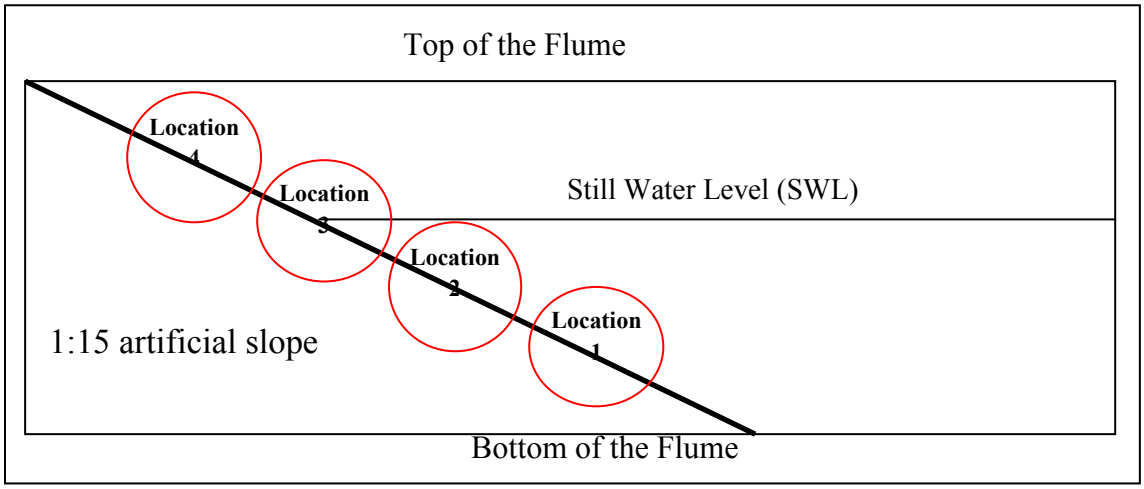

Figure 5.9.2: Side view of the location for sample collection on the slope

For observing the changes of soil sample gradation due to wave action arbitrarily three runs were taken (Run No. 2, 4 and 9). Fig. 5.9.3 represents the soil sample

gradation of a particular run in the location 1. Other soil sample gradation curves are represented in the Appendix B for detail.

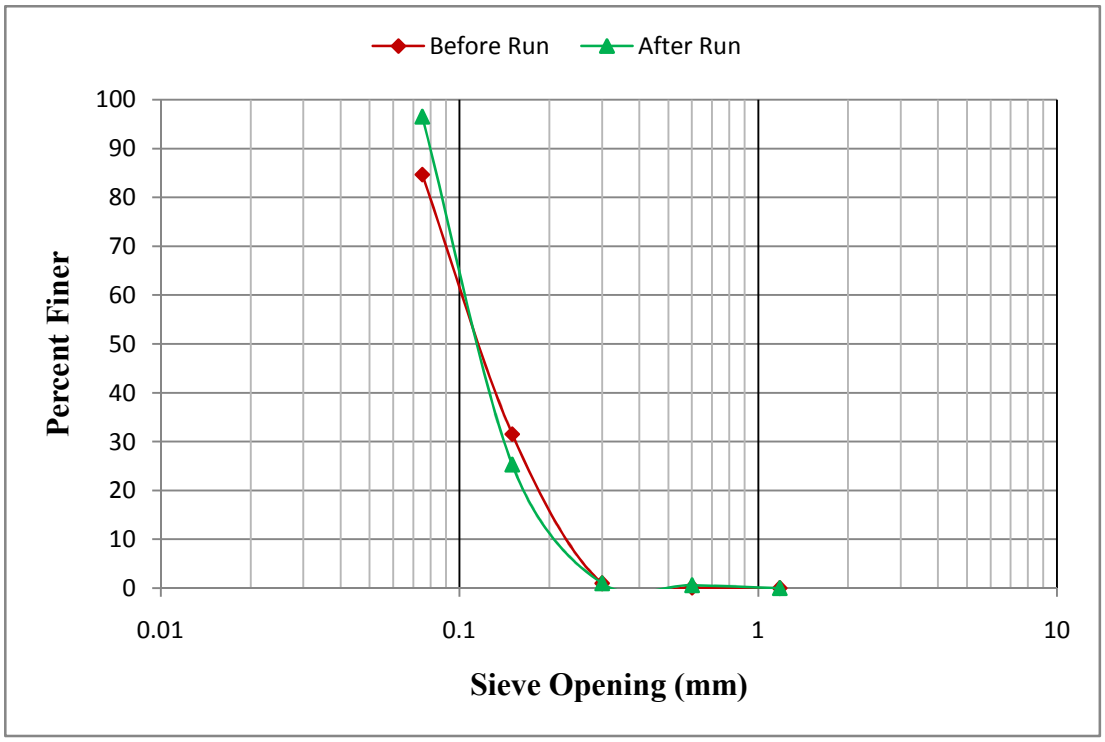

Figure 5.9.3: Grain size distribution at location 1 for Run No 2

Form these analyses it has been observed that the value of d_{50} for run no 2 (before and after run) remains same for the Location 1, but for Location 2 the d_{50} value was found as 0.125 (before run) and 0.12 (after run).

The value of d_{50} for the Location 3 was found as 0.16 mm (before run) and 0.2 mm (after run). This value indicates that the gradation of soil sample is increased by a significant amount hence the finer particles moves towards the sea and the coarser particle moves towards the shore. In Location 4 same trend was also observed as the d_{50} value changes from 0.12 mm to 0.14 mm.

The gradation changes for the other two runs at four different locations are represented in the Appendix B.

From this analysis, it is evident that the change of sediment gradation on the slopping beach varies at different locations (Table 5.9.1). In the four locations selected for observation, Location 1 and Location 2 shows no or very insignificant gradation change for sediment particle for all the representative runs.

But the picture is completely different in the Location 3 and Location 4 on the slope. In these locations, the median diameter of sediment particle is increased greatly as the incident wave breaks to some extent in the Location 3, but for Location 4 wave run-up plays a crucial role as it transports the coarser suspended sediment towards the onshore zone.

Another important observation is evident that, for the maximum representative cases the gradation curve shifts towards the right direction after the wave action. Hence, it can be stated that the overall grain size of the sediment is increased towards the onshore zone by the wave attack for newly constructed beach profile.

Table 5.9.1: Comparison Table for change of d_{50} values at different locations

Run No	**Location**	**d_{50} (mm) Before Run**	**d_{50} (mm) After Run**
Run No 2	Location 1	0.12	0.12
	Location 2	0.125	0.12
	Location 3	0.16	0.2
	Location 4	0.12	0.14
Run No 4	Location 1	0.12	0.115
	Location 2	0.13	0.12
	Location 3	0.14	0.17
	Location 4	0.17	0.18
Run No 9	Location 1	0.13	0.128
	Location 2	0.11	0.11
	Location 3	0.17	0.21
	Location 4	0.15	0.21

Therefore, for constructing new structures in the near-shore zone the sediment induced load should be taken into account as the gradation curves state that the gradation of sand particles are not uniform before and after the incident wave action.

5.10 Summary

In this chapter the experimental values have been compared with some well established formula to calculate the sediment transport rate in the cross-shore direction. Therefore, some non-dimensional correlations have been formed as well as the experimental bed profile is compared with the model data.

Furthermore, the response of bed profile with different breakwater and CC blocks has been observed. In addition to this the variation of sediment gradation has been observed due to wave incidence on the slope.

CHAPTER 6

Conclusions and Recommendations

6.1 General

The simplest concept for sediment transport is that wave makes the sand suspended in the water by the back and forth movement of the oscillatory wave when the current is not present. After that the deposition or erosion in the bed takes place depending on the sediment properties and wave properties. Therefore, the final bed profile is formed in the standing wave when it does not break.

The waves produce asymmetric bottom orbital velocities in shallow water. The wave orbital velocity is stronger in the direction of wave propagation under the crests. It is weaker against the direction of wave propagation under the troughs. This complex phenomenon causes the sediment to move in the cross-shore direction.

In addition to this, grain size is another fundamental feature for sediment movement in the cross-shore direction. Furthermore, with different wave parameters, the response of transport varies as found from the study and shown in different literature studied by the author.

6.2 Conclusions

By conducting detail and rigorous experimental investigation, data analysis and model study, presented in the previous chapters, the synopsis of the study has been presented as follows:

1. In the study it has been observed that the prepared laboratory beach slope is an erosion type beach. (Section 5.3).
2. The experimental result has revealed that, the volume of sediment to the onshore zone was increased with the increase of wave period when water depth was

decreasing. Hence wave period and water depth have significant functions for sediment movement or beach formation (Section 5.4).

3. From this study it has been found that, the movement of sediment to the offshore direction is dominating (Section 5.5).
4. The correlation formed between non-dimensional cross-shore sediment transport rate and Shields parameter were found as $\Phi = 6.8\,(\Psi_m - \Psi_c)\Psi_m{}^{0.48}$ and $\Phi' = 11.6\Psi_m{}^{2.8}$ (Section 5.5).
5. In this study an important relationship between non-dimensional cross-shore sediment transport rate and Critical Shear Velocity has been developed. The relationship is found to be $\Phi' = 2.0(\mathbf{u_*/w_0})^3$ (Section 5.5).
6. The study result has been found quite similar to that of Parabolic Wave Model for predicting the bed profile. It has been observed that the velocity (V_x and V_y) data obtained from the experiment showed good matching with the model predicted data (Section 5.6 and Section 5.7).
7. The experimental results suggested that for protecting the beach erosion, CC blocks are more effective than breakwaters. But the use of submerged breakwaters requires further elaborative study as this experiment shows unexpected result regarding their use (Section 5.8).
8. From this study it has been found that, the median grain diameter of sand particle is increased form the initial value in the onshore region, whereas the change is quite insignificant in the offshore zone after completing a run (Section 5.9).

6.3 Recommendations for further Study

Based on present research work, some recommendations can be suggested for further study on cross-shore sediment transport. They are as follows:

- In current study, the slope was taken as 1:15, but in real cases the slope is much milder. Hence for real life problem it is required to conduct study on such slopes as well to fully understand the sediment transport process.
- In this study, the bed material was same throughout the every run. Hence it can be recommended that by using different bed material the same study on cross-shore sediment transport is to be performed.

- In this study non-breaking wave was taken as a consideration to investigate the sediment transport process. In future same study can be done by producing breaking waves.
- This study represents the final bed level, which was measured after completing the run due to scarcity of sophisticated instrument to measure the bed level. But it is required to investigate the change of bed profile after certain time interval. So, in future this sort of study might be performed.
- For the protection of coastal region the effective use of breakwaters (submerged and floating) requires more elaborative study as the coast of Bangladesh faces severe erosion problem.

References

Bagnold, R., 1963. An approach of marine sedimentation. In: Hill, M.N. (Ed.), The Sea Interscience, New York, Vol 3, pp507–528.

Bagnold, R., 1966. An approach of sediment transport model from general physics. US Geol. Survey Prof. Paper 422-I.

Bailard, J., 1981. An energetics total load sediment transport model for a plane sloping beach. J. Geophys. Res. Vol 86 (C11), pp10938–10954.

Bijker, E., 1968. Littoral drift as function of waves and current. 11th Coastal Eng. Conf. Proc. ASCE, London, UK, pp 415–435.

Bird, E., 1984. Coasts: An Introduction to Coastal Geomorphology. Blackwell, Oxford, pp 320.

Bowen, A.J., 1980. Simple models of nearshore sedimentation; beach profiles and longshore bats. In: S.B. McCann (Editor), The Coastline of Canada. Geological Survey of Canada, pp l-l1.

Butt, T. and Russell, P., 1999. Suspended sediment transport mechanisms in high energy swash. Mar. Geol. Vol 161, pp361–375.

Byatt-Smith, J. G. B., and Longuet-Higgins, M. S., 1976. On the Speed and Profile of Steep Solitary Waves, Proc. Roy. Soc. London, Series A, Vol 350, pp175-189.

Camenen, B. and Larroude, P., 2000. Numerical comparison of sediment transport formulae. Sandwave Dynamics Workshop, Lille, France, pp 37– 42.

Camenen, B. and Larson, M., 2005. A general formula for non-cohesive bed load sediment transport. Estuarine, Coastal and Shelf Science Vol 63, pp249–260.

Camenen, B. and Larson,M., 2007. A unified sediment transport formulation for coastal inlet application. Technical report ERDC/CHL CR-07-1, US Army Engineer Research and Development Center, Vicksburg, MS.

Camenen, B. and Larson, M., 2008. A general formula for noncohesive suspended sediment transport. Journal of Coastal Research Vol 24 (3), pp 615–627.

CEM, 2006. Coastal Engineering Manual, Department of the Army, US Army Crops of Engineers, Washington DC 230314-1000, Part II.

Dally, W.R., 1980. A numerical model for beach profile evolution. Masters Thesis, University of Delaware, Newark, DE.

Dally, W.R. and Dean, R.G., 1984. Suspended sediment transport and beach profile evolution. J. Waterw. Port Coastal Ocean Eng. ASCE, Vol 1l (1), pp 15-33.

Dalrymple, R. A. and Dean R. G., 1975. Waves of Maximum Height on Uniform Currents, ASCE Jour. Waterw., Port, coastal and Ocean Engr., Vol 101, pp 259-268.

de Meijer, R.J., 2002. Gradation effects in sediment transport. Coastal Engineering, Vol 47 (2), pp179– 210.

Dette, H.H., Larsonb, M., Murphyc, J., Newe, J., Peters, K., Reniers, A. and Steetzel, H.,

2002. Application of prototype flume tests for beach nourishment assessment, Coastal Engineering, Vol 47, pp137–177.

Dibajnia, M. and Watanabe, A., 1992. Sheet flow under nonlinear waves and currents. Coast. Eng., pp2015– 2029.

Dibajnia, M., 1995. Sheet flow transport formula extended and applied to horizontal plane problems. Coast. Eng. J. Jpn. 38 (2), pp178– 194.

Dohmen-Janssen, M., 1999. Grain size influence on sediment transport in oscillatory sheet flow, phaselags and mobile-bed effects. PhD thesis, Delft University of Technology, ISBN 90-9012929-4, The Netherlands.

Dyer, Keith R., 1986. Coastal and Estuarine Sediment Dynamics. John Wiley and Sons, Toronto, 342 pp. Waterway, Port, Coastal and Ocean Engineering Division of ASCE Vol. 118(2) pp193-200.

Einstein, H., 1972. A basic description of sediment transport on beaches, waves on beaches and resulting sediment transport. Academic Press, New York, pp. 29– 34.

Elfrink, B. and Baldock, T., 2002. Hydrodynamics and sediment transport in the swash zone: a review and perspectives. Coastal Engineering, Vol 45, pp149–167.

Frijlink, H., 1952. Discussion des formules de de ´bit solide de Kalinske, Einstein et Meyer-Peter and Muller compte tenue des mesures re ´centes de transport dans les rivie `res ne ´erlandaises. 2nd Journal Hydraulique, Socie ´te ´ Hydraulique de France, pp98–103.

Hallermeier, R. J., 1982. Oscillatory bedload transport: Data review and simple formulation. Cont. Shelf Res., Vol. 1 pp159-190.

Horikawa, K., Watanabe, A. and Katori, S., 1982. Sediment transport under Sheet Flow Conditions. Proc. Coastal Eng. Conf, Vol. II, pp1335-1352, Cape Town, S. Africa.

Hsu, T. J., Elgar, S. and Guza, R.T., 2006. Wave-induced sediment transport and onshore sandbar migration. Coastal Engineering Vol. 53, pp817–824.

Hughes, M.G., Masselink, G., Hanslow, D. and Mitchell, D., 1997. Toward a better understanding of swash zone sediment transport. Proc. Coastal Dynamics ’97. ASCE, Plymouth, pp804– 813.

Ippen, A. T., 1966. Estuary and Coastline Hydrodynamics, McGraw-Hill Book Company, Inc, New York.

Jonsson, I.G., 1966. Wave boundary layers and friction factors. Proceedings of the 10th Coastal Engineering Conference, ASCE, pp. 127–148.

King, D. and Seymour, R., 1982. State of the art in oscillating sediment transport models. 17th Coastal Eng. Conf. Proc., pp371– 385.

Komar, P.D.,1976. Beach processes and Sedimentation, Prentice-Hall, pp429

Larson, M. and Wamsley, T.V., 2007. A formula for longshore sediment transport in the swash. Proceedings Coastal Sediments '07. InASCE, New Orleans, pp1924–1937.

Longuet-Higgins, M. S., 1976. Recent Developments in the Study of Breaking Waves,

Proc. 15th Coastal Engr. Conf., Vol 1, pp441-460.

Madsen, O. and Grant, W., 1976. Sediment transport in the coastal environment. Vol 209, M.I.T. Ralph M. Parsons Lab.

Matin M. A., 1995. Sorting Characteristics of Beach Materials Along Cox's Bazar-Teknaf Coast M. Engg. Thesis, Department of Water Resources Engineering, BUET, Dhaka.

Miles, J. W. 1980. Solitary Waves, Annual Rev. Fluid Mech., Vol 12, pp11-43.

Miles, J. W. 1981. The Korteweg de Vries Equation: A Historical Essay, Jour. Fluid Mech., Vol 106, pp131-147.

Navera U. K., 2004. Development of a Model for Predicting Wave-Current Interactions and Sediment Transport Process in Nearshore Coastal Waters. Ph. D Thesis, University of Wales, Cardiff, Wales, United Kingdom.

Ogawa, Y. and Shuto, N., 1981. On the dynamics of swash zone. Proc. 29th Japanese Conf. on Coastal Eng., JSCE, pp135-139.

Ogawa, Y. and Shuto, N., 1982. Field measurements of hydraulics and sediment movements in swash zone. Proc. 28th Japanese Conf. on Coastal Eng., JSCE, pp212-216.

Peregrine, D. H. 1976. Interaction of Water Waves and Currents, Advances in Applied Mechanics, Academic Press, New York, Vol 16, pp9-117.

Quick, M.C., 1991. Onshore-offshore sediment transport on beaches. Coastal Engineering, Vol 15, pp313-332.

Quick, M.C. and Patricia L. D., 1994. Cross-shore transport for beaches of mixed sand and gravel. Proc. International Symposium: Waves—Physical and Numerical Modelling, Vancouver, B. C. pp1443-1452.

Ribberink, J. and Chen, Z., 1993. Sediment transport of fine sand under asymmetric oscillatory flow. Delft Hydraulics, Report H840, Part VII, The Netherlands.

Richmond, B.M. and Sallenger, A.H. Jr., 1984. Cross-shore sediment transport of bimodal sands. Proc. 19th International Coastal Engineering Conference pp1997-2008.

Sato, S. and Horikawa, K., 1986. Laboratory study on sand transport over ripples due to asymmetric oscillatory flows. In: Proceedings, 20th International Conference on Coastal Engineering, Taipei. ASCE, Vol 2, pp1481-1495.

Sawamoto, M. and Yamashita, T., 1987. Sediment Transport in Sheet Flow Regime. Coastal Sediments, New Orleans, USA.

Seymour, R. J., 1987. Discussion of the paper by Dally and Dean (1984). J. Waterw. Port Coastal Ocean Eng. ASCE, Vol 113(1), pp85-86.

Shore Protection Manual., 1984. U.S. Army Engineer Waterways Experiment Station, U.S. Government Printing Office, Washington, DC, 4th ed., Vol 2.

Sunamura, T., 1982. Onshore-offshore sediment transport rate in the swash zone of laboratory beaches. Coast. Eng. Jap. Vol 27, pp205-212.

Sunamura, T. and Horikawa, K., 1974. Two-dimensional beach transformation due to

waves, Proc. 14th Coastal Eng. Conf., ASCE, pp 920-928.

Sekiguchi, T. and Sunamura, T., 2004. Effects of bed perturbation and velocity asymmetry on ripple initiation: wave-flume experiments, Coastal Engineering, Vol 50, pp 231–239.

Van Rijn, L.C., 1984a. Sediment transport: Part I: Bed load transport. ASCE J. Hydraul. Div. 110, pp. 1431–1456.

Van Rijn, L.C., 1984b. Sediment transport: Part II: Suspended load transport. ASCE J. Hydraul. Div. 110, pp. 1613–1641.

Van Rijn, L.C., 1984c. Sediment transport: Part III: Bed forms and alluvial roughness. ASCE Journal of Hydraulics Division, Vol. 110, pp. 1733–1754.

Van Rijn, L.C., 1989. Handbook of Sediment Transport by Currents and Waves. Delft Hydraulics, Delft, the Netherlands.

Van Rijn L.C., 1993. Principle of Sediment Transport in river, Estuaries and Coastal Seas. Aqua Publications, The Netherlands.

Watanabe, A., 1982. Numerical models of nearshore currents and beach deformation. Coastal Eng. Jpn., Vol 25, pp147- 161.

Watanabe, A., Riho, Y. and Horikawa, K., 1980. Beach profiles and on-offshore sediment transport. 17th International Conference on Coastal Engineering, pp1106–1121.

Weigel, R. L., 1964. Oceanological Engineering. Prentice-Hall, Englewood Cliffs, NJ, USA

Walsh, B. W., 1989. Onshore-offshore transport mechanisms. M. A. Sc. Thesis, Dep. Civ. Eng. University of British Columbia, Vancouver, B. C , pp213.

Yamashita, T., Sawamoto, M. and Yokoyama, H., 1984. Experimental Study on the sand transport rate and the mechanism of sand movement due to wave. Proc. 31st Japanese Conf. on Coastal Eng., JSCE, pp281-285.

APPENDIX-A

Step wise procedure of wave generator operation:

- **Desk Works:**
    1. From wind speed and fetch length wave height can be obtained by following wave forecasting formula or using nomograms (SPM, 1984). Then model T and h has been fixed.
    2. Find ω by following the formula $\omega = \frac{2\pi}{T}$ from T and determine a dimensionless wave parameter $\frac{\omega^2 h}{g}$.
    3. Set e and f from figure A.2 and find $\frac{f+e}{f}$.

- **Setting Wave Generator:**
    4. Mark h on the side glass of flume.
    5. Empty the flume if there is water.
    6. Turn on the switch of wave generator.
    7. Fix frequency of wave generator as slow as possible by rotating dial (don not change frequency while it is at rest).
    8. Make the vertical arms perfectly vertical (see Figure A.1) for pure translation.
    9. Keep the vertical arms apart from each other as possible for pure rotation.
    10. Measure f at bottom and $f+e$ on marked line (desired water level).
    11. Find $\frac{f+e}{f}$ and compare with the value obtained in step 3. If it does not satisfy adjust vertical arms to alter translation and rotation of paddle.

12. Turn the switch off.

- **Start runs:**
    1. Pour water in the flume up to desired water level.
    2. Turn the switch on and quickly increase frequency of wave generator by rotating dial.
    3. Measure frequency of wave generator. If it is not satisfied then adjust frequency by rotating dial.

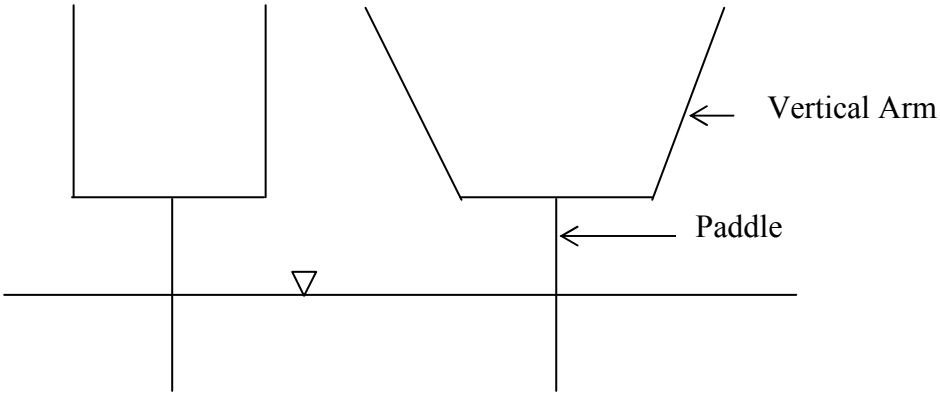

Figure A.1: Line sketch of wave generator (pure translation is shown in left sketch)

Parameters:

T = wave period

h = water depth

ω = $\frac{2\pi}{T}$ angular frequency

f = translation of paddle of eave generator

e = rotation of paddle of wave generator

Example:

Model wave period, T is 1.0 sec and depth of water, h is 50 cm. Then dimension less parameter becomes 2.01. From figure A.2, e and f have been obtained as 0.81and 0.09 respectively.

The ratio $\frac{f+e}{f}$ is then obtained as 10.0. In the laboratory wave generator has been adjusted by trial and error such that $e+f$ has been obtained as = 6.20 and f as 0.62. Then $\frac{f+e}{f}$ has been obtained as 10.0.

Thus the setup has been completed.

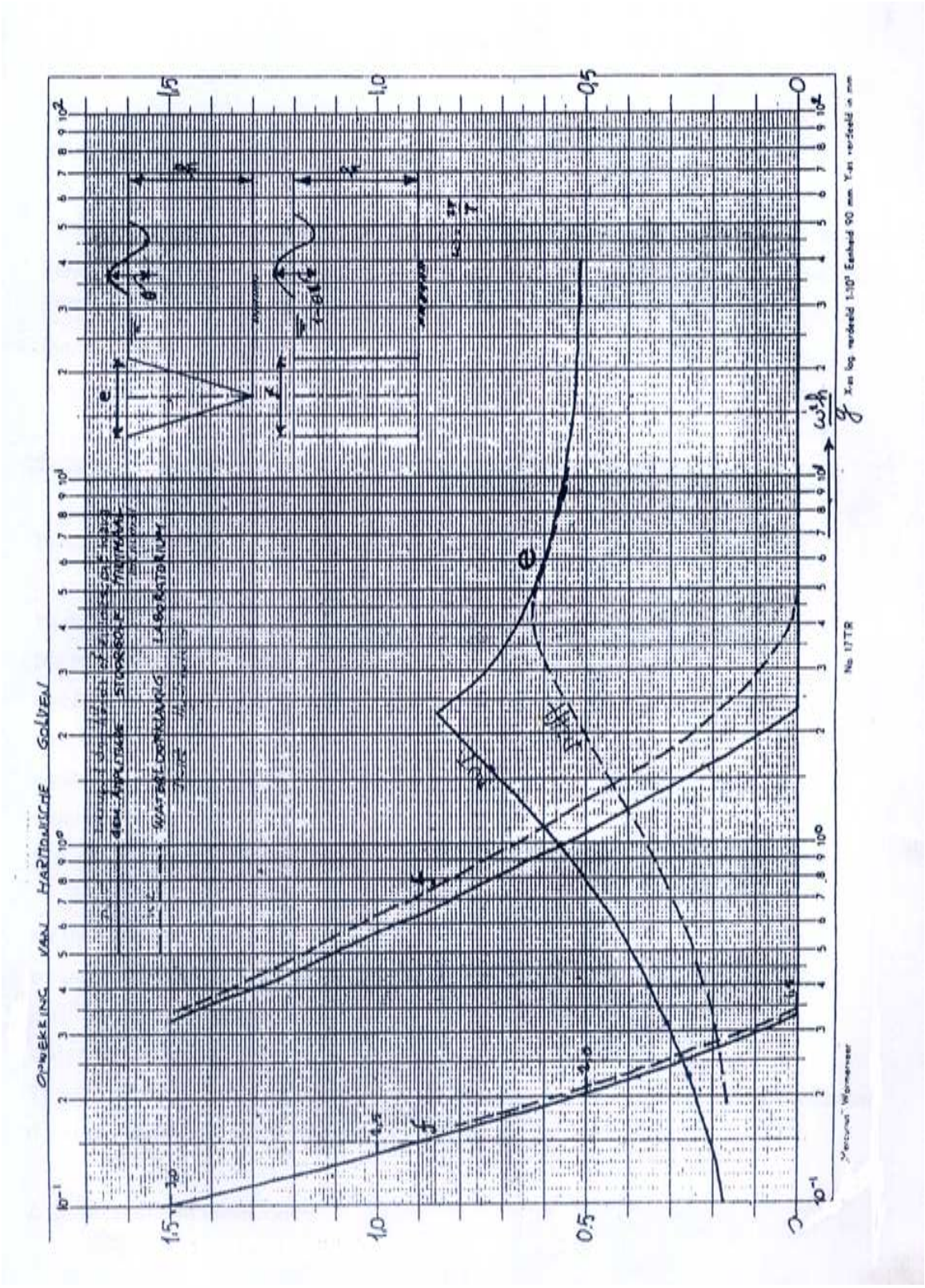

Figure A.2: Nomogram to obtain the value of ***e*** and ***f***

APPENDIX-B

Sieve analysis results for Run No. 2 in three locations are represented in the figure B.1 to B.3.

Figure B.1: Grain size distribution at location 2 for Run No 2

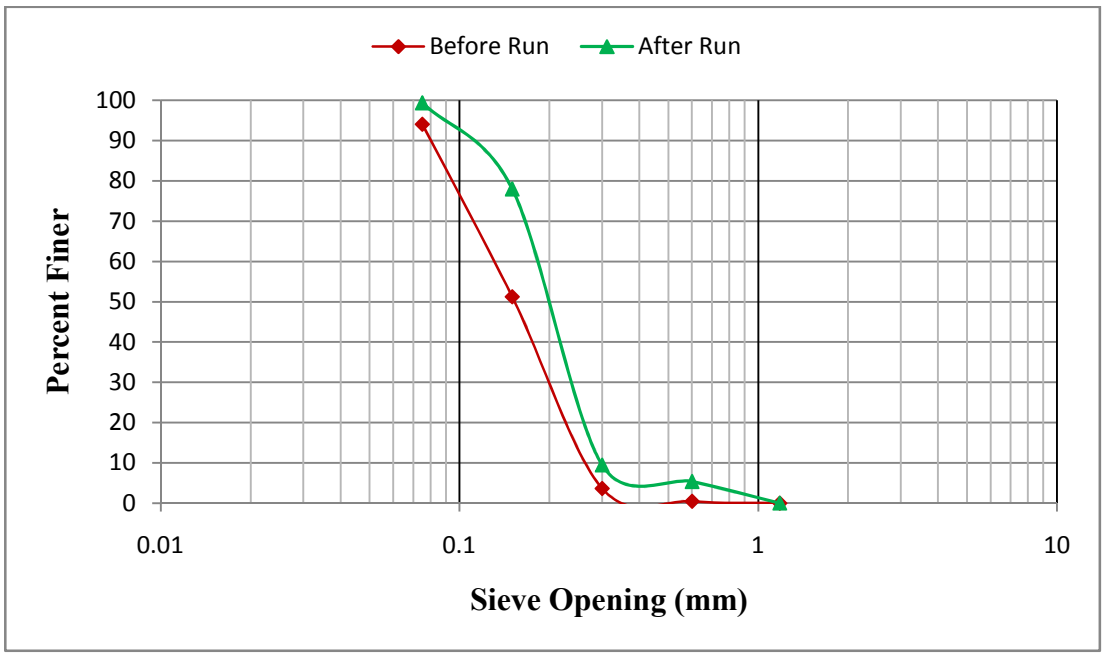

Figure B.2: Grain size distribution at location 3 for Run No 2

Figure B.3: Grain size distribution at location 4 for Run No 2

Sieve analysis results of the collected sediment sample for run number 4 at four selected locations are represented in the Fig. B.4 to B.7.

Figure B.4: Grain size distribution at location 1 for Run No 4

Figure B.5: Grain size distribution at location 2 for Run No 4

Figure B.6: Grain size distribution at location 3 for Run No 4

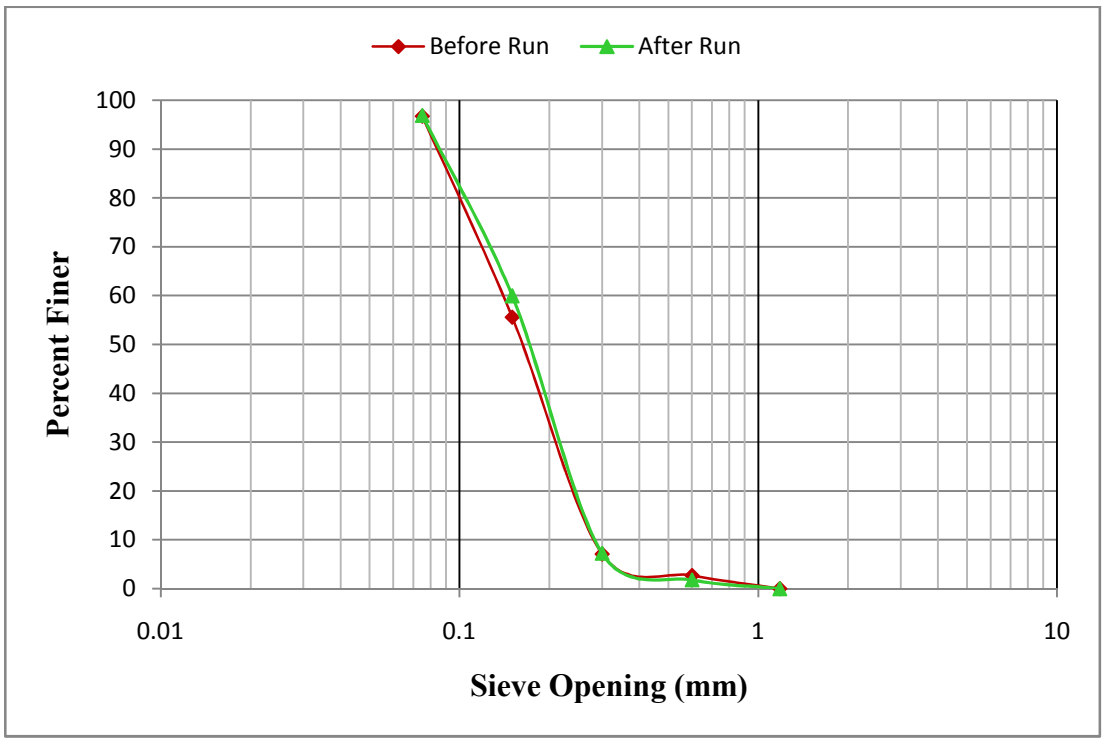

Figure B.7: Grain size distribution at location 4 for Run No 4

Sieve analysis results of the collected sediment sample for run number 9 at four selected locations are represented in the Fig. B.8 to B.11.

Figure B.8: Grain size distribution at location 1 for Run No 9

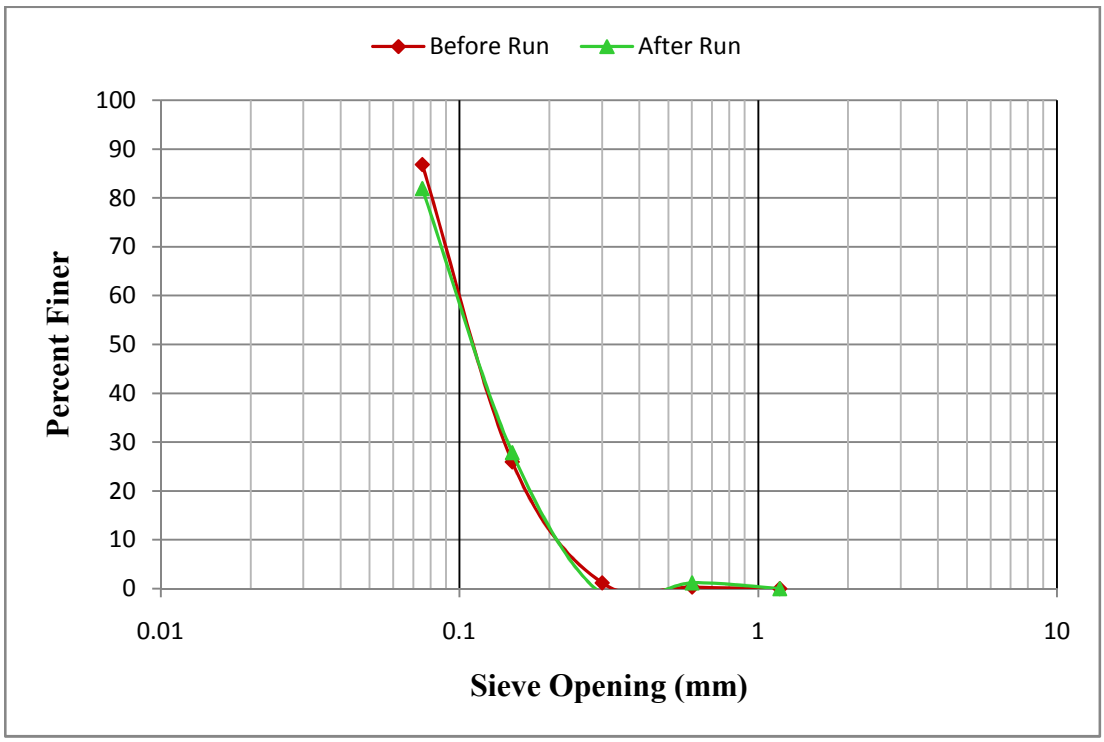

Figure B.9: Grain size distribution at location 2 for Run No 9

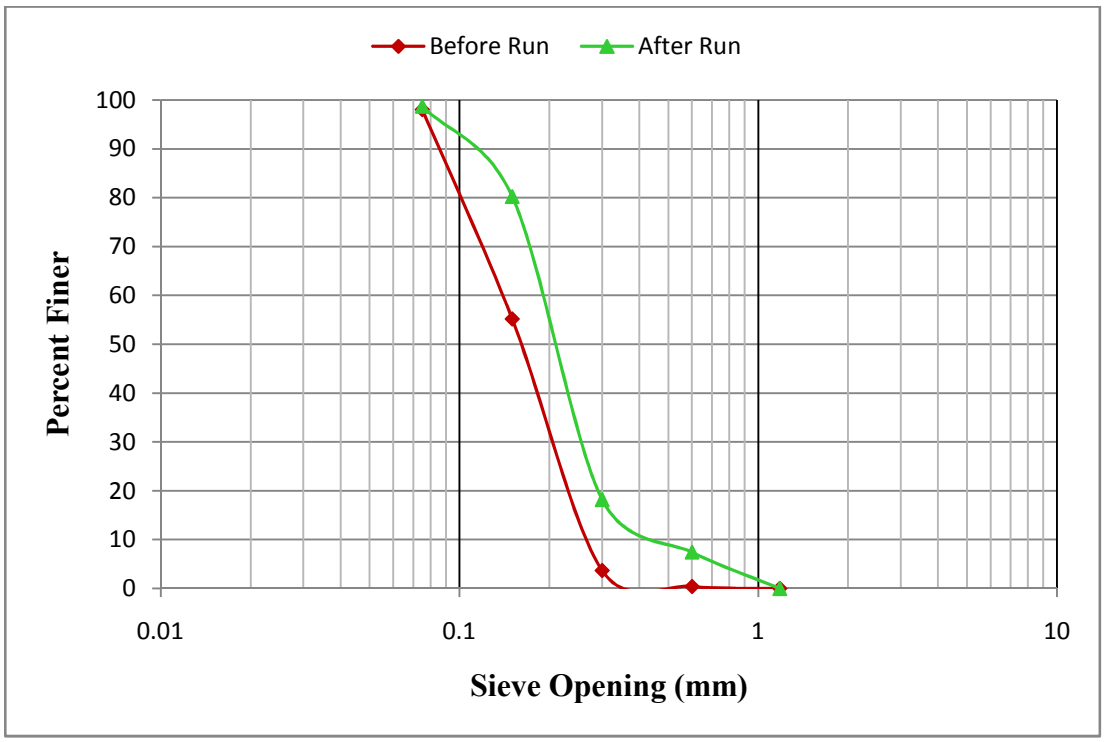

Figure B.10: Grain size distribution at location 3 for Run No 9

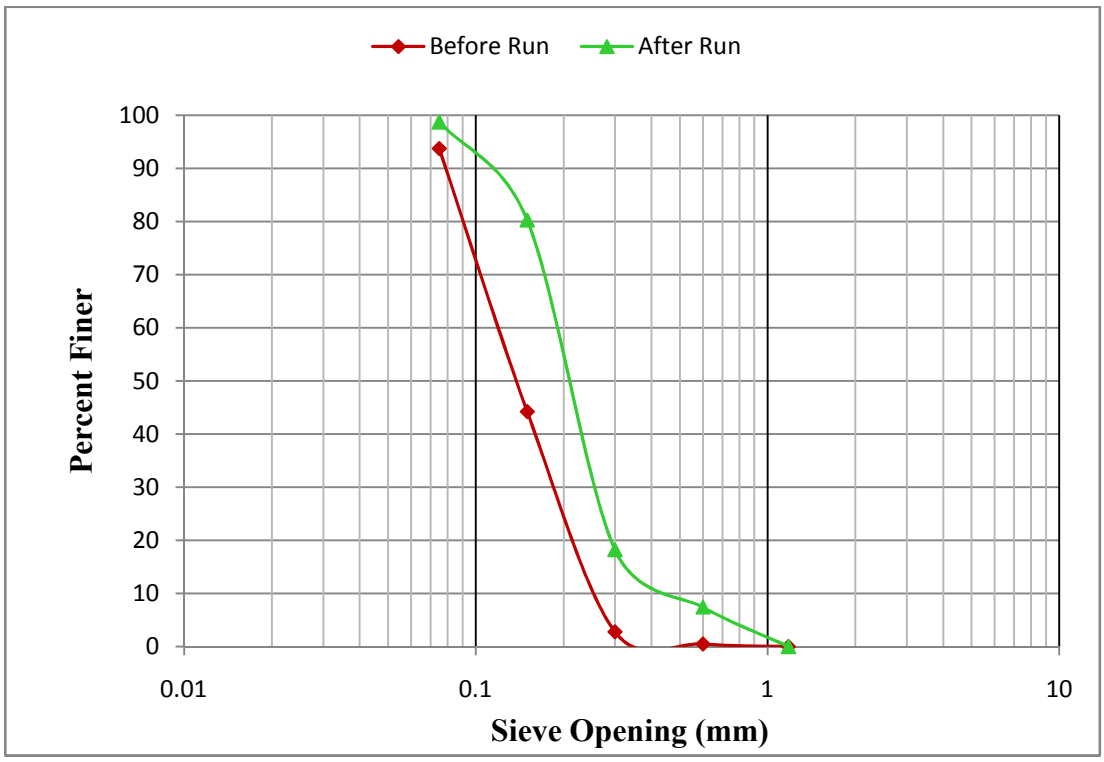

Figure B.11: Grain size distribution at location 4 for Run No 9